

We are IntechOpen, the world's leading publisher of Open Access books Built by scientists, for scientists

6,300

Open access books available

171,000

International authors and editors

190M

Downloads

Our authors are among the

154

Countries delivered to

TOP 1%

most cited scientists

12.2%

Contributors from top 500 universities



WEB OF SCIENCE™

Selection of our books indexed in the Book Citation Index
in Web of Science™ Core Collection (BKCI)

Interested in publishing with us?
Contact book.department@intechopen.com

Numbers displayed above are based on latest data collected.
For more information visit www.intechopen.com



Advanced Oxidation Processes: A Powerful Treatment Option for the Removal of Recalcitrant Organic Compounds

Damodhar Ghime and Prabir Ghosh

Abstract

Advanced oxidation processes (AOPs) are the technologies that generally use the hydroxyl radicals, the ultimate oxidant for the remediation of organic contaminants in wastewater. These are highly effective novel methods speeding up the oxidation process. AOP can combine with ozone (O_3), catalyst, or ultraviolet (UV) irradiation to offer a powerful treatment of wastewater. Future research should be focused on enhancing the properties of heterogeneous catalysts in AOPs. This chapter reports general review of different AOPs utilized for the removal of various phenolic compounds and textile dyes in wastewater. The chapter also aimed at an investigation of efficiency for different photochemical AOPs. The authors have carried out the experimental runs at a laboratory scale for the removal of malachite green oxalate (MGO) dye with photochemical AOPs. The influence of ferrous ions and oxidant dosage on percentage decolorization of MGO in wastewater has been reported. The discussion extends to the utilization of different modified photocatalysts for the photocatalysis process. The future challenges, such as the adoption of strategies for the integration of processes and the decrement in operational cost of AOPs, are discussed. The discussion covers the utilization of different heterogeneous catalysts, the reduction of input demands of chemicals and energy for the processes.

Keywords: advanced oxidation processes (AOPs), wastewater treatment, organic contaminants, heterogeneous catalysts, hydroxyl, sulphate radicals

1. Introduction

Advanced oxidation processes (AOPs) are the most attractive and favorable option for the effective removal of organic pollutants in wastewater. In recent years, many harmful chemicals in the released effluent from industries have been identified in the environment. These chemicals are hazardous to both human beings and aquatic biota. They can cause severe damages to human beings and the marine environment. So, there is a strong need to treat toxic pollutants with a proper treatment option. Thus, AOPs find its suitable applicability for the treatment of wastewater containing harmful chemicals. Advanced oxidation technologies are based on the in situ generations of strong oxidants, i.e. hydroxyl radicals and sulphate radicals,

for the oxidation of organic pollutants [1]. Some of the AOPs use ozone and UV irradiation for better treatment efficiency. These AOP technologies have already been established and started at full scale for the treatment of drinking water and the facilities of water reuse. Also, several AOPs such as electrochemical treatment, use of electron beam, plasma, microwave and ultrasound related processes are continually being studied by the environmental researchers and scientists.

AOPs are very well known for bridging the gap between the treatability obtained by traditional physicochemical and biological processes, and from day to day more stringent regulations are set by the environmental laws. As extensive research is going on in AOPs from the last two decades, still these technologies are well matured, and there are again some fields worthy of research [2].

1.1 Different AOPs for wastewater remediation

Different AOPs such as photocatalysis, Fenton-like processes and ozonation were investigated for the treatment of an integrated solution of produced water that contains toluene, xylene, naphthalene, phenol, malonic and acetic acids. This integrated solution of produced water was referred as a seawater matrix [3]. The efficiency in terms of total organic carbon (TOC) was studied. Among different applied AOPs, photocatalysis was less efficient for the treatment of a seawater matrix. The removals of TOC lower than 20% were noticed in 4 h of treatment. The better results were obtained in the ozonation process that combined with oxidant hydrogen peroxide (H_2O_2). The combined effect of H_2O_2 and ozone leads to the complete removal of organics, consisting of a high-percentage removal of acetic acid that was not entirely oxidized with the rest of AOPs used. 74% TOC removal efficiency was observed in ozonation for the optimum conditions of 4 g/h ozone, 500 mg/L H_2O_2 and pH of 10 in 2 h of treatment time.

Several AOPs such as O_3 , $\text{O}_3/\text{H}_2\text{O}_2$, UV, UV/ O_3 , UV/ H_2O_2 , $\text{O}_3/\text{UV}/\text{H}_2\text{O}_2$, $\text{Fe}^{2+}/\text{H}_2\text{O}_2$ and photocatalysis processes were investigated for the oxidation of phenol in aqueous medium [4]. The comparison of these different AOPs was undertaken considering some of the experimental parameters. Among all, the Fenton process showed the fastest removal rate for phenol in wastewater. The lower costs were observed for ozonation. Single ozonation provides the best results for phenol degradation in ozone combinations.

The viability of the ozonation and ozone combined with UV photolysis processes was investigated for the degradation of direct blue 86 dye in wastewater [5]. The batch experiments were conducted for studying the effect of solution pH, initial dye concentration and reaction time. The obtained results show that the pH and initial dye concentration controls the efficiency of the process. More than 98% decolorization efficiency was obtained at pH 11, 100 mg/L of initial dye concentration in 35 min of ozone treatment.

All AOPs are characterized by their potential of exploiting the higher reactivity of hydroxyl radicals while driving in oxidation processes. The different AOPs with their essential features are discussed and presented for the wastewater remediation [6]. The number of investigations was carried out with the Fenton process for the abatement of organic pollutants in wastewater. Fenton's reagent can destroy the toxic contaminants in the wastewater like phenols and pesticides. The use of Fenton's reagent for the oxidation purpose is an attractive option for the wastewater treatment due to the iron abundances, and hydrogen peroxide is more comfortable to handle and environmentally safe. Sometimes, UV irradiation is also used with the Fenton process to increase the process efficiency. This process can overcome the shortcomings of the Fenton process. Photolysis allows the regeneration of

ferrous ions (Fe^{2+}) from ferric ions (Fe^{3+}) that produce sludge in the Fenton process. Besides, the titanium dioxide (TiO_2) in anatase form finds its application in photocatalysis at a greater level due to its higher stability, low cost and better performance for the degradation of organics.

1.2 Organic pollutants in industrial wastewater

The contamination of water resources continuously exists due to the release of organic pollutants from industrial discharges. The presence of organic pollutants affects the freshwater quality and causes severe effects on aquatic biota. The recent improvement in very sensitive analytical techniques is able to measure the concentration of organic pollutants, even in $\mu\text{g/L}$ concentrations. The organic content generally measures in terms of total organic carbon, chemical oxygen demand (COD), and biological oxygen demand (BOD) [7]. In most of the cases, the dyes and phenolic compounds were taken as model pollutants as per the published literature in recent years. Among different organic pollutants, the phenolic compounds have deserved more attention owing to their high toxicity and frequency of industrial wastewaters [8]. The presence of phenolic compounds in wastewater gives unpleasant smell and taste even at deficient concentrations.

Agro-industrial wastewaters are characterized by the presence of a higher amount of organic and inorganic pollutants of environmental concern [9]. Some parameters, such as high pollutant dose and production of more volume, make the treatment of agro-industrial waters an ecological challenge. For the effective treatment of industrial effluents, the wastewater treatment should consist of degradation as well as the mineralization of water pollutants. During oxidation, the conversion of identified pollutants in wastewater to its more stable oxidation state is necessary.

1.3 Aim and objectives of the chapter

This chapter studies the general review of different AOPs employed for the oxidation of organic pollutants in wastewater. The chapter also aimed at an investigation of the efficiency of different photochemical AOPs. Experimental runs using a UV photochemical reactor were performed at a laboratory scale for the decoloration of malachite green oxalate (MGO) dye using photochemical AOPs. The influence of ferrous ions and oxidant dosage on percentage decolorization of MGO in wastewater has been reported. The discussion was also extending to the utilization of different modified photocatalysts for the photocatalysis process. Some of the future challenges, such as the adoption of strategies for the integration of processes and the decrement in operational cost of AOPs, are discussed.

2. Different photochemical AOPs

Photochemical AOPs are frequently used as an efficient barrier for the oxidation of organic pollutants in wastewater. The combined effect of UV irradiation and hydrogen peroxide (H_2O_2) reaction confirms the removal of a broader range of compounds. Common photochemical AOPs used are UV alone, UV/ H_2O_2 , UV/ Fe^{2+} , UV/ H_2O_2 / Fe^{2+} , UV/ O_3 , UV/ $\text{S}_2\text{O}_8^{2-}$, UV/ TiO_2 , UV/chlorine and UV with some other photocatalysts [10]. Therefore, UV AOPs can show better removal rates with both the radicals, i.e. hydroxyl and sulphate radicals.

2.1 Hydroxyl radical-based photochemical AOPs

The removal of targeted micro-pollutants, including naproxen, carbamazepine, diclofenac, gemfibrozil, ibuprofen, caffeine and mecoprop, were reported with photolysis and UV/H₂O₂ processes [11]. The medium-pressure UV lamp was used for the UV irradiation. The obtained results indicate that UV photolysis alone is not useful for the removal of micro-pollutants, excluding diclofenac and mecoprop. So, there was a need to treat the rest of the micro-pollutants with the UV/H₂O₂ process. It was found that the overall rates of oxidation for all selected organic pollutants were enhanced in the presence of H₂O₂, especially in the case of caffeine and carbamazepine at an oxidant dose of 25 mg/L on comparing with direct UV photocatalysis. Accordingly, the addition of H₂O₂ is critical in the photolysis process for better removal efficiency as it can promote the degradation of micro-pollutants in wastewater. The radical species are generated through the transfer of electrons by transition metal oxidation of oxidants or by the photolysis of H₂O₂ or thermolysis of H₂O₂ and in heterogeneous TiO₂ photocatalysis [12].

Recently, UV photolysis of hydrogen peroxides has earned considerable significance as they are comparatively a benign process concerning the environmental and economic considerations. The activation of symmetrical peroxides, mainly H₂O₂ with UV irradiation, generates the hydroxyl radical species ([•]OH) through the homolytic cleavage of the peroxide bond. These hydroxyl radicals are responsible for the oxidation of water pollutants.

2.2 Sulphate radical-based photochemical AOPs

Sulphate radical-based photochemical AOPs have drawn considerable attention because of the typical advantages of sulphate radicals such as higher redox potential (2.5–3.1 V), stability, selectivity and its use on the broader pH ranges. These radicals could be generated from different persulphates under the application of light, heat and transition metal and sometimes in an alkaline atmosphere or during electrochemical treatment [13]. The combined effect of UV irradiation with persulphate confirms the destruction of a broader range of water pollutants in wastewater.

The UV-activated persulphate advanced oxidation process was investigated for the degradation of sulfamethoxypyridazine (SMP) [14]. The sulphate radical-based photochemical AOP can significantly remediate SMP from aqueous solutions. In a comparative study of kinetics, the second-order reaction rate constant for SMP with sulphate radicals was obtained to $2.73 \times 10^{10} \text{ M}^{-1} \text{ s}^{-1}$, whereas the use of hydroxyl radicals was $2.22 \times 10^{10} \text{ M}^{-1} \text{ s}^{-1}$. Therefore, the faster reaction kinetics was in the case of sulphate radical-based photochemical AOPs.

Moreover, the uses of different heterogeneous catalysts such as cobalt, silver, copper and ruthenium-based catalysts have been studied to efficiently activate peroxymonosulphate (PMS) and peroxydisulphate (PDS) for the removal of water contaminants. Comparing to other activation methods, the activation of persulphates with heterogeneous catalysts has its own merits, such as the requirement of lesser energy, ease of scale-up and higher reactivity. Nevertheless, the use of cobalt- or copper-based catalysts might create some health problems because of the leaching of harmful metal into the aqueous phase, which can stop their practical applications. Again, the use of ruthenium-based catalysts for persulphate activation can be more costly. Thus, Mn-based catalysts are the best option to use for the activation of persulphate. Mn-based materials show some crucial advantages like its higher natural abundance, lower level of toxicity and environmental friendliness.

So, these materials have paid more attention to further improvement in Mn-based catalysts for the activation of persulphates [15].

3. Decolorization of malachite green oxalate dye through photochemical AOPs

The cylindrical type of photochemical reactor was used for the decolorization of malachite green oxalate dye in wastewater. The technical details for the reactor were that it was having the effective volume of 1.47 L and feeding tank volume of 5 L. The reactor was also built with an inside reflecting surface and four tubes of UV source (low-pressure mercury-vapor lamp of intensity 8 W each) surrounded with glass/quartz tube which was placed centrally in reactor [16]. The feeding tank was made up of SS304 material. The wastewater was circulated into the system with the help of a magnetic pump that was composed of polypropylene material. The maximum working temperature for the photochemical reactor was 80°C. The unknown concentration of MGO dye in wastewater after the treatment was measured with a UV-vis spectrophotometer. Absorbance values were detected at 618 nm of maximum wavelength for MGO dye.

3.1 Comparative assessment of different photochemical AOPs for MGO dye

The comparative assessment of various photochemical AOPs, including UV alone, UV/H₂O₂, UV/TiO₂, UV/H₂O₂/TiO₂ and UV/Fe²⁺/H₂O₂, were investigated for the decolorization of MGO dye. The reaction conditions used were initial dye and H₂O₂ concentrations of 100 mg/L and 12 mM, pH 3, ferrous ion concentration of 60 mg/L and TiO₂ dose to 0.6 g/L with irradiation of 32 W for 60 min of treatment time. A higher rate of decolorization was found in the case of UV/H₂O₂/TiO₂ and UV/Fe²⁺/H₂O₂ processes. It was about 97 and 98% for UV/Fe²⁺/H₂O₂ and UV/H₂O₂/TiO₂ processes, respectively. This was happened due to the higher rate of generation for hydroxyl radicals in both the processes. The use of photocatalyst (i.e. TiO₂) enhances the production of hydroxyl radicals in the process, leading to the higher percentage removal of MGO dye. UV photolysis alone was not able to decolorize the MGO completely (77% for a treatment time of 60 min). UV/H₂O₂ and UV/TiO₂ processes almost achieved 95% decolorization efficiency. In short, the decolorization of MGO dye was reduced in the order of [16]:

$$\text{UV/Fe}^{2+}/\text{H}_2\text{O}_2 > \text{UV/H}_2\text{O}_2/\text{TiO}_2 > \text{UV/TiO}_2 > \text{UV/H}_2\text{O}_2 > \text{UV alone} \quad (1)$$

3.2 Influence of ferrous ions on MGO dye decolorization in the photo-Fenton process

The influence of ferrous ions on MGO dye decolorization was studied by taking the concentrations of Fe²⁺ in the range of 20–80 mg/L. **Figure 1** shows the effect of varying ferrous ion concentration on MGO dye decolorization in the photo-Fenton process. It was seen that the rate of decolorization was enhanced as the ferrous ion concentrations increased up to 20–60 mg/L. Further increase in ferrous ions to 80 mg/L decreased the rate of decolorization. This might have happened due to the rise in the generation of hydroxyl radicals for a higher concentration of Fe²⁺ ions. It can show some scavenging effects of hydroxyl radicals. More concentration of ferrous ions in solution brings about the brown turbidity of ferric hydroxides, and this can cause the recombination of hydroxyl radicals in the aqueous medium [16].

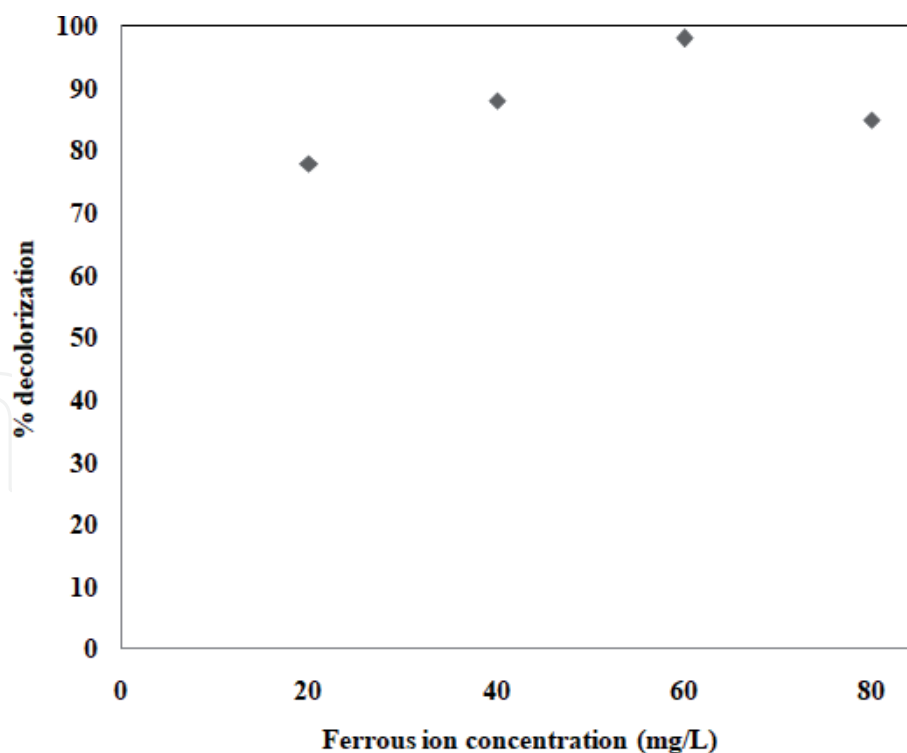


Figure 1.

Influence of ferrous ions (Fe^{2+}) on MGO dye decolorization with the photo-Fenton process by using dye concentration of 100 mg/L, 12 mM of H_2O_2 and pH 3 with irradiation of 32 W for 60 min of treatment time.

3.3 Effect of H_2O_2 concentrations in UV/ H_2O_2 , photo-Fenton and TiO_2 photocatalysis processes

The concentration of oxidant in the photochemical AOPs (UV/ H_2O_2 , photo-Fenton and TiO_2 photocatalysis) was varied in the range of 6–36 mM. About 88.61% of decolorization was observed for a dose of 6 mM in the photo-Fenton process [16]. This shows the existence of the generation of hydroxyl radicals into the system. Increment in percentage decolorization was observed with an increase in oxidant concentration up to 12 mM. Beyond 12 mM, it was found to decrease. **Figure 2** shows the influence of H_2O_2 concentration in UV/ H_2O_2 , photo-Fenton and TiO_2 photocatalysis processes at an oxidant concentration of 12 mM. The decrement in % decolorization beyond 12 mM of oxidant was due to the scavenging action of using extra H_2O_2 or possible recombination of hydroxyl radicals. Sometimes, the excessive amount of H_2O_2 acts as a hole scavenger, which can produce per-hydroxyl radicals. The per-hydroxyl radicals are less reactive than hydroxyl radicals. Thus, it is always advisable to use an optimum dose of oxidant.

3.4 Pseudo-first-order reaction kinetics for hydroxyl and sulphate radical-based AOPs

The pseudo-first-order reaction kinetics was reported for the decolorization study of MGO dye in wastewater. Both processes, hydroxyl and sulphate radical-based AOPs, were employed to calculate the reaction rates and compared to study their efficiencies. The parameters of kinetic models for decolorization efficiency of MGO dye at 12 mM dose of H_2O_2 and 1.68 mM of persulphate concentrations using UV irradiation were studied with the application of linear regression analysis to $[\ln(C_0/C_t) \text{ versus } t]$ data for pseudo-first-order model [16]. The obtained values of correlation coefficients for sulphate and hydroxyl radical-based AOPs were 0.9904 and 0.9261, respectively. The reaction rate constant values were 0.0276 min^{-1} for

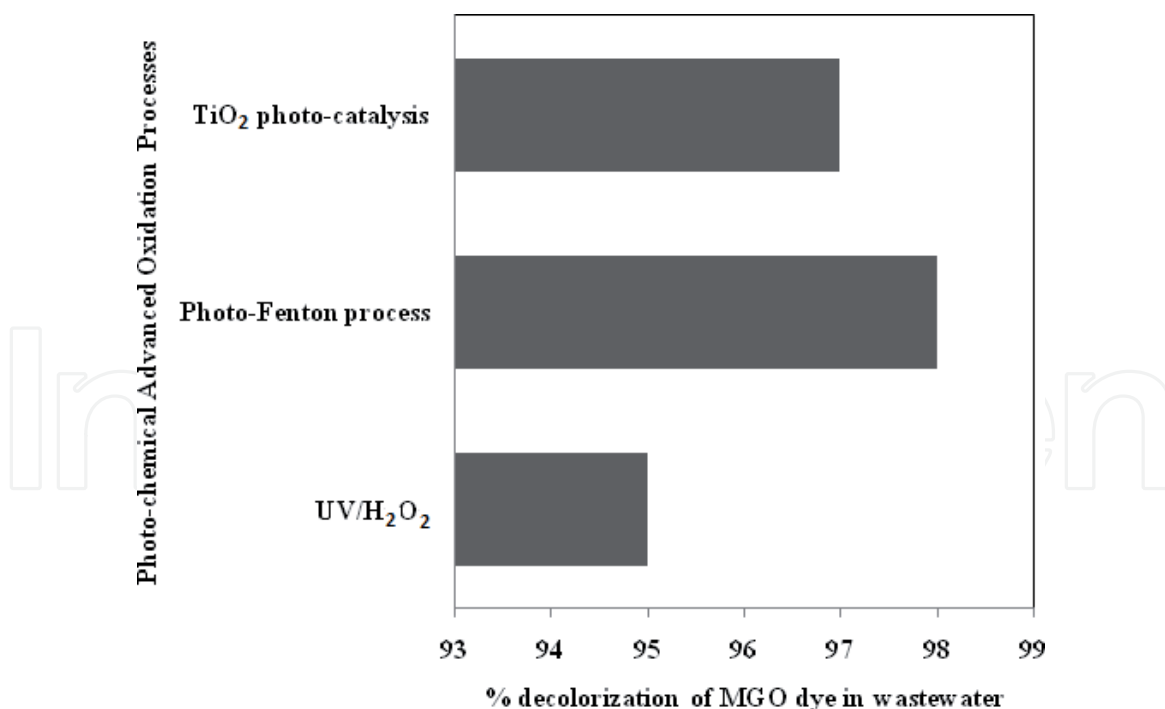


Figure 2.
 Influence of H₂O₂ concentration in UV/H₂O₂, photo-Fenton and TiO₂ photocatalysis processes (experimental conditions: flow rate of 10 LPH, 12 mM of oxidant (H₂O₂), ferrous ion concentration of 60 mg/L, TiO₂ dosage of 0.6 g/L with irradiation of 32 W for 60 min of treatment time).

sulphate radical-based AOP and 0.0031 min⁻¹ for hydroxyl radical-based AOP. This means that the decolorization was faster in sulphate radical-based AOP.

4. Utilization of different modified photocatalysts in photocatalysis

The use of different photocatalysts in the photocatalysis processes is a useful alternative and attractive option in advanced researches. The photocatalyst should possess higher photochemical stability and can effectually use UV irradiation for wastewater treatment. The word ‘photocatalyst’ is made up of two parts: photo and catalyst. The word ‘photo’ means light, and a ‘catalyst’ means the process in which the oxidation rate is enhanced with catalyst.

Activation energy ‘E_a’ was found to decrease with an increase in the rate of reaction. In addition, the photocatalysts possess some properties such as higher surface area, better crystallinity, low cost, non-toxicity, ease handling and cost-effective applicability [17]. Recently, the application of semiconductors like titanium dioxide (TiO₂) shows great potential in photocatalysis processes. This is because of its low cost and environmentally friendly nature. TiO₂ is generally used as a standard reference for the comparison of the photochemical activity of other catalysts. The fine powdered form of TiO₂ is normally used in the slurry form. This leads to the higher volumetric production of reactive oxygen species (ROS) that can be proportional to the number of active surface sites [18].

The post-separation of TiO₂ after the treatment is an additional step while using this photocatalyst in slurry form. It is an important step for avoiding any loss of catalyst and can be reused for the photooxidation of new pollutants. The catalyst can be recovered through conventional sedimentation or via crossflow filtration or some types of membrane filtrations. The applicability of immobilized form of photocatalysts can increase the operational difficulty as the photon might not penetrate to every single surface active site for its activation. Silver orthophosphate (Ag₃PO₄)

has also gained much attention for its use as photocatalysts as it shows higher photooxidative capabilities for O_2 evolution from the split-up of water and better removal efficiency for textile wastewater [19]. Approximately 90% of quantum efficiency can be achieved with Ag_3PO_4 at a wavelength of 420 nm in the oxidation of wastewater. During this phenomenon, $AgNO_3$ acts as a scavenger. This mentioned quantum efficiency was extremely higher than other photocatalysts, such as 20% in the case of N-doped TiO_2 and $BiVO_4$ photocatalysts. But the uncontrolled and unwanted photo-corrosion of Ag_3PO_4 is the main hurdle for its application in photocatalytic systems.

The photo-corrosion of Ag_3PO_4 happens due to its slighter solubility (0.02 g/L) in water and its characteristics of energy band structure. Thus, it's a big challenge for the researchers to improve and modify Ag_3PO_4 for their stability and to increase its activity without the help of any sacrificial reagents. Sometimes, the semiconductor, TiO_2 , is doped to slow down the recombination of fast charge and to enable the visible light absorption with the generation of defect states in the bandgap. In the earlier case, the conduction band electrons or valence band holes are trapped in the defect sites, retarding their recombination and enhancing the interfacial charge transfer. In the latter case, the electronic transitions from the valence band to defect state or from defect state to conduction band are permitted under UV irradiation [20, 21].

The dopants are categorized into metal and nonmetal ions, and their selection is critical in considering their overall photocatalytic activity. Using noble metal ions (platinum, gold and silver) as dopants has gained less attention than the use of transition metals. Metallic doping serves the purpose of both a conduction band electron trapping and a cocatalyst in photocatalysis. Doping of TiO_2 is also possible with some nonmetallic elements such as carbon, sulfur, nitrogen and boron for studying their visible light photocatalysis.

The photocatalytic decomposition of water pollutants on nitrogen-doped TiO_2 under the illumination of visible light is essentially induced by the surface intermediates formed by oxidation of water or by the reductive activation of oxygen. It does not happen by the direct reactions with positively charged holes trapped at N_2 -induced mid-gap level. Moreover, the use of the carbon-doped TiO_2 in photocatalysis is also controversial. Different methods have been proposed for the synthesis of C-doped TiO_2 , such as carbon coating and carbon mounting. Two carbon dopants are there: the first one is anions that can substitute oxygen (O_2) in the lattice structure, and the second one is cations that can occupy an interstitial lattice site. The oxidation states that are linked with its bonding phases are +4 (carbonates having C-O bond) and -4 (carbides having Ti-C bond). These oxidation states are strongly dependent on the method of catalyst preparation and operating conditions used. Both states can be even copresent in the prepared photocatalysts. Sometimes, the TiO_2 is also doped with more than two elements for further enhancement in the photocatalytic activity under UV and visible light. This type of activity makes the doped TiO_2 more stable via compensation of charge. The metal/metal (Pt/Cr), nonmetal/nonmetal (N/S) and metal/nonmetal pair (Pt/N) combinations can be used further for doping [20]. Therefore, TiO_2 photocatalysts are doped with different elements, as discussed above, to overcome its demerits before use in oxidation, i.e. less absorbance with visible light and possible recombination of electron-hole pairs [22].

5. Conclusions

Advanced oxidation technologies represent a powerful option for the removal of organic pollutants in industrial wastewater. Different AOPs have been investigated,

and thus, it allows the selection of the most suitable process for the specific wastewater treatments. Different photochemical AOPs also have much potential for the reduction of organics in wastewater. The combination of UV and radicals (hydroxyl or sulphate) can effectively eliminate the organics with higher removal efficiency than direct UV photolysis or persulphate oxidation alone. Decolorization of malachite green oxalate was performed with different homogeneous and heterogeneous AOPs. The influence of ferrous ions and oxidant concentration and comparative assessment of different photochemical AOPs are reported. 12 mM of H_2O_2 and 60 mg/L of ferrous ion concentrations have been observed to be optimum in the photo-Fenton process. In the comparative assessment studies of photochemical AOPs, the percentage dye decolorization efficiency has been decreased in the order: $\text{UV/Fe}^{2+}/\text{H}_2\text{O}_2 > \text{UV/H}_2\text{O}_2/\text{TiO}_2 > \text{UV/TiO}_2 > \text{UV/H}_2\text{O}_2 > \text{UV alone}$. The experimental results show that the MGO dye removal efficiency from wastewater is higher in the case of sulphate radical-based AOP than hydroxyl radical-based AOP. Although the pure form of TiO_2 is a well-liked photocatalyst for many reasons, it suffers from lower efficiency for photochemical oxidation and becomes deficient in the visible light activity that obstructs its practical applications. Thus, the surface-modified TiO_2 photocatalysts have been continuously investigated to overcome the shortcomings of pure TiO_2 .

6. Future perspectives

The conceptual proof of advanced oxidation processes has already been offered after years of research for wastewater treatment. However, something is indeed missing, the application of AOPs from laboratory scale to large scale (i.e. totally operational use). The main hindrance is the level of operating cost (money required for per unit mass of organic pollutant eliminated or unit volume of wastewater treated) allied with AOPs in comparison with other traditional wastewater treatment techniques. How can advanced oxidation treatment techniques become more striking cost-wise? Some useful thoughts that can be considered for its broader applicability are as follows:

- The utilization of renewable energy is essential in this case. AOPs driven by sun irradiation have an apparent head start not only for the treatment of industrial wastewater but also for the production of energy simultaneously. This is the more economical solution for the issue of water purification and its reuse.
- Every time, AOPs should not be our first choice for the treatment of wastewater. It must be imposed to become selective, i.e. they must have a definite treatment target. Otherwise, valuable and expensive elements such as oxidants, energy and different catalysts are wasted without cause.
- Advanced oxidation technologies have been intensely benefitted from the advances in the field of material science. Novel materials have been identified continuously with better characteristics. Consequently, the use of AOPs for environmental applications is a topic in engineering, science and other multiple disciplines. All the researchers and scientists working on the same field from various disciplines must join forces to solve the problem successfully. Moreover, the use of waste materials as a catalyst, such as red mud (waste from bauxite processing industries), can reduce the cost of AOP treatment. This phenomenon is waste valorization. It is a new, impressive and somewhat unexploited concept.

So, it is not possible to replace accessible wastewater treatment technologies with AOPs from an economic standpoint. But this problem can be solved by using the combination of advanced oxidation processes with the ancient treatment technologies. It is feasible and cost-effective, also comparing to a fully AOP application.

IntechOpen


IntechOpen

Author details

Damodhar Ghime and Prabir Ghosh*
Department of Chemical Engineering, National Institute of Technology, Raipur,
Chhattisgarh, India

*Address all correspondence to: prabirg.che@nitrr.ac.in

IntechOpen

© 2020 The Author(s). Licensee IntechOpen. Distributed under the terms of the Creative Commons Attribution - NonCommercial 4.0 License (<https://creativecommons.org/licenses/by-nc/4.0/>), which permits use, distribution and reproduction for non-commercial purposes, provided the original is properly cited. 

References

- [1] Miklos DB, Remy C, Jekel M, Linden KG, Hubner U. Evaluation of advanced oxidation processes for water and wastewater treatment—A critical review. *Water Research*. 2018;**139**:118-131
- [2] Dewil R, Mantzavinos D, Poulios I, Rodrigo MA. New perspectives for advanced oxidation processes. *Journal of Environmental Management*. 2017;**195**:93-99
- [3] Jimenez S, Andreozzi M, Mico MM, Alvarez MG, Contreras S. Produced water treatment by advanced oxidation processes. *Science of the Total Environment*. 2019;**666**:12-21
- [4] Contreras S, Pascual E, Esplugas S, Gim J, Rodri M. Comparison of different advanced oxidation processes for phenol degradation. *Water Research*. 2002;**36**:1034-1042
- [5] Hassaan MA, El A, Madkour FF. Testing the advanced oxidation processes on the degradation of direct blue 86 dye in wastewater. *Egyptian Journal of Aquatic Research*. 2017;**43**:11-19
- [6] Andreozzi R, Caprio V, Insola A, Marotta R. Advanced oxidation processes (AOP) for water purification and recovery. *Catalysis Today*. 1999;**53**:51-59
- [7] Bedding ND, McIntyre AE, Perry R, Lester JN. Organic contaminants in the aquatic environment. *Science of the Total Environment*. 1982;**25**:143-167
- [8] Luan M, Jing G, Piao Y, Liu D, Jin L. Treatment of refractory organic pollutants in industrial wastewater by wet air oxidation. *Arabian Journal of Chemistry*. 2017;**10**:S769-S776
- [9] Amor C, Marchao L, Lucas MS, Peres JA. Application of advanced oxidation processes for the treatment of recalcitrant agro-industrial wastewater: A review. *Water*. 2019;**11**:1-31
- [10] Wols BA, Hofman-caris CHM. Review of photochemical reaction constants of organic micropollutants required for UV advanced oxidation processes in water. *Water Research*. 2012;**46**:2815-2827
- [11] Shu Z, Bolton JR, Belosevic M, Gamal M, Din E. Photodegradation of emerging micropollutants using the medium-pressure UV/H₂O₂ advanced oxidation process. *Water Research*. 2013;**47**:2881-2889
- [12] Olmez-Hanci T, Arslan-Alaton I. Comparison of sulfate and hydroxyl radical based advanced oxidation of phenol. *Chemical Engineering Journal*. 2013;**224**:10-16
- [13] Gu D, Guo C, Lv J, Hou S, Zhang Y, Feng Q, et al. Removal of methamphetamine by UV-activated persulfate: Kinetics and mechanisms. *Journal of Photochemistry and Photobiology A: Chemistry*. 2019;**379**:32-38
- [14] Gao Y, Gao N, Chu W, Zhang Y, Zhang J, Yin D. UV-activated persulfate oxidation of sulfamethoxypyridazine: Kinetics, degradation pathways and impact on DBP formation during subsequent chlorination. *Chemical Engineering Journal*. 2019;**370**:706-715
- [15] Huang J, Zhang H. Mn-based catalysts for sulfate radical-based advanced oxidation processes: A review. *Environment International*. 2019;**133**:1-23
- [16] Ghime D, Ghosh P. Oxidative decolorization of a malachite green oxalate dye through the photochemical advanced oxidation processes. 2019;**21**:195-203

[17] Singh P, Shandilya P, Raizada P, Sudhaik A, Rahmani-sani A, Hosseini-bandegharai A. Review on various strategies for enhancing photocatalytic activity of graphene based nanocomposites for water purification. *Arabian Journal of Chemistry*. 2018. DOI: 10.1016/j.arabjc.2018.12.001

[18] Nan M, Jin B, Chow CWK, Saint C. Recent developments in photocatalytic water treatment technology: A review. *Water Research*. 2010;**44**:2997-3027

[19] Chen X, Dai Y, Wang X. Methods and mechanism for improvement of photocatalytic activity and stability of Ag_3PO_4 : A review. *Journal of Alloys and Compounds*. 2015;**649**:910-932

[20] Park H, Park Y, Kim W, Choi W. Surface modification of TiO_2 photocatalyst for environmental applications. *Journal of Photochemistry and Photobiology C: Photochemistry Reviews*. 2013;**15**:1-20

[21] Dedkova K, Matejova L, Matejova K, Peikertova P, Kutlakova KM, Kukutschova J. Study of the antibacterial activity of cerium doped TiO_2 photocatalysts. In: *NANOCON 2013 Proceedings, Brno, Czech Republic, EU. Vol. 10*. 2013. pp. 16-21

[22] Patil SB, Basavarajappa PS, Ganganagappa N, Jyothi MS, Raghu AV, Raghava K. Recent advances in non-metals-doped TiO_2 nanostructured photocatalysts for visible-light driven hydrogen production, CO_2 reduction and air purification. *International Journal of Hydrogen Energy*. 2019;**44**:13022-13039

Heterogeneous Catalytic Process for Wastewater Treatment

Ting Zhang

Abstract

This chapter introduced heterogeneous catalysis and described diverse heterogeneous catalytic processes for wastewater treatment. The main advantages of heterogeneous catalysis were explained compared with homogeneous catalysis. The methods of synthesis and characterization of heterogeneous catalysts with some examples were then elaborated. The principle of heterogeneous catalytic treatment process of refractory wastewater was analyzed, and several different types of heterogeneous catalytic oxidation processes, technical progresses, and application examples were presented. The mechanisms of heterogeneous catalytic oxidation degradation of pollutants in wastewater were also discussed. According to the review, the heterogeneous catalytic oxidation technology was considered having a good application prospect, and the further research directions of heterogeneous catalysis were proposed.

Keywords: heterogeneous catalysis, synthesis, characterization, wastewater treatment, refractory wastewater, catalytic oxidation processes, mechanism

1. Introduction

Water pollution, especially organics pollution, has become a global environmental problem. The severity, nature, and harm to organisms and human beings of organic pollution are continually changing with the development of society and industry. In recent years, the pollution of refractory organics and their treatment have become a hot topic to researchers all over the world. Refractory organic pollutants, such as halogenated organics, surfactants, nitro compounds, heterocyclic compounds, phenolic compounds, and polycyclic aromatic hydrocarbon, among others, with high toxicity, are difficult to be degraded by microorganisms. Many of these pollutants have toxic effects on humans and organisms, such as carcinogenic, teratogenic, and mutagenic effects. The harmfulness of refractory organic compounds has posed a severe threat to human health and ecosystems. Therefore, how to control the pollution of refractory organics has always been an important research topic in the field of environmental protection.

Researchers have conducted in-depth studies on the treatment of wastewater containing refractory organics. Refractory organics can be removed by adsorption, advanced oxidation, and membrane separation, among others (**Figure 1**). Among these technologies, advanced oxidation processes (AOPs) have made remarkable progress and achievements in the treatment of wastewater containing refractory organics. AOPs, including photochemical oxidation, catalytic wet oxidation,

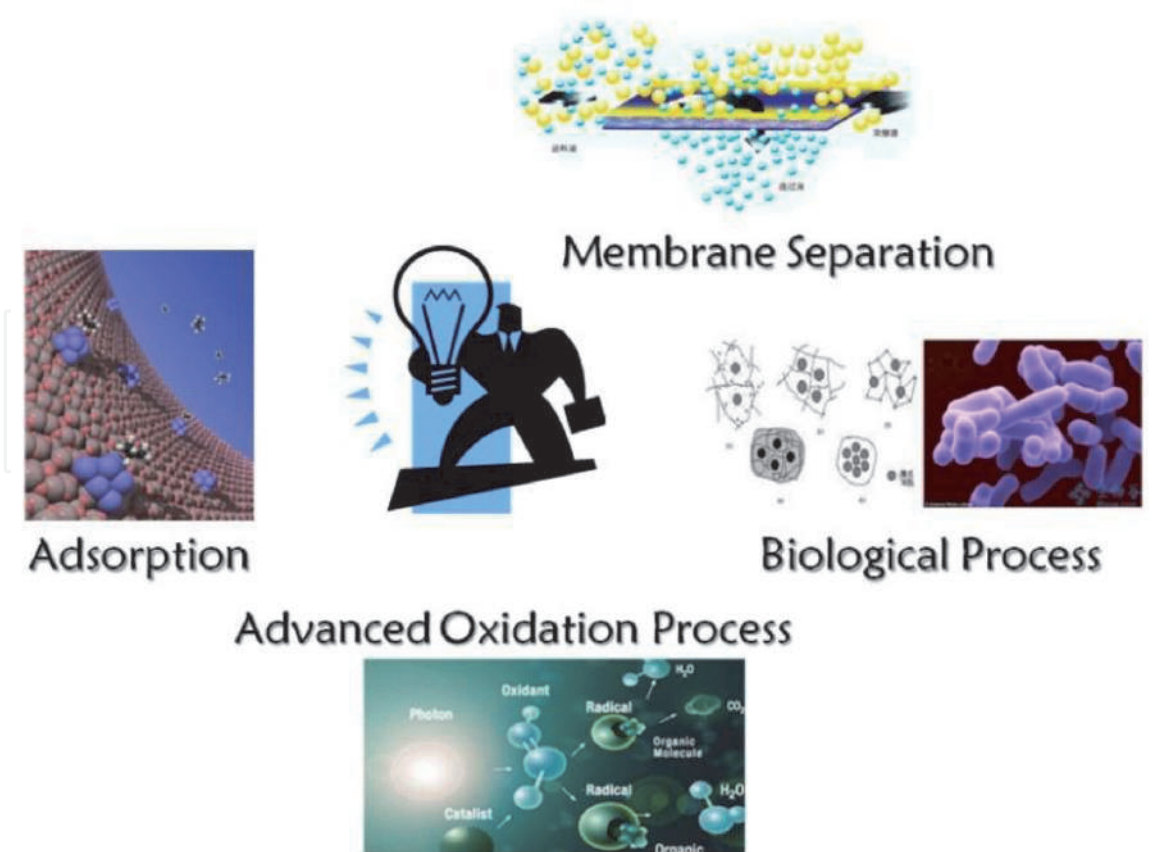


Figure 1.
Refractory organics removing methods.

sonochemical oxidation, electrochemical oxidation, and ozone oxidation, can decompose and transform toxic, harmful, and refractory macromolecular organics into nontoxic, harmless, and biodegradable small molecular organics. The final products of the oxidation are carbon dioxide, water, and inorganic ions, while no excess sludge is produced.

The catalysis term implies the process of increasing the rate of a chemical reaction by adding a catalyst, which is ultimately regenerated so that its amount remains unchanged. Catalysis is inhibited if the catalyst or the reactant is removed, or inhibitors alter the reaction. Inhibitors are materials that slow down the overall reaction by shortening the reaction chains, generally by reacting with one of the chemical components that maintain the chain and entering into a nonchain reaction. A wide variety of substances, such as phenols, sugars, and alcohols, have been found to act as inhibitors during the catalysis process.

The homogeneous catalysis occurs in a single phase, in which the catalyst is dispersed in an aqueous solution or gas mixture with the reactants. Conversely, heterogeneous catalysis occurs in more than one phase; for instance, the reactants are liquids, and the catalyst is solid [1].

AOPs' aim is to generate hydroxyl radicals ($\cdot\text{OH}$), which can oxidize most chemical species, especially hard-to-degrade organics. Hydroxyl radicals are nonselective when oxidizing organics, while their oxidation potential has been estimated as 2.8 and 1.9 V at pH 0 and 14, respectively [2].

The heterogeneous Fenton reaction has demonstrated better catalytic performance and environmentally friendly characteristics when compared with the homogeneous Fenton reaction. Although homogeneous catalysts are generally very efficient for the degradation of organic compounds, the catalysts of iron ions are dissolved in water, their separation and reuse are rather difficult at the end of treatment, and ferric ions are generated as by-products. The removal of iron ions

from the treated water needs a large number of chemicals and manpower, which will increase the cost of treatment. Another drawback is the tight range of pH in reactions of homogeneous Fenton systems. The pH of the solution in a Fenton system should be adjusted to around 3.0 before carrying out the wastewater treatment, and the reagents for acidification are very costly [3].

In this chapter, the preparation processes and characterization methods of heterogeneous catalysts, as well as treatment applications, are reviewed. This chapter aims to provide a basis for further studies on new heterogeneous catalysts for the treatment of refractory organics.

2. Heterogeneous catalysis

Many catalytic processes, in which the catalyst and the reactants are not present in the same phase, are heterogeneous catalytic reactions. They include reactions of gases (or liquids) at the surface of a solid catalyst. The surface is where reactions take place, so the catalysts are generally prepared to provide large surface areas per unit. Metals, metals coated onto supporting materials, metalloids, metallic films, and doped metals have all been used as heterogeneous catalysts.

With solid catalysts, at least two of the reactants are chemisorbed by the catalyst, and they will react at the surface of the catalyst, with which the products are formed as readily as possible. Then, the products are released from the catalyst surface, as can be seen in **Figure 2**.

Heterogeneous catalysts can be divided into two categories: unsupported catalysts (bulk catalyst) and supported catalysts. Unsupported catalysts include metal oxide catalysts, such as Al_2O_3 , SiO_2 , and B_2O_3 , and zeolite molecular sieve catalysts, such as ZSM-5, X, Y, and B types of zeolite. Supported catalysts often employ porous materials as supporters, and active components, metals or metal oxides, for example, are coated on the surface of the supporters to form the catalysts. Heterogeneous catalysts can accelerate many chemical processes, including CO oxidation, selective oxidation, water-gas shift, selective hydrogenation, electrocatalysis, photocatalysis, organic reactions, deNO_x , and reforming reactions, among others, as shown in **Figure 3**.

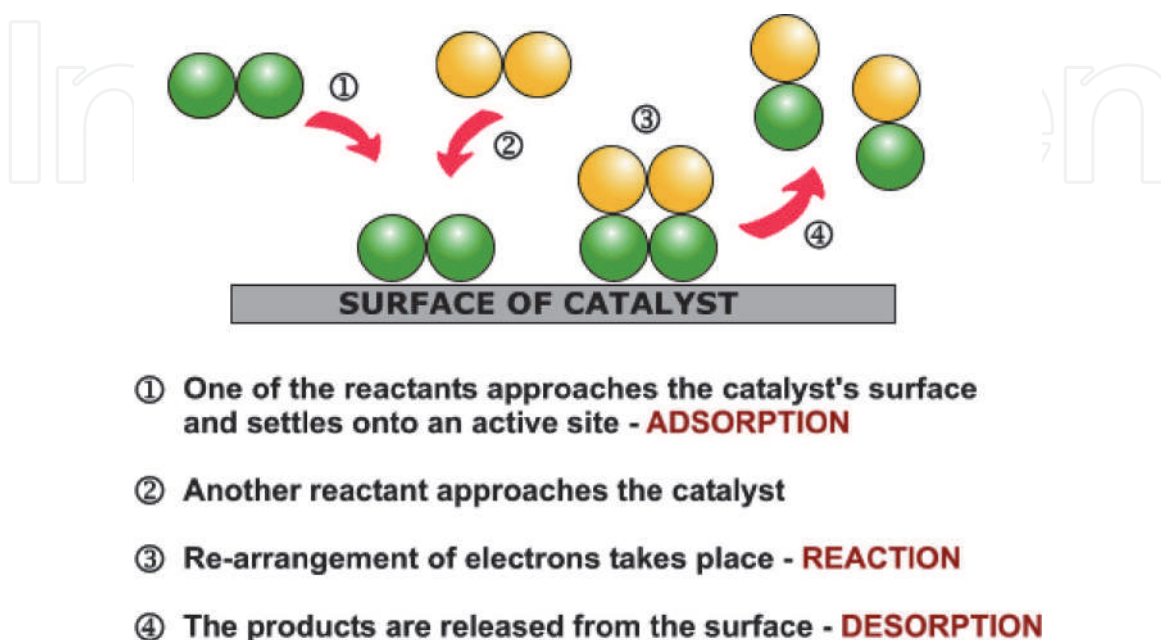


Figure 2.
Catalytic processes on a solid catalyst.

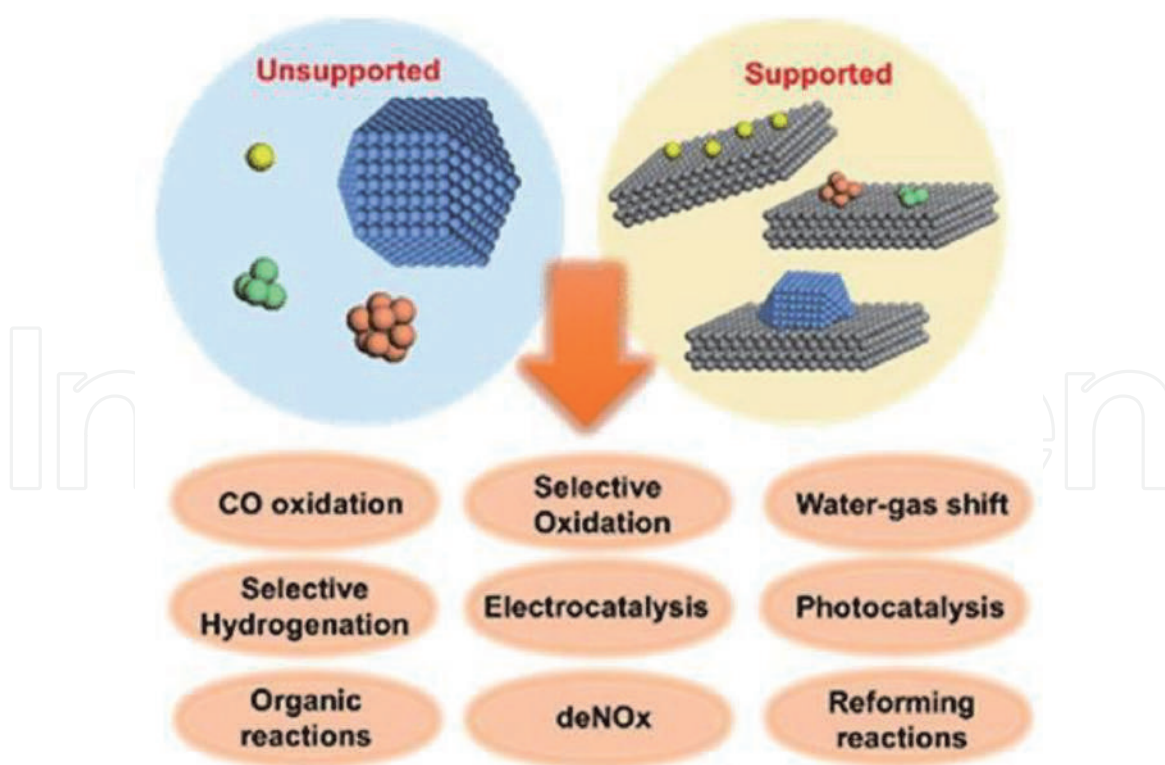


Figure 3.
Types of heterogeneous catalysts and their usages.

The heterogeneous catalytic process, as an efficient green method coping with organic wastewater, has attracted considerable attention in the last two decades. The highly reactive and nonselective hydroxyl radicals can oxidize and mineralize most organic compounds at near diffusion-limited rates, mainly unsaturated organic compounds.

3. Synthesis and characterization of heterogeneous catalysts

Catalysis is a surface phenomenon occurring on the surface or interface; in order for the catalyst to have more active sites, it is necessary to maximize its surface area, that is, to increase the porosity of solid catalysts. There are two ways to increase porosity. First, if the solid catalyst is composed of nonporous crystals, the catalyst should be prepared with the smallest grain size (i.e., to increase its external surface area). Second, if the solid catalyst is composed of grains with regular channels, the catalyst should be prepared by particles with regular channels (i.e., to increase its internal surface area). **Figure 4** shows the schematic of various catalyst development strategies, which aim to increase the number of active sites or increase the intrinsic activity of each active site.

To characterize heterogeneous catalysts, BET surface area, scanning electron microscope (SEM), transmission electron microscope (TEM), Fourier transform infrared spectroscopy (FT-IR), and X-ray diffraction (XRD) are commonly used characterizing methods.

The specific surface areas and pore volumes of the samples are often determined by physisorption of nitrogen at -196°C using a Micromeritics ASAP instrument. The specific surface area is calculated using the BET method and pore size distribution was obtained by using the BJH method.

A field-emission scanning electron microscope is utilized to determine the crystal morphology and chemical element composition. Measurements are made with

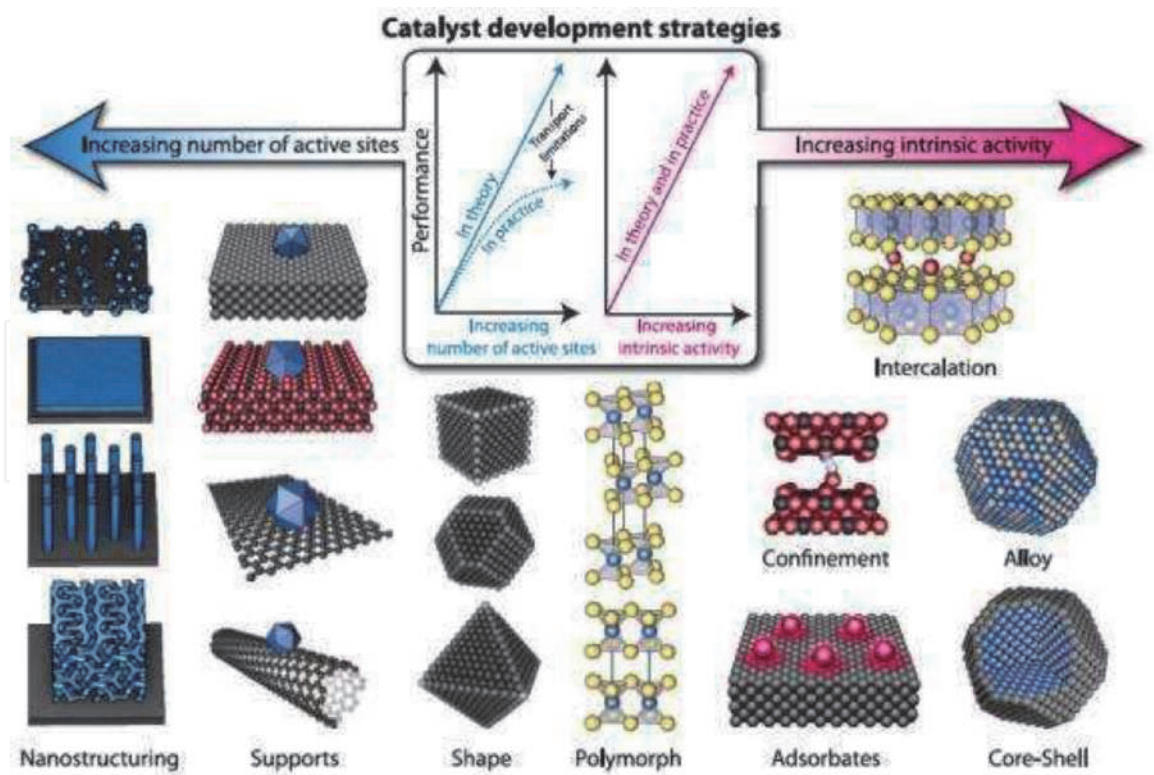


Figure 4.
Catalyst development strategies.

SEM using a digital imaging processing at room temperature and acceleration voltage of 20 kV. The samples are usually prepared as electrically conductive by sputter coating with a thin layer of gold under vacuum conditions to avoid charge accumulations of nonmetal catalysts, and all samples are dispersed in ethanol before tests.

A transmission electron microscopy is utilized to observe and analyze the micromorphology and microstructure. FT-IR spectroscopy is used to confirm the chemical structure, any changes in the compositional or functional group during the preparation of catalysts. Measurements are made on a FT-IR spectrometer after samples are mixed with 300 mg of spectroscopic grade KBr and ground in an agate mortaring in the range of $4000\text{--}400\text{ cm}^{-1}$ at room temperature.

To investigate the crystalline structure and stability of catalyst composites, powder X-ray diffraction patterns are recorded by X-ray diffractometer using $\text{Cu } K_{\alpha}$ radiation ($\lambda = 0.1542\text{ nm}$) at a rate of $0.02^{\circ}/\text{s}$ in the range of $5\text{--}80^{\circ}$ with an operating voltage of 40 kV and electric current of 150 mA.

If the catalysts contain metals, XPS (X-ray photoelectron spectroscopy) of the samples are often tested. XPS was used to identify metal oxidation states of the composites.

3.1 Bulk catalysts

Bulk catalyst refers to the whole catalyst particle, its external surface, and internal components, where almost all of them are active substances. Some examples of bulk catalysts are silica-aluminum catalysts for catalytic cracking and ammonia synthesis, zinc-chromium oxide or copper-zinc-aluminum catalysts for hydrogen production, and iron molybdate catalysts for methanol oxidation [4–7]. The main chemical processes for the preparation of such catalysts are precipitation, gelation, and crystallization. **Figure 5** shows the synthesis processes of bulk catalysts.

$\text{LiFe}(\text{WO}_4)_2$ catalyst for decolorization of methylene blue is an example of bulk catalysts. $\text{LiFe}(\text{WO}_4)_2$ particles are prepared using solid-state reactions. The

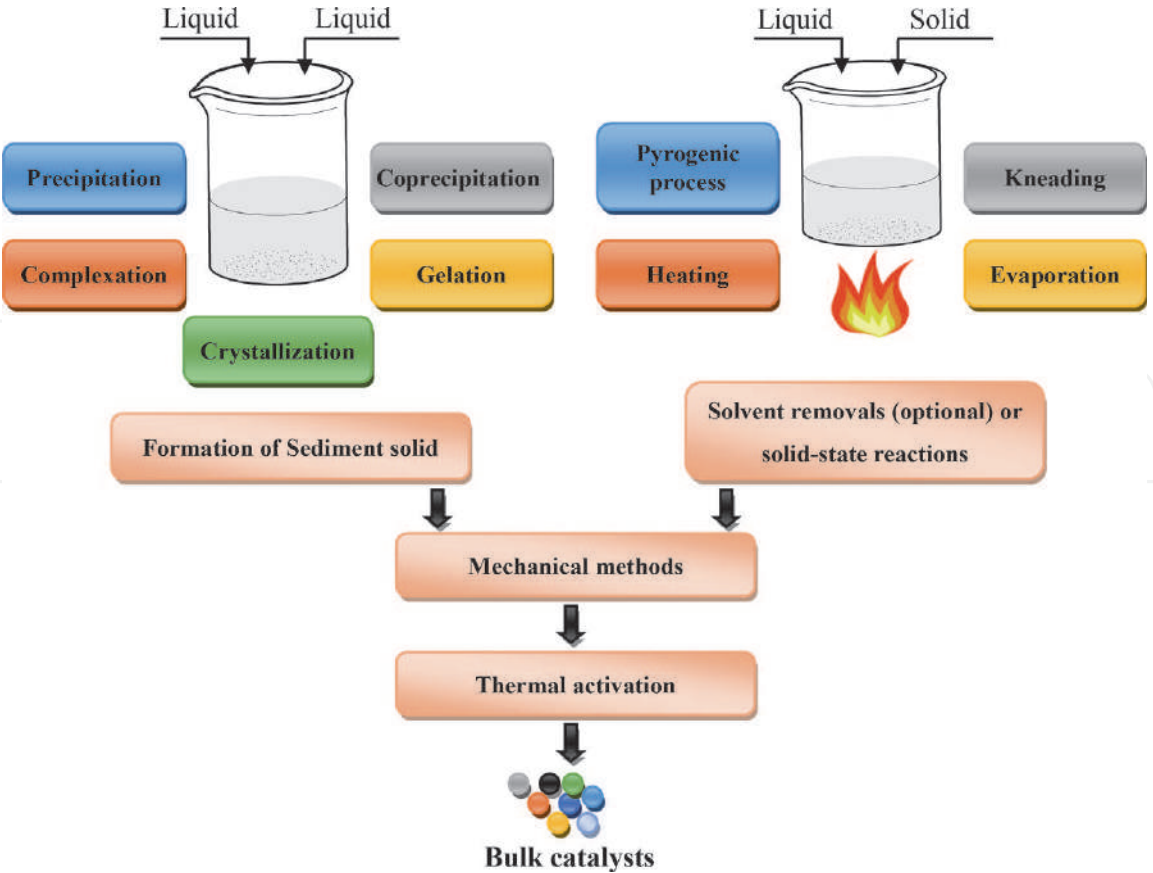


Figure 5.
Synthesis process of bulk catalysts.

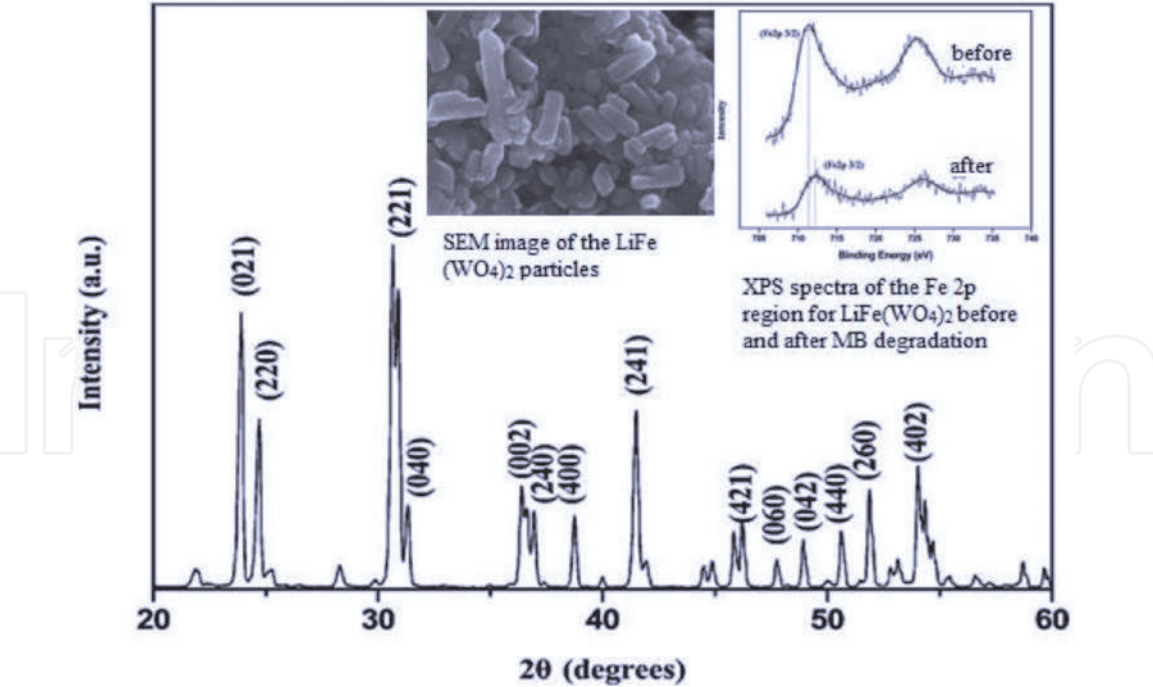


Figure 6.
Characterizations of $\text{LiFe}(\text{WO}_4)_2$ catalyst [8].

powders, consisting of Li_2CO_3 , Fe_2O_3 , and WO_3 with a molar ratio of 1:1:4, are mixed uniformly in a glass mortar. Then, the mixture is mechanically milled with hydrous ethanol as a lubricating agent. Afterwards, the powders are dried to remove the ethanol. Finally, the powder is calcined and yields well-crystallized $\text{LiFe}(\text{WO}_4)_2$ [8].

The characterizations of $\text{LiFe}(\text{WO}_4)_2$ can be seen in **Figure 6** [8]. The XRD patterns of the $\text{LiFe}(\text{WO}_4)_2$ show that the peaks of the sample match well with the published standard data (PDF 01-072-0751), and $\text{LiFe}(\text{WO}_4)_2$ has a highly crystalline and single-phase structure, without any peaks of unreacted precursors. The morphological characteristic of the $\text{LiFe}(\text{WO}_4)_2$ particles shows that the $\text{LiFe}(\text{WO}_4)_2$ crystal was rod-like, that the average length of the samples varied over the range of 300–500 nm, and that the width of the sample was about 200 nm. XPS spectra show that the binding energy of 711.94 eV belongs to $\text{Fe}2p_{3/2}$. The binding energy value slightly decreased after 1 h reaction of MB decolorization due to the transformation of $\text{Fe}(\text{III})$ to $\text{Fe}(\text{II})$ after heterogeneous photo-Fenton reaction [8].

3.2 Supported catalysts

Supported catalysts are the most often used catalysts in wastewater treatment processes. They include the surface-loaded catalysts, core-shell catalysts, and thin-film catalysts.

3.2.1 The active catalytic components loaded onto the carrier surface

Surface-loaded catalysts mean active catalytic components loaded onto the carrier, which can be divided into two categories: one is concentrating the active components to the surface of porous solid carriers by means of dipping the carriers into the precursor contained ions or molecules and the other is that the predecessors or catalyst solid particles are adhered or deposited to the surface of the carrier, such as sol-gel method.

Carriers are inorganic porous materials, such as alumina, silicon oxide, activated carbon, zeolite, molecular sieve, and clays, among others. Commonly used catalyst carriers' structure data are shown in **Table 1**.

The most important supported catalysts are metal- or oxide-supported catalysts. Metal precursors are usually metal salts, such as nitrates, carbonates, sulfates, and chlorides. These salts are also the raw materials for preparing metal oxide supporters and bulk catalysts. When they dissolve in water, they will be dissociated into ions, and metal ions will further form hydrated ions. If the catalyst supporters are added to these metal salt solutions, the active components can be loaded onto the supporters by impregnation or sol-gel methods, thereby obtaining heterogeneous catalysts. **Figures 7** and **8** are typical processes of impregnation and sol-gel methods for heterogeneous catalyst synthesis.

Carriers		Specific surface area/(m^2/g)	Pore volume/(mL/g)
Oxide	Al_2O_3	200~500	0.3~0.9
	SiO_2	400~800	0.4~4.0
	$\text{SiO}_2\text{-Al}_2\text{O}_3$	400~600	0.5~0.9
	MgO	30~140	0.3
Carbon	Activated carbon	~1000	0.3~2.0
Clay	Bentonite	150~280	0.3~0.5
	Attapulgate	100~200	0.3~0.5

Table 1.
Structure data of commonly used catalyst carriers.

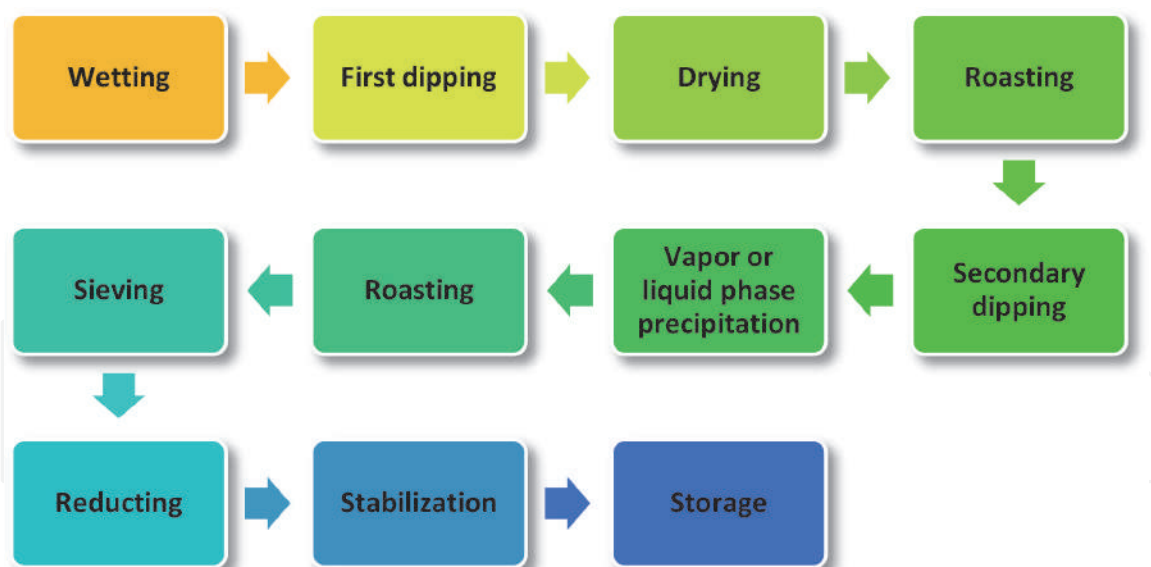


Figure 7.
Typical process of impregnation for heterogeneous catalyst synthesis.

3.2.1.1 Carbon-based catalysts

Carbon is often used as a catalyst supporter due to its large surface area and porous structure. There are many types of carbon: activated carbon, activated carbon fiber, mesoporous carbon, and multiwalled carbon nanotubes, among others. Here are some examples of carbon supporters for heterogeneous catalysts.

Ordered mesoporous carbon-supported iron catalysts (Fe/OMC) were prepared by the incipient wetness impregnation method [9]. OMC was prepared by triconstituent coassembly of resols, oligomer silicates from TEOS, and triblock copolymer F127 template, followed by carbonization and silica removal. The OMC was impregnated in an iron nitrate solution; then, the catalyst was dried, followed by calcination under N_2 flow.

Characterizations of Fe/OMC are shown in **Figure 9** [9]. From the XRD patterns, all of the samples show a broad peak at 23.5° corresponding to amorphous carbon. The crystallinity of iron oxides is improved with the increase of calcination temperature. TEM images showed a highly ordered array in the structure of OMC and Fe/OMC catalysts, which suggests the preservation of the long ordered arrangement of the channels after the iron deposition. The iron oxide particles are not clearly seen in the TEM image at a low calcination temperature of the samples, as the calcination temperature increases, the iron particles become more prominent and are revealed in the TEM images. The iron particles are well dispersed from the TEM pictures [9].

Fe_3O_4 /multiwalled carbon nanotubes (MWCNTs) were synthesized by in situ chemical oxidation coprecipitation. MWCNTs were pretreated by stirring in a flask, containing a mixture of sulfuric acid/nitric acid and refluxing in an ultrasound wave cleaner. The as-treated MWCNTs were suspended in deionized water and put into a $95^\circ C$ water bath. $FeSO_4 \cdot 7H_2O$ was added into the MWCNT suspended solution and NaOH and $NaNO_3$ solution was added dropwise, which is heated up to $95^\circ C$ into the heating MWCNT-metal solution with vigorous stirring as well as stable N_2 flow during the entire reaction period. After 2 hours, the Fe_3O_4 /MWCNT nanocomposites were formed [10].

Characterizations of Fe_3O_4 /MWCNTs are shown in **Figure 10** [10]. The TEM images show the octahedron Fe_3O_4 nanoparticles with diameters ranging from 40 to 100 nm growing on the MWCNTs surface regularly and most of the Fe_3O_4 nanoparticles were strung by MWCNTs. The room-temperature Raman spectra

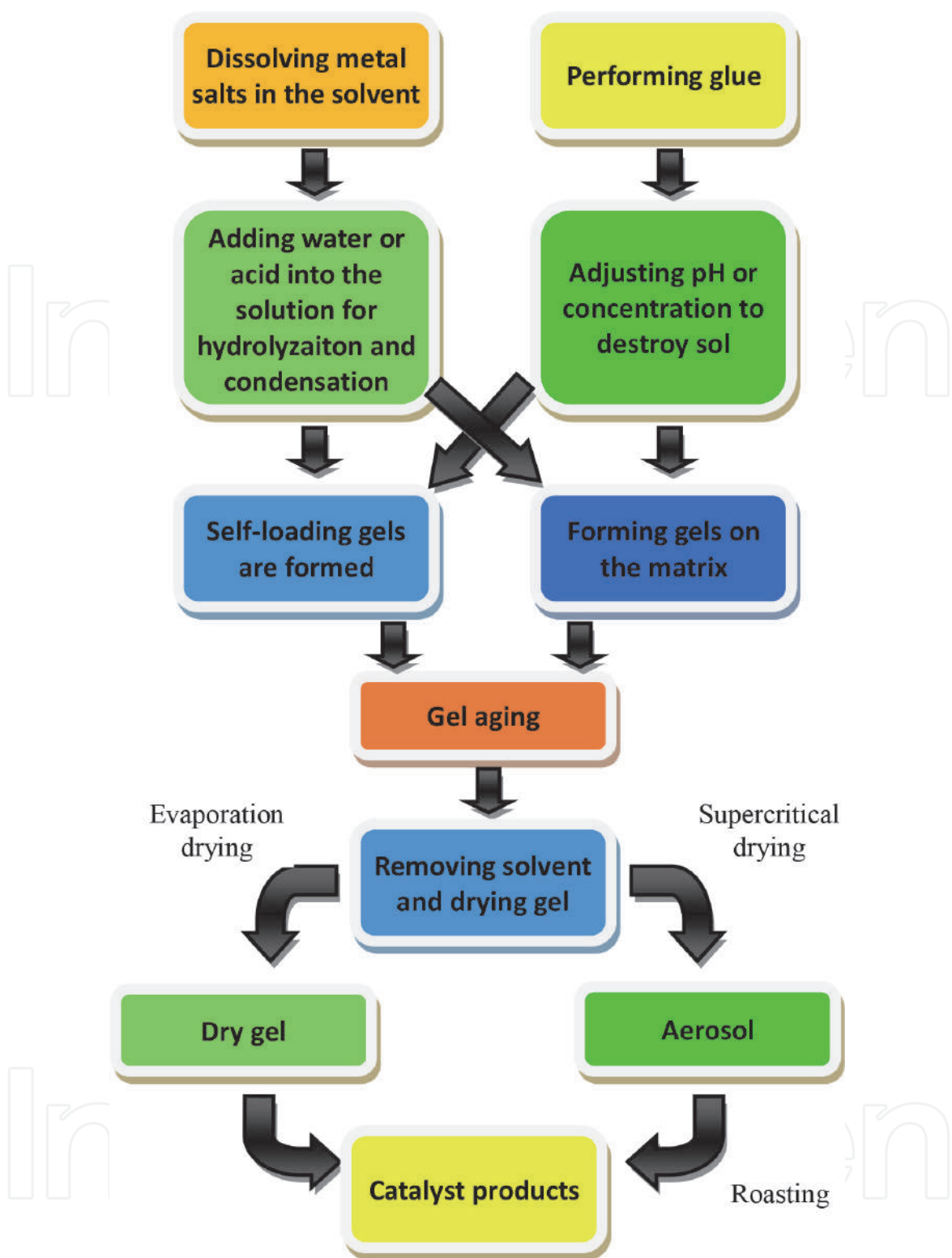


Figure 8.
Typical process of the sol-gel method for heterogeneous catalyst synthesis.

show a difference in the crystallinity of MWCNTs before and after the Fe_3O_4 loading process. Some extra peaks were observed at lower wave numbers corresponding to vibration modes of Fe–O bonds of Fe_3O_4 nanoparticles, and Fe–C bonds confirm the formation of Fe_3O_4 nanoparticles on the surface of MWNTs [10].

3.2.1.2 Oxide-based catalysts

Recently, metal-containing oxide-based (mesoporous silica, Al_2O_3 , and ZnO , among others) catalysts have attracted much attention because the oxide-based

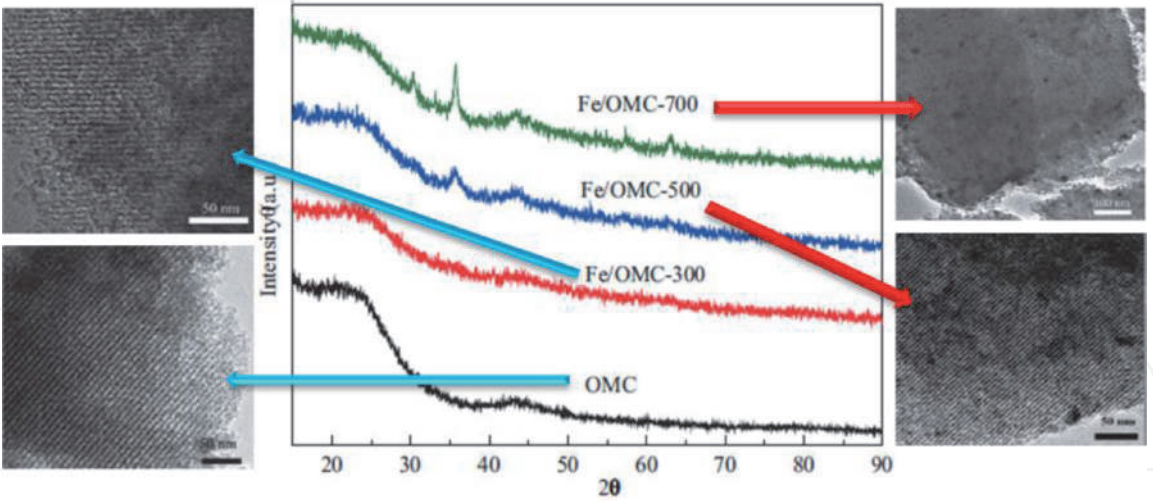


Figure 9.
Characterizations of Fe/OMC [9].

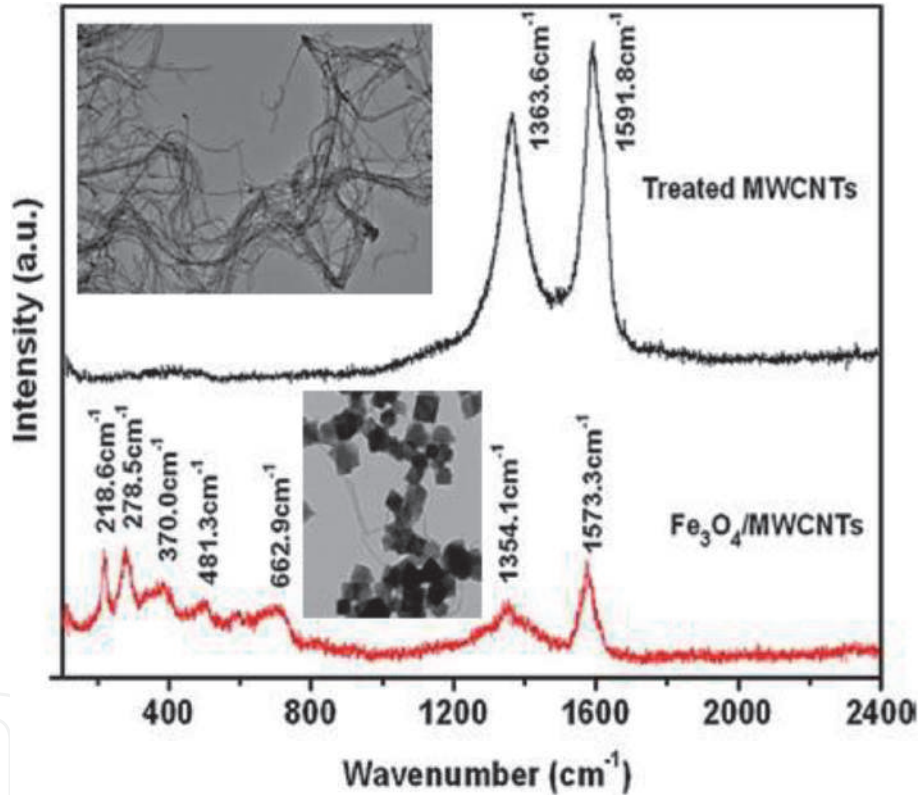


Figure 10.
Characterizations of $\text{Fe}_3\text{O}_4/\text{MWCNTs}$ [10].

materials have a high surface area, good thermal stability, and favorable hydrothermal stability. Numerous oxide-based composites were synthesized for degrading organic compounds such as methyl orange, acid orange, polyarylamide, and phenol [11–16].

The porous $\text{Fe}_2\text{O}_3\cdot\text{SiO}_2$ composite was prepared by a facile impregnation method [17]. Typically, silica powder was immersed in $\text{Fe}(\text{NO}_3)_3$ and the mixture was vigorously stirred for 24 h at room temperature; then, the sample was dried and calcined. The obtained powder was cooled to room temperature to get as-synthesized $\text{Fe}_2\text{O}_3\cdot\text{SiO}_2$ for catalytic experiments.

Characterizations of $\text{Fe}_2\text{O}_3\cdot\text{SiO}_2$ are shown in paper [17]; those figures present the FE-SEM and TEM images, EDS spectrum and EDS mapping image, XRD

patterns, N_2 adsorption/desorption isotherms, and FT-IR spectra of as-synthesized $Fe_2O_3 \cdot SiO_2$ and as-synthesized SiO_2 . As shown in SEM images, silica is like light clouds and showed an aggregate shape, while the as-synthesized $Fe_2O_3 \cdot SiO_2$ seems to become darker and denser after iron-loading, and $Fe_2O_3 \cdot SiO_2$ composite exhibited higher aggregation than silica due to impregnation and calcination processes, as can be seen in TEM images. Both samples were a bulk shape, which consisted of many small particles, approximately 10–20 nm in size. In TEM images, the iron oxide nanoparticles with about 5 nm in size were well dispersed on silica particles, while the iron oxide was not clearly distinguished from the silica in SEM images. The elemental composition of $Fe_2O_3 \cdot SiO_2$ composite from EDS stated that the composite contained 8.1 wt.% Fe and showed the dispersion of Fe on the surface of SiO_2 . The wide-angle XRD diffractions of SiO_2 and $Fe_2O_3 \cdot SiO_2$ composite showed that the diffraction peak of 20.1° belongs to amorphous silica, and the diffraction peaks at 21.8 , 25.0 , 35.39 , and 49.3° belong to α - Fe_2O_3 . The broad and low-intensity peaks of Fe_2O_3 could result from low loading deposition level, well dispersion, and poor crystalline structure with a small size of metal oxide particles in the composite. According to the N_2 adsorption/desorption isotherms of as-synthesized SiO_2 and as-synthesized $Fe_2O_3 \cdot SiO_2$ and IUPAC classification, both samples clearly showed a type II with an H1 hysteresis loop indicating material with agglomerates or compacts of approximately uniform spheres. The FT-IR spectra of the sample showed the small bands found at 685 and 604 cm^{-1} could be assigned to stretching vibrations of Fe-O and Si-O-Fe, respectively, which confirmed that SiO_2 indeed binds with Fe_2O_3 [17].

3.2.1.3 Clay-based catalysts

Clays such as montmorillonite, kaolin, and bentonite [18–20] are often employed as supporters in the use of heterogeneous catalysts, in order to lower the treatment cost of wastewater. Among the perspective clays, attapulgite clay is also a promising choice. Attapulgite clay is a kind of clay mineral with attapulgite as its main component. It is a crystalline hydrated magnesium aluminum silicate mineral with a unique layer-chain structure. Due to its particular structure, attapulgite has various excellent properties, such as good adsorption and catalytic properties [21–23]. Some examples of ATP for catalyst supporters are as below.

The first example is the preparation of the Fe_3O_4 /ATP catalyst [24]. ATP clay was mixed with water evenly and aged 24 h at room temperature. The aged ATP was granulated to microparticle and dried and then roasted. Spherical ATP particles were put into the mixture solution of thoroughly mixed oleylamine (or ethanol), and n-hexane was added with $Fe(acac)_3$ and immersed for a particular time in an ultrasonic instrument. After separating ATP particles from the mixture solution, they were dried at a vacuum drying oven and then the particles were put in a muffle furnace and roasted without air. Thus, the particle heterogeneous catalyst Fe_3O_4 /ATP was obtained. The process of preparing the Fe_3O_4 /ATP catalyst can be seen in **Figure 11**.

The characterizations of Fe_3O_4 /ATP are shown in **Figure 12**. Rod-shaped particles with lengths of 500~700 nm and widths of 100~150 nm are visible in SEM micrographs. After the introduction of iron species into ATP, nano- Fe_3O_4 particles were coated evenly onto the surface of ATP. TEM micrographs confirmed that the Fe_3O_4 nanoparticles with an average diameter of 10~25 nm stuck to the attapulgite rod-like fibers. The FT-IR results of Fe_3O_4 /ATP show some peaks at lower wave numbers (480 and 565 cm^{-1}) corresponding to vibration modes of Fe-O bonds of Fe_3O_4 nanoparticles on the surface of ATP. XRD patterns of Fe_3O_4 /ATP are contrasted with those of ATP. Sample Fe_3O_4 /ATP showed the characteristic peaks

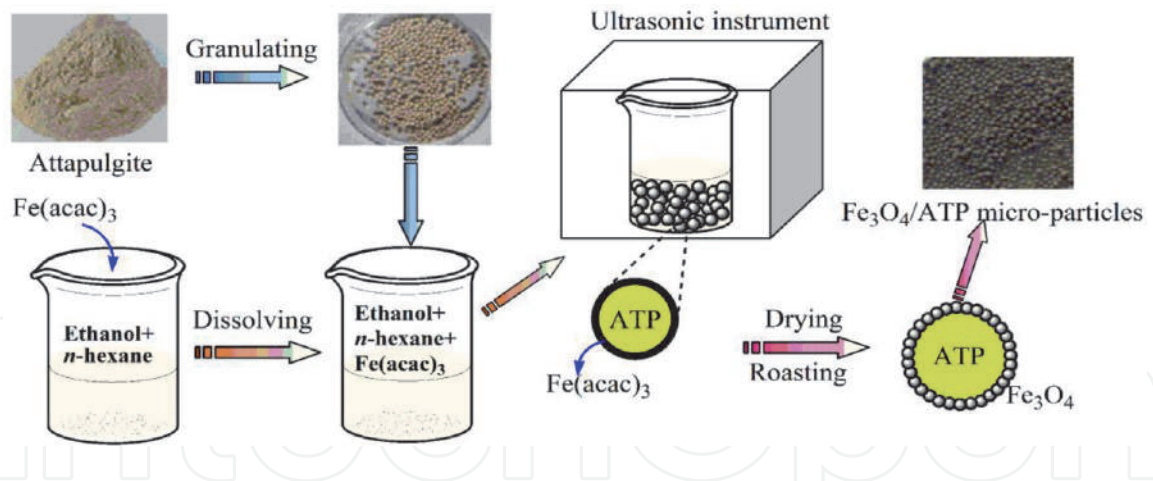


Figure 11.
Schematic of preparing Fe₃O₄/ATP catalyst [24].

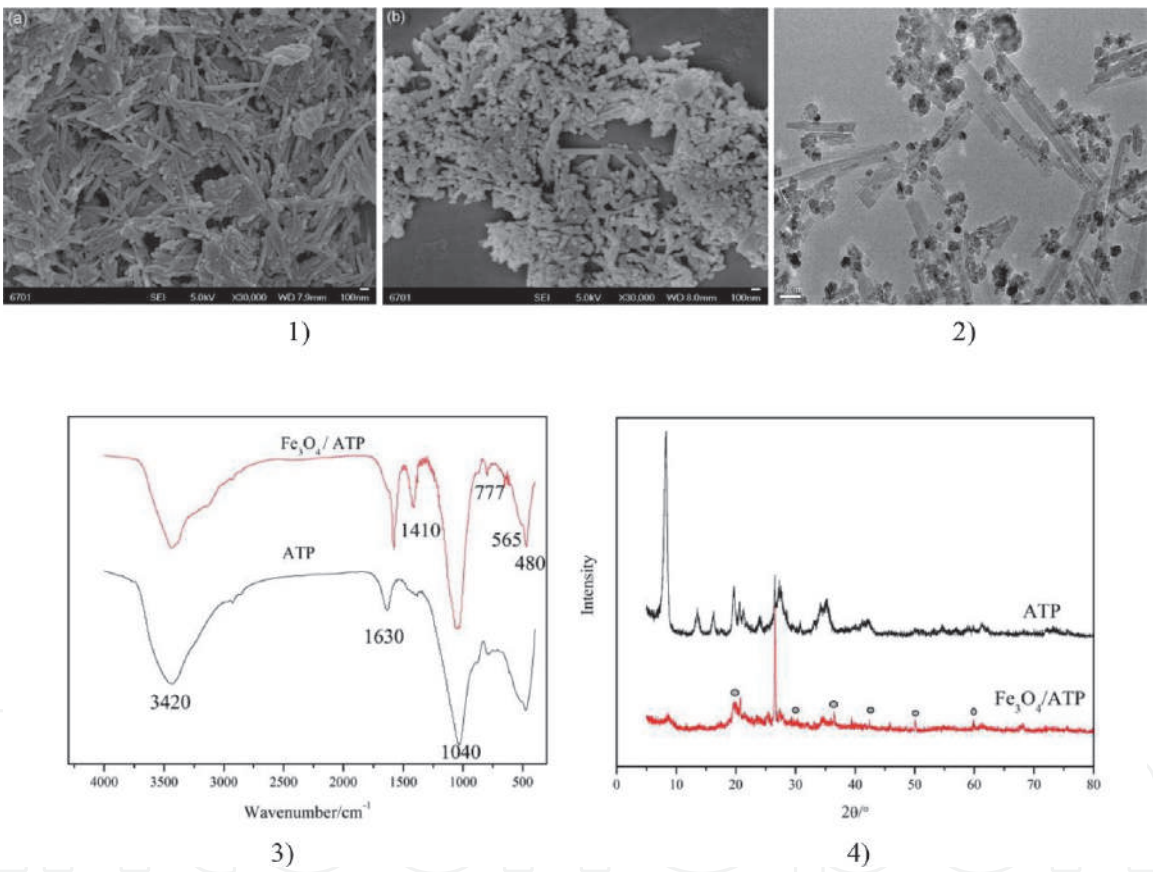


Figure 12.
Characterizations of Fe₃O₄/ATP [24]. (1) SEM micrographs of samples (a) ATP, (b) Fe₃O₄/ATP. (2) TEM micrographs of Fe₃O₄/ATP. (3) FT-IR spectra of samples. (4) XRD patterns of samples.

(5.3, 8.4, 19.7, 27.5, 34.6, and 42.6°) of cubic spinel structure known from bulk Fe₃O₄ phase [24].

Some researchers organo-modified attapulgite to make it have a larger surface area and more pores. Fe/OATP is a kind of catalyst for HA-Na degradation, which employed organo-modified attapulgite as a supporter [25]. Attapulgite (ATP) was firstly acidified with 1 mol/L of HCl solution, then washed with distilled water three times, and dried. Octadecyl trimethyl ammonium chloride (OTAC) was weighed according to a particular proportion and dissolved in distilled water. Then acidified ATP was added into the OTAC solution at 60°C. The mixture was stirred and treated in an ultrasonic instrument for 15 minutes. After that, the clay was washed

with distilled water three times and dried in vacuum to obtain the organo-modified attapulgite (OATP). OATP and FeSO_4 were put into a beaker containing distilled water and stirred continuously. Sodium borohydride (NaBH_4) was slowly put into the beaker and stirred continuously. A large number of black floccules were produced. They were filtered and washed with ethanol for at least three times and dried in a vacuum drying oven to obtain the catalyst Fe/OATP . The synthesis process of Fe/OATP can be seen in **Figure 13**.

Characterizations of Fe/OATP are shown in **Figure 14** [25]. From SEM images, we can see that the length of the rod crystal had not changed after modification, but the layered structure, the surface area, and pore volume of the particles increase significantly, which means that the organic modification successfully enlarges the specific surface area of the ATP particles. After introducing nano-Fe into modified ATP particles (OATP), the spherical material with a diameter of about 80 nm is loaded on the rod structure of OATP, which showed that the nanoiron was loaded on the structure of OATP successfully. Some peaks, observed at 2923 and 2850 cm^{-1} in FT-IR curves of OATP and Fe/OATP samples, are symmetric stretching vibration peaks of $-\text{CH}_3$ and $-\text{CH}_2$, respectively. These peaks indicate that organics successfully modify attapulgite clay. After introducing the Fe species, the peaks at 2923 and 2850 cm^{-1} become weak. The strong peaks at 5.3 , 19.7 , 34.6 , 35.2 , 42.6 , and 78.7° could be found in the XRD patterns of all these three samples, which means the crystal structure of ATP has not been broken during the process of modification or preparation. The characteristic peaks at 50.4 , 61.9 , and 73.14° shown in the sample of Fe/OATP indicate that Fe^0 was successfully located on the clay structure [25].

3.2.2 Core-shell structured catalysts

In recent years, the preparation and application of core-shell structured materials have attracted extensive attention [26–28]. The catalysts compounded with the core-shell structure often exhibit high overall activity, large specific surface area, excellent shape-selective catalytic effect, and good thermal stability in catalytic reactions [29, 30]. The existence of shell layers not only provides available active

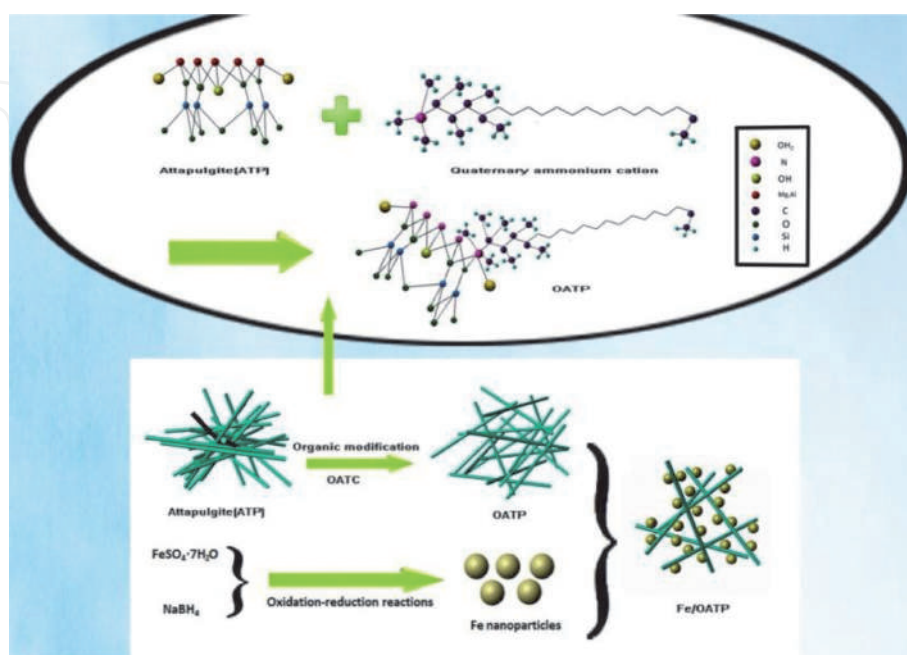


Figure 13.
Synthesis process of Fe/OATP [25].

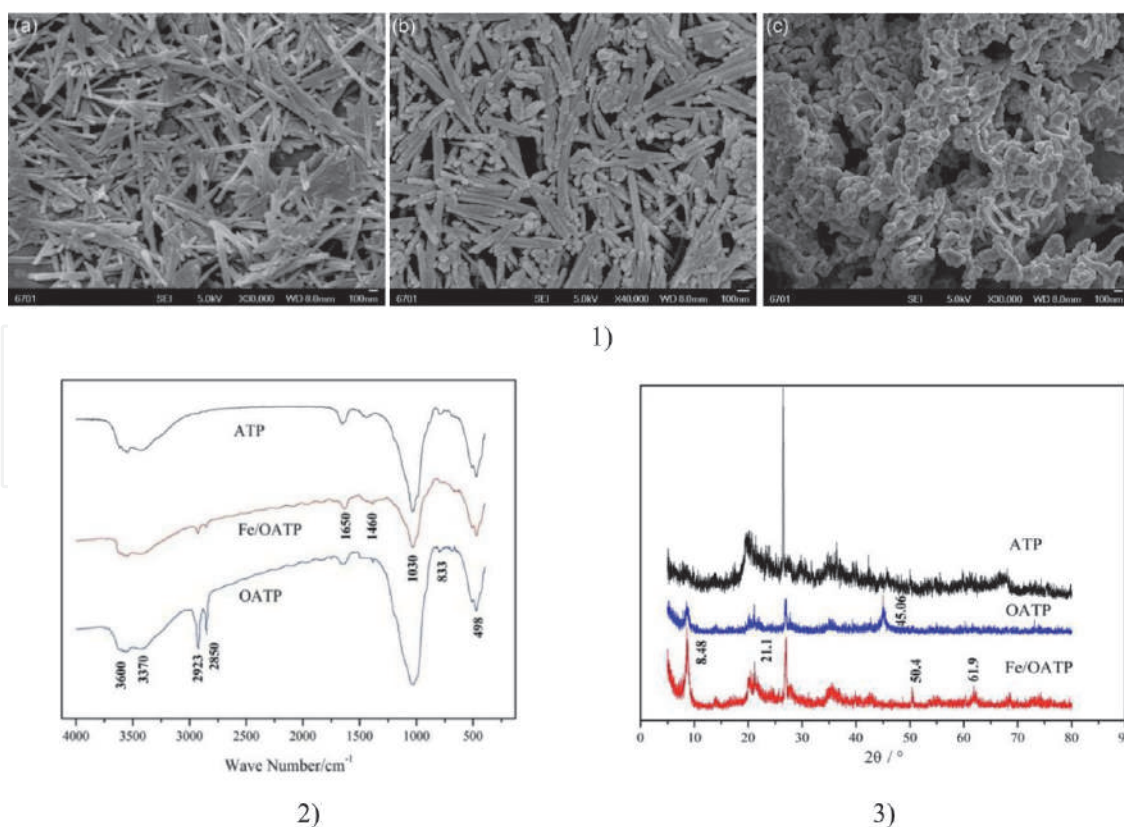


Figure 14.

Characterizations of Fe/OATP [25] (1) SEM images of the samples (a) ATP (b) OATP (c) Fe/OATP. (2) FT-IR spectroscopies of the samples (ATP, OATP, and Fe/OATP). (3) XRD patterns of the samples (ATP, OATP, and Fe/OATP).

sites for catalytic reactions but also protects for the core to avoid the collapse or sintering of the core catalyst structure leading to deactivation [31, 32].

Moreover, by selecting the chemical compositions of the core and shell, several inorganic substances with different characteristics can be incorporated into core-shell structure catalysts by appropriate methods, so that it can reach the goals of dual-function catalysis or even multifunction catalysis that single-component catalysts cannot achieve. It dramatically simplifies the experimental steps and saves precious time for researchers. Therefore, core-shell catalysts play an increasingly important role in the field of catalysis [33, 34]. The core-shell catalysts can comprise solid cores (such as inorganic, metal, or metal oxides) coated with polymers, inorganics, metal, or metal oxides [35–37]. The shell material can change the functionality, reactivity, and charge of the core surface, and also can strengthen the dispersibility and stability of the colloidal core. Catalytic or magnetic functions may be easily imparted to the colloidal core matter, depending on the coating materials. Metal oxides and zeolites are often used supporters of core-shell structured catalysts.

Ag@Fe₂O₃ core-shell structured catalysts were prepared using a homogeneous deposition precipitation method [38]. The core of silver colloids was first synthesized through a chemical reduction method using reagent grade silver nitrate as a precursor, NaBH₄, as the reducing agent and polyvinylpyrrolidone as the protecting agent. Then, an aqueous solution of urea and variable quantities of Fe₂(SO₄)₃·7H₂O were added to the solution of silver colloids. The mixture was heated for 1 h and then cooled to room temperature. The precipitate was washed thoroughly with warm water to remove as much sulfate ions as possible and then separated by centrifugation. At last, the product was dried. As shown in **Figure 15**, silver colloids

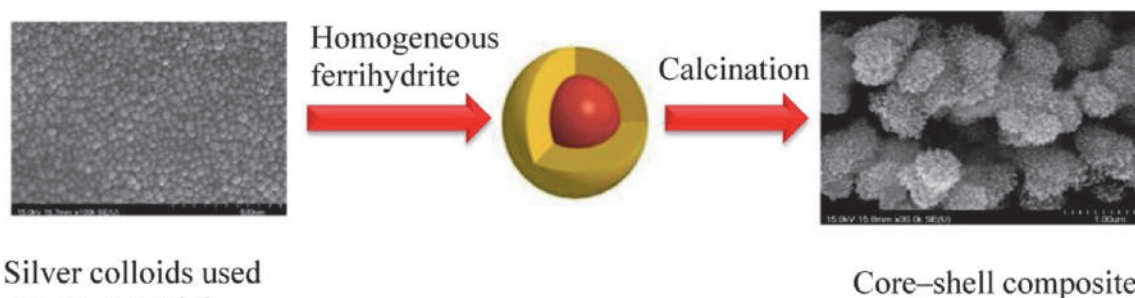


Figure 15.
Formation of $\text{Ag@Fe}_2\text{O}_3$ core-shell composite [38].

with about 40–50 nm in diameter were used as cores and the homogeneous ferrihydrite was used as shell. After being calcined, the rice-shaped $\text{Ag@Fe}_2\text{O}_3$ was formed, and the diameter and length of the $\text{Ag@Fe}_2\text{O}_3$ core-shell composite were about 10 and 20 nm, respectively. The calcined core-shell composites were aggregated with the size of 300–500 nm, which showed the porous nature of the $\text{Ag@Fe}_2\text{O}_3$ core-shell composite for catalytic reactions [38].

3.2.3 Thin-film catalysts

Thin films are a reliable and potential way of structuring the materials with tunable properties and flexible device construction in the field of energy and environment. It has gained technological importance as it helps to miniaturize the devices. Thin films are mostly modification methods to change the physical structure of materials. For example, the desired photocatalytic materials can be grown into thin films through the process of depositing molecular phase materials onto a substrate to form a solid material. The deposited thin films also can be grown along with the substrate and peeled off from the substrate and utilized as free-standing thin films. Thin-film catalysts have the potential to be used in the industries because synthesis processes of thin-film catalysts are simple in the handling of catalytic materials in several aspects such as their convenient design, adaptable form for the reactors, recyclability, recovery, etc. Therefore, the design of catalytic thin-film catalysts would be ideal for their wide applications.

Thin-film catalysts with good quality could be obtained by two methods: chemical depositions and physical depositions. Thin-film catalysts may consist of a layer and the substrate where the films are deposited on it, or consist of multiple layers. The following table shows different methods of thin-film deposition (**Table 2**) [40].

Thin-film catalysts can be used for hydrogen generation, photocatalytic CO_2 reduction to valuable chemicals, water treatment of toxic organic dyes, and bacterial disinfection. **Table 3** shows some examples of thin-film catalysts for water treatment.

For instance, Islam et al. have prepared zinc oxide (ZnO) and aluminum-doped zinc oxide (AZO) thin films onto a microscopic glass substrate using the sol-gel dip-coating technique at room temperature [49]. For both doped and undoped ZnO thin films, precursor solutions were prepared by dissolving $[\text{Zn}(\text{CH}_3\text{COO})_2 \cdot 2\text{H}_2\text{O}]$ in ethanol followed by stirring for 1 h; then, DEA was added as a stabilizer and water was added for hydrolysis. The resultant solution was stirred at room temperature for two more hours to obtain a clear and homogeneous sol. For AZO film, sols with different concentration of Al was prepared by dissolving an appropriate amount of $[\text{AlCl}_3 \cdot 6\text{H}_2\text{O}]$ and $[\text{Zn}(\text{CH}_3\text{COO})_2 \cdot 2\text{H}_2\text{O}]$ in ethanol. In both cases, the precursor solution was deposited on clean glass substrates by the dip-coating technique. The dip-coated thin films were dried at room temperature

Physical deposition	Evaporation techniques	Vacuum thermal evaporation
		Electron beam evaporation
		Laser beam evaporation
		Arc evaporation
	Sputtering techniques	Direct current sputtering
		Radiofrequency sputtering
Chemical deposition	Sol-gel technique	
	Chemical bath deposition	
	Spray pyrolysis technique	
	Plating	Electroplating technique
		Electroless deposition
	Chemical vapor deposition (CVD)	Low pressure chemical vapor deposition (LPCVD)
		Plasma-enhanced chemical vapor deposition (PECVD)
		Atomic layer deposition (ALD)

Table 2.
Different methods of thin-film deposition [39].

Thin films	Applications	Reference
TiO ₂ -anatase films	Trichloroethylene degradation	[41]
Au-buffered TiO ₂ thin films	Methylene blue degradation	[42, 43]
TiO ₂ /SiO _x	Dye degradation	[44]
ZnO thin films	Methylene blue degradation	
ZnO deposited on silicon	Dye degradation	[45]
ZnO nanorods grown on ZnO film	Dye degradation	[45]
α-Fe ₂ O ₃ thin films on Si(100) substrates	Dye degradation	[46]
SrTiO ₃ α-Fe ₂ O ₃ thin films	Dye degradation	[47]
PbO/TiO ₂	Stearic acid degradation	[48]

Table 3.
Different thin-film catalysts with application in wastewater treatment.

followed by calcinations at 400°C for 1 h to remove the organic compounds from the thin films.

Characterizations of Al-doped ZnO thin film can be seen in **Figure 16(a)** [49]. The crystal structure and different structural parameters of the films were analyzed from the X-ray diffraction (XRD) spectrum of the ZnO and AZO thin films. The undoped ZnO exhibits well-defined diffraction reflections corresponding to the wurtzite hexagonal phase of ZnO lattice planes. The intensity of all peaks decreases with Al doping suggesting deterioration of the crystallinity of ZnO films due to the incorporation of defects in the lattice site. From FE-SEM images, it can be seen that nanoparticles are formed and deposited on the film depositing area in all cases. For the pure ZnO thin film, the nanoparticle size varies from 10 to 70 nm. After the incorporation of Al, the particle size becomes more uniform, and the distribution of size is between 15 and 30 nm [49].

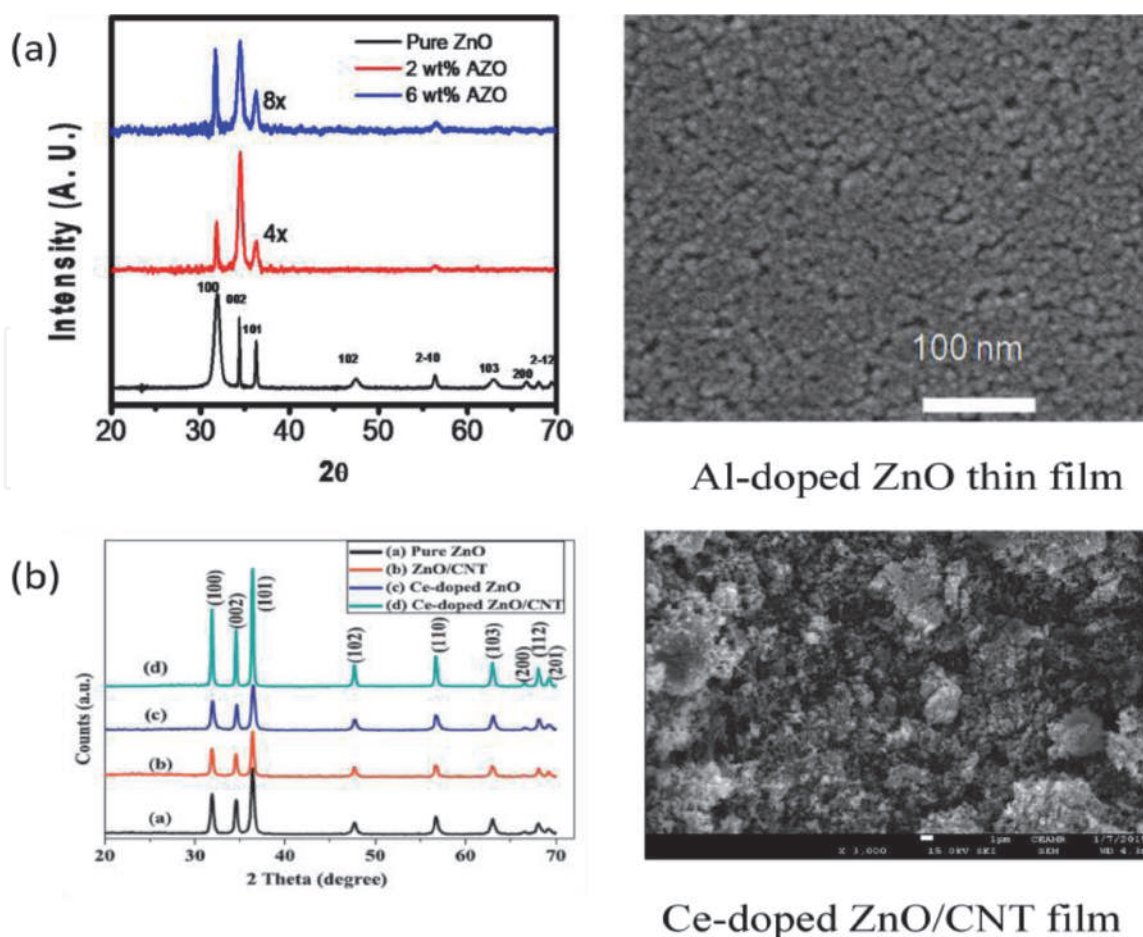


Figure 16. Characterizations of Al-doped ZnO thin film (a) and Ce-doped ZnO/CNT thin film (b) [49, 50].

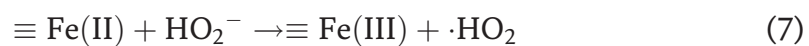
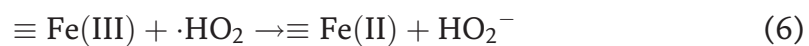
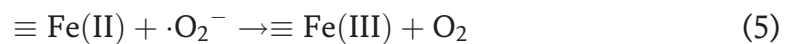
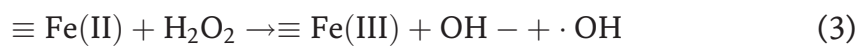
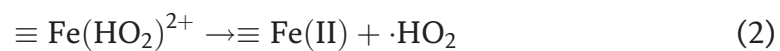
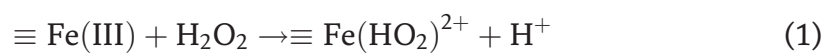
Another example is Ce-doped ZnO/carbon nanotube (CNT) thin film, which was prepared using a sol-gel drop coating method [50]. TEA and zinc acetate dehydrate were added into anhydrous ethanol under vigorous stirring. CNT and cerium sulfate were added into the above solution, and the solution was sonicated to get a uniform dispersion. The solution was heated at $(55 \pm 5)^{\circ}\text{C}$ with constant stirring at 200 rpm to get the ZnO/CNT sol, which was transparent and quite stable. The ZnO/CNT sol aged for 24 h before the preparation of the Ce-doped ZnO/CNT film. To synthesize Ce-doped ZnO/CNT thin film, the precursor solution was given dropwise on each of that frosted glass substrate using a pipette and then heated for 20 min at 80°C . The coating process was repeated twice for a thick film (~ 4 μm) preparation, and finally, the film was annealed at 500°C for 2 h using a muffle furnace.

To evaluate the crystallinity and crystal phases of the prepared thin film, XRD and FESEM spectra were acquired and are displayed in **Figure 16(b)** [50]. Ce and CeO_2 , Ce_2O_3 or other crystalline forms were not identified in the patterns, so the authors believed that Ce ions were uniformly substituted by Zn sites or interstitial sites in ZnO crystals. The addition of dopant and functionalized CNTs on the ZnO matrix presented the sharp and high-intense peak indicating the well-crystalline phase of ZnO. From the FESEM spectra of Ce-doped ZnO/CNT thin film, it is observed that that the sample ZnO/CNT is ZnO decorated on the surface of CNT, and the Ce-doped ZnO sample presents 3D flower-like microstructures consisting of many nanoflakes. It is worth noting that many different-size pores were generated in the 3D microstructures, which might act as transport paths for molecules and active sites for catalytic reaction and improve the catalytic properties of the thin-film material [50].

4. Heterogeneous catalysts for wastewater treatment: the process and mechanism

4.1 Heterogeneous Fenton catalysis

Heterogeneous Fenton catalysis, as one of the advanced oxidation technologies, is of great interest for environmental remediation owing to its benign process and general applicability [51]. Heterogeneous Fenton-like reactions on solid catalysts can effectively catalyze the oxidation of organic pollutants at wide pH conditions, which is beneficial for in situ remediations of polluted groundwater and soil and can be reused for further runs. Heterogeneous Fenton-like reaction is a surface-controlled reaction that depends on the catalyst surface area, on H_2O_2 concentration, on the reaction temperature, and on solution pH and ionic strength [52]. Kwan and Voelker [53] have suggested the chain of reactions in the catalyzed oxidation system as follows:



If only Fe(III) is originally present, Fe(II) is slowly generated by reactions (1) and (2) initiating oxidation reactions. A simple schematic of heterogeneous Fenton catalysis processes can be seen in **Figure 17**.

The magnetic $\text{Fe}_3\text{O}_4@\beta\text{-CD/MWCNT}$ nanocomposites were prepared by a hydrothermal method and used as a heterogeneous Fenton-like catalyst to degrade Tetrabromobisphenol A (TBBPA) [54]. $\text{Fe}_3\text{O}_4@\beta\text{-CD/MWCNT}$ presented good catalytic performance when removing TBBPA from water and got about 97% removal rate of under the optimum condition. Comodification of MWCNT and

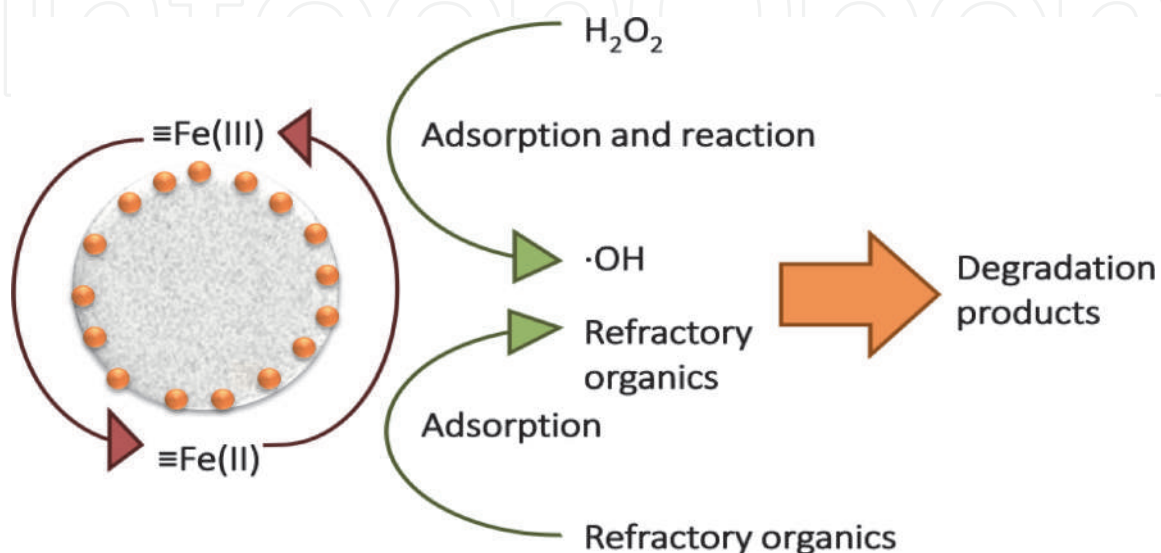


Figure 17.
A simple schematic of heterogeneous Fenton catalysis processes.

β -CD could distinctly promote the removal efficiency of TBBPA, which certified the existence of the synergistic effect between Fe_3O_4 , β -CD, and MWCNT. The catalyst has good regeneration ability; it still possessed excellent catalytic activity of TBBPA removal rate at about 86.2% after three cycles. Debromination and bridge fracture between two benzene rings were the primary process of TBBPA mineralization. This catalyst can provide a potential application in the degradation of refractory pollutants [54].

Except for Fe, Cu also can act as an active component of heterogeneous Fenton catalysts. Cu-V bimetallic catalyst (CuVOx) with abundant surface defects was successfully synthesized by the hydrothermal method [55]. Degradation experiment of emerging pollutant fluconazole confirmed that CuVOx exhibited higher catalytic activity, broader pH applicability, and more satisfactory reusability than monometallic copper compounds. By the introduction of vanadium into copper-based materials, several surface properties that are closely related to the reactivity of the copper catalysts, such as adsorption capacity, surface defects, and active site concentration, were improved. The electron-rich center around Cu/V active sites and surface oxygen vacancies are responsible for the rapid dissociation of H_2O_2 and the efficient catalytic oxidation of fluconazole in CuVOx Fenton system. The introduction of vanadium increased active sites and electron density and improved the surface chemical properties of the bimetallic catalyst. FLC and H_2O_2 were firstly adsorbed on the surface of CuVOx , which was beneficial to shorten the mass transfer process of pollutant oxidation. Around oxygen vacancies, there are abundant electrons with high transfer capability, which weaken the O-O bond of adsorbed H_2O_2 and transfer from the material surface to H_2O_2 . Under the reaction of catalyst, the adsorbed H_2O_2 was rapidly dissociated to produce a considerable amount of $\cdot\text{OH}$. Then, $\cdot\text{OH}$ attacked FLC adjacent to the active site, thereby achieving oxidative degradation of the pollutant [55].

4.2 Heterogeneous photocatalysis

Photocatalysis is the process of light-induced redox reactions upon the surrounding molecules to produce radical species for the subsequent utilization in

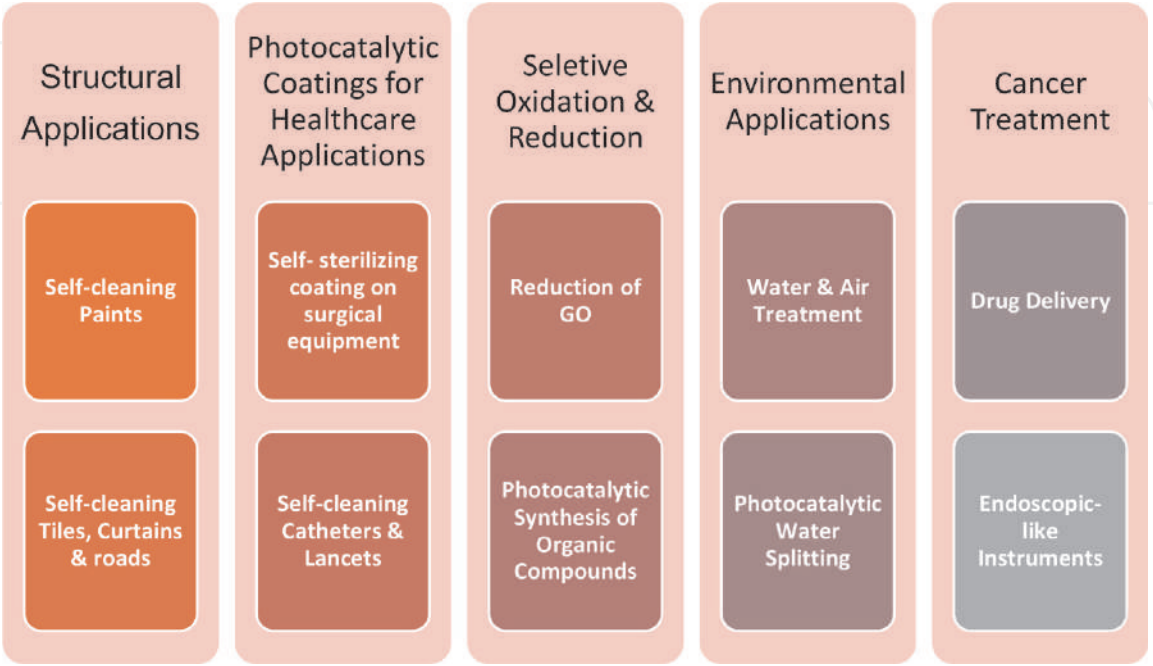


Figure 18.
Applications of heterogeneous photocatalysis [57].

various pollutant degradations, CO₂ conversion into hydrocarbon fuels, and disinfection of microorganisms, and so on, [56] as shown in **Figure 18**. Photocatalysis has many advantages: low reaction temperature, high oxidizability, complete purification, and using solar as an energy source. Furthermore, the careful selection of materials and structures of photocatalysts for photocatalysis is essential to perform the photocatalytic reactions efficiently. An ideal photocatalyst is bound to possess good performances such as narrow band gap energy, suitable band edge potential, reduced recombination, enhanced charge separation, and improved charge transportations [58]. For this purpose, photocatalytic materials are modified for their chemical compositions, which can be done through doping [59], composite formation [60], metal sensitization, and molecule functionalizations [61], among others, and physical structures, which include the size, shape, and surface morphology modifications of the materials.

The principle of photocatalysis is based on the theory of a solid energy band. When the energy of light irradiation absorbed by the semiconductor catalyst is larger than the photon band gap width, the electron-hole pairs are generated due to the transition of electrons. The light irradiation on the semiconductor causes the excitation of electrons from the valence band (VB) to the conduction band (CB) and the creation of holes in the valence band (VB) [62]. Electrons and holes stimulated by light radiation will migrate to the surface of semiconductor particles after various interactions and react with water or organics adsorbed on the surface of semiconductor catalyst particles to produce a photocatalytic effect, as shown in **Figure 19**. The typical photocatalytic process toward pollutant degradation can be described as follows.



Here are some examples of photocatalysis and photocatalysts.

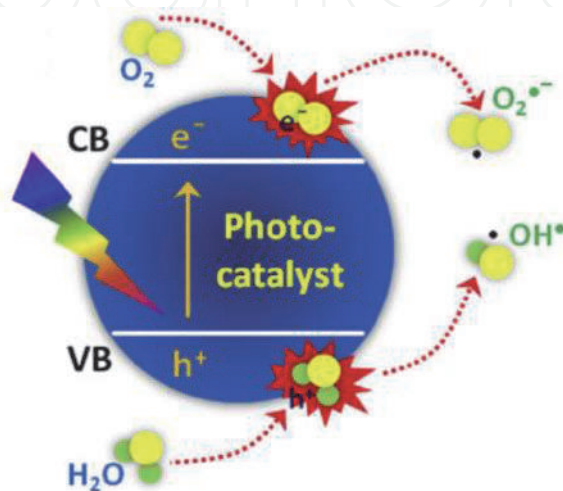


Figure 19.
Photocatalytic process in semiconductor.

A series of TiO_2 /biochar composite catalysts were prepared by the hydrolysis method for the degradation of methyl orange, where biochar was obtained from the pyrolysis of waste walnut shells [63]. The photocatalytic activity results showed that TiO_2 /biochar composite catalysts exhibited higher catalytic activity than that of pure TiO_2 . The decolorization efficiency of 96.88% and the mineralization efficiency of 83.23% were obtained, attributed to the synergistic effect of biochar and TiO_2 . After repeated uses, the catalyst still exhibited rather high activity toward the degradation of MO, where the decolorization efficiency and mineralization efficiency of MO achieved 92.45 and 76.56%, and the loss of activity was negligible. The possible degradation mechanism of MO with TiO_2 /biochar composites can be explained as follows. MO molecules firstly adsorbed by biochar due to the well-developed pore structure, which provides more opportunities for the contact of catalysts and pollutants. With irradiation of ultraviolet light, TiO_2 was excited to generate electrons from the valence band, transferring to the conduction band, and holes were left in the valence band. Biochar transferred electrons and acted as acceptors, inhibiting the recombination of electron-hole pairs. Then, the electrons would react with oxygen molecules and water molecules to generate superoxide anion radicals and hydroxyl radicals. Holes would also be trapped by water molecules to engender hydroxyl radicals. Thus, holes, superoxide anion radicals, and hydroxyl radicals cofunctioned as active species would interact with the MO molecules, and finally, carbon dioxide was formed [63].

Sun et al. evaluated the photocatalytic efficiency of activated carbon-supported TiO_2 catalyst (AC/ TiO_2) for degradation of aflatoxin B1 (AFB1) under UV-Vis light. AC/ TiO_2 was prepared by simple hydrothermal synthesis [64]. According to the experiments, the higher degradation efficiency of AFB1 by AC/ TiO_2 composite (98%) than that by bare TiO_2 (76%) was attributed to a higher surface area of AC/ TiO_2 and enhanced visible-light intensity by the synergistic effect of TiO_2 and AC. Moreover, the catalyst can be easily separated from the solution and can still keep high activity. The authors found that the hole (h^+) and the hydroxyl radicals ($\cdot\text{OH}$) played an essential role in the degradation of AFB1 and proposed the possible photocatalytic oxidation mechanism of AC/ TiO_2 for AFB1 degradation. When irradiated by UV light, the excited AC/ TiO_2 composite produces electrons (e^-) to the conduction band and holes (h^+) on the valence band. The photo-generated electrons can react with O_2 to produce superoxide radicals ($\text{O}_2^{\cdot-}$) and further produce hydroxyl radicals ($\cdot\text{OH}$). The photo-generated holes can react with hydroxide ions (OH^-) in the solution to directly produce $\cdot\text{OH}$. Some of these holes (h^+) and $\cdot\text{OH}$ would oxidize AFB1, which is absorbed on the surface of the catalyst [64]. Most of the photocatalysis processes have the same mechanism and they can be illustrated by (Figure 20).

4.3 Heterogeneous electrocatalysis

Electrocatalysis is a kind of catalysis that accelerates the charge transfer reaction at the interface of electrodes and electrolytes. The range of electrode catalysts is limited to electrical materials such as metals and semiconductors. There are many kinds of semiconductor oxides, such as skeleton nickel, nickel boride, tungsten carbide, sodium tungsten bronze, spinel and tungsten minerals, as well as various metals and phthalocyanines. Electrocatalysis is mainly used in the treatment of organic wastewater, degradation of chromium-containing wastewater, desulfurization of flue gas and raw coal, the simultaneous removal of NO_x and SO_2 , and the reduction of carbon dioxide and nitrogen. The selection of appropriate electrode materials plays a critical role in accelerating the electrode reaction. The selected electrode materials play a catalytic role in the process of electrification, thus

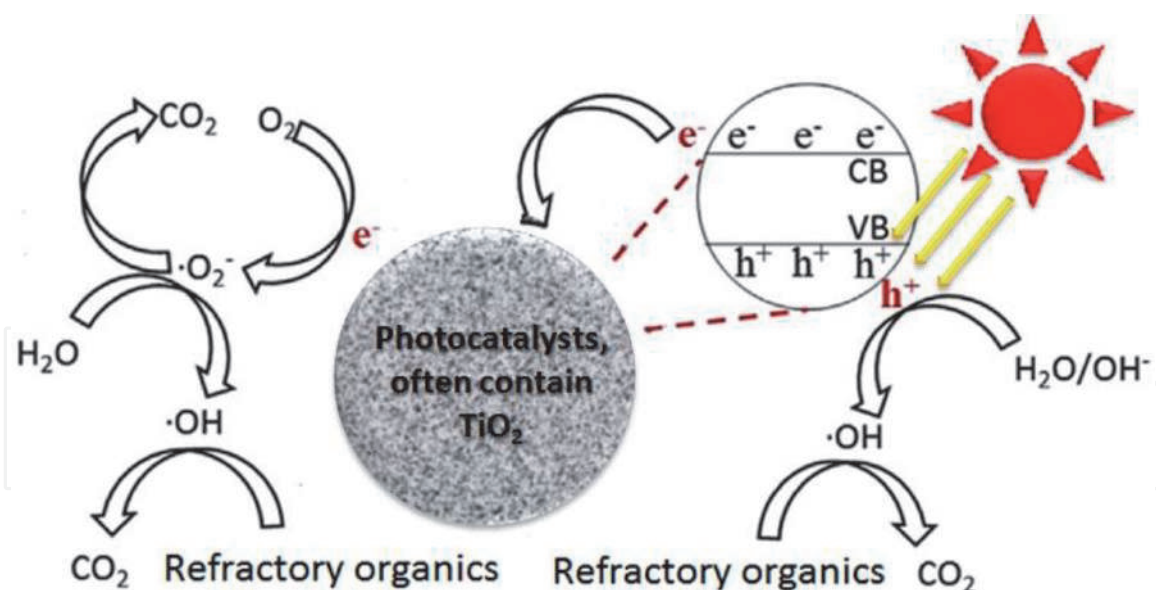


Figure 20.
The schematic of photocatalysis processes.

changing the reaction rate or direction of the electrode without any qualitative change in itself. Electrocatalysis covers two aspects of electrode reaction and catalysis, so electrocatalysts must have two functions at the same time: conductive and relatively free transfer of electrons; and effective catalytic activation. Therefore, the feasible way to design electrocatalysts is to modify the electrodes. Combining active components with conductive base electrodes in the form of covalent bonds or chemical adsorption can achieve the dual purposes of both transferring electrons and activating substrates.

Chao Zhang et al. investigated modified iron-carbon with polytetrafluoroethylene (PTFE) as a heterogeneous electro-Fenton (EF) catalyst for 2,4-dichlorophenol (2,4-DCP) degradation in near-neutral pH condition [65]. The degradation performance of the catalyst modification with 20% PTFE maintained well with low iron leaching. Moreover, the degradation efficiency of 2,4-DCP could exceed 95% within 120 min treatment at catalyst dosage of 6 g/L, initial pH of 6.7, and the current intensity of 100 mA. Two-stages of 2, 4-DCP degradation were observed: the first stage is a slow anodic oxidation stage, and the second one is a much faster heterogeneous EF oxidation stage. The automatic decrease of pH in the first stage initiated the Fe^{2+} release from microelectrolysis and benefited to the subsequent EF reaction. Aromatic intermediates including 2-chlorohydroquinone, 4,6-dichlororesorcinol, and 3,5-dichlorocatechol were detected by GC-MS. A possible mechanism and degradation pathway for 2,4-DCP were proposed. Air permeated from the prepared ADE cathode and was utilized to produce H_2O_2 . Simultaneously, Fe-C microelectrolysis would produce Fe^{2+} , which reacted with H_2O_2 as Fenton reagent. Considering the results of GC-MS and IC analyses, 2,4-DCP can be hydroxylated by $\cdot\text{OH}$ addition's reaction onto the aromatic ring, resulting in the formation of 3,5-dichlorocatechol and 4,6-dichlororesorcinol. Meanwhile, the chlorine atom located in the paraposition on the aromatic ring was substituted by $\cdot\text{OH}$ to yield 2-chlorohydroquinone. The aromatic organics mentioned above would be further oxidized to organic acids by $\cdot\text{OH}$, such as oxalic, acetic, and formic acids until mineralized to CO_2 completely. The possible degradation paths of 2,4-DCP can be seen in **Figure 21**.

Nanolayered double hydroxide (NLDH) decorated with Fe and Cu was applied as a novel heterogeneous catalyst for catalytic degradation of gentamicin by the electro-Fenton (EF) process [66]. The EF process was equipped with a graphite

plate under aeration. The highest removal efficiency was 91.3% when the Cu-Fe--NLDH-equipped EF process applied in comparison with the Fenton (50%) and the electro-oxidation alone (25.6%). Increasing the current resulted in the enhanced degradation of gentamicin, while the excessive electrolyte concentration and catalyst dosage led to the tangible drop in the reactor performance. At a specified reaction time, the injection of O₃ gas enhanced the efficiency of the Cu-Fe-NLDH-equipped EF process. The presence of ethanol led to a more suppressing effect than benzoquinone, indicating the dominant role of ·OH radical in the degradation of gentamicin compared with other free radical species such as O₂^{·-} radical. Most of

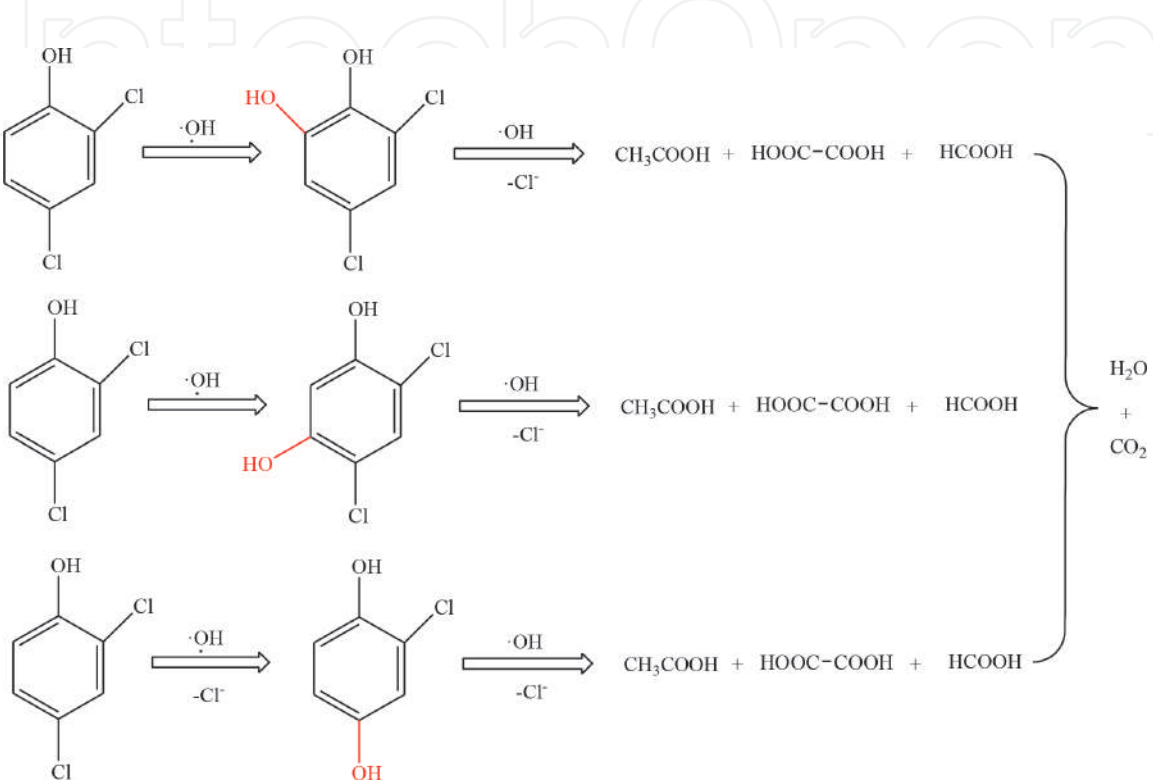


Figure 21.
Proposed degradation pathway of 2,4-DCP [65].

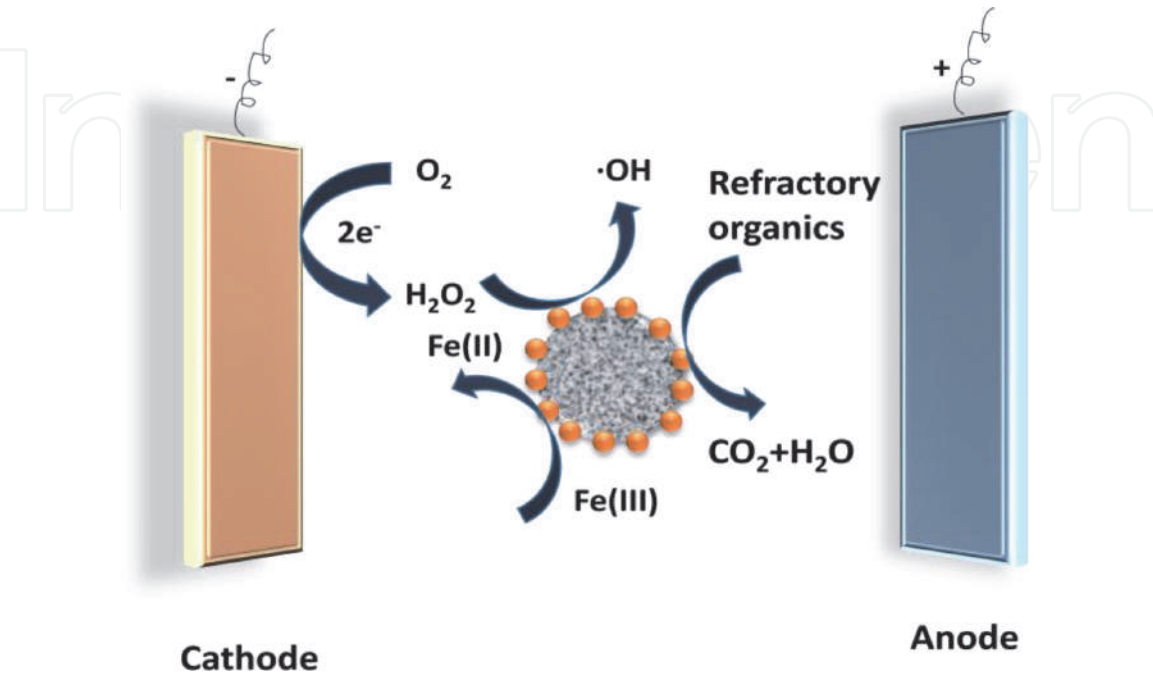


Figure 22.
The schematic of electrocatalysis processes [66].

Catalysts	Target pollutants	Assistant	Degradation efficiency	Reference
Fe/OATP	HA-Na	—	97%	[24]
Fe ₃ O ₄ @β-CD/ MWCNT	Tetrabromobisphenol A	—	97%	[54]
CuVOx	Fluconazole	—	99%	[55]
Fe ₂ O ₃ /ATP	Methylene blue	—	99%	[67]
CuO/SiO ₂	RhB	—	95%	[68]
TiO ₂ /biochar	Methyl orange	UV-Vis light	98%	[63]
AC/TiO ₂	Aflatoxin B1	UV-Vis light	96.88%	[64]
Mg-ZnO-Al ₂ O ₃	Caffeine	UV-Vis light	98.9%	[69]
Fe-C/PTFE	2,4-DCP	Electric	95%	[65]
Cu-Fe-NLDH	Gentamicin	Electric	91.3%	[66]
DG@Fe ₃ O ₄	Methylene blue	Electric	99%	[70]

Table 4.
Comparison of some catalysts for different pollutant degradation.

the photocatalysis processes have the same mechanism, they just used different electrodes and catalysts, and they can be illustrated by (Figure 22).
The comparison of some catalysts for different pollutant degradation was shown in Table 4.

5. Conclusions

Heterogeneous catalytic processes, as an efficient green method coping with organic wastewater, have attracted considerable attention. Heterogeneous catalysts, such as bulk catalysts and supported catalysts (including surface-loaded catalysts, core-shell catalysts, and thin-film catalysts), are often synthesized by impregnation, sol-gel, and coprecipitation methods. To characterize heterogeneous catalysts, BET surface area, scanning electron microscope (SEM), transmission electron microscope (TEM), Fourier transform infrared spectroscopy (FT-IR), and X-ray diffraction (XRD) are common characterizing methods. Heterogeneous catalytic processes are efficient in treating organic wastewater due to the generation of highly reactive and nonselective hydroxyl radicals ($\cdot\text{OH}$), which can oxidize and mineralize most organic compounds, with the advantages of no secondary pollution, easy separation, and recycling. The researchers often employed heterogeneous catalysts to degrade dyes, pesticides, and antibiotics, among others. The reactions and mechanisms of different heterogeneous catalytic processes might be different according to the target pollutants.

At present, the researches on heterogeneous-supported catalysts should focus on the following problems: (1) how to prepare heterogeneous catalysts (especially nanocatalysts) with high efficiency, low cost, and low energy consumption, which can be widely used in the treatment of industrial wastewater; (2) how to prepare the catalysts with larger specific surface area and higher activity, and how to make the loaded active components distribute more evenly on the surface of the carrier; and (3) how to expand the application fields of heterogeneous catalysts, such as the application in degradation of microplastics in wastewater.

IntechOpen


IntechOpen

Author details

Ting Zhang
School of Petrochemical Engineering, Lanzhou University of Technology, Lanzhou,
China

*Address all correspondence to: zhangting@lut.cn

IntechOpen

© 2020 The Author(s). Licensee IntechOpen. Distributed under the terms of the Creative Commons Attribution - NonCommercial 4.0 License (<https://creativecommons.org/licenses/by-nc/4.0/>), which permits use, distribution and reproduction for non-commercial purposes, provided the original is properly cited. 

References

- [1] Taylor HS. Catalysis—Chemical Process. 1957. Available from: www.britannica.com
- [2] Wang Q, Tian S, Long J, Ning P. Use of Fe(II)Fe(III)-LDHs prepared by co-precipitation method in a heterogeneous-Fenton process for degradation of methylene blue. *Catalysis Today*. 2014;41-48
- [3] Cheng M, Ma W, Li J, Huang Y, Zhao J, Wen YX, et al. Visible-light-assisted degradation of dye pollutants over Fe(III)-loaded resin in the presence of H₂O₂ at neutral pH values. *Environmental Science & Technology*. 2004;38:1569-1575
- [4] Socci J, Osatiashtiani A, Kyriakou G, Bridgwater T. The catalytic cracking of sterically challenging plastic feedstocks over high acid density Al-SBA-15 catalysts. *Applied Catalysis A: General*. 2019;570:218-227
- [5] Lu P, Cai F, Zhang J, Liu Y, Sun Y. Hydrogen production from methanol steam reforming over B-modified CuZnAlO_x catalysts. *Journal of Fuel Chemistry and Technology*. 2019;47:791-798
- [6] Cai F, Lu P, Ibrahim JJ, Fu Y, Zhang J, Sun Y. Investigation of the role of Nb on Pd—Zr—Zn catalyst in methanol steam reforming for hydrogen production. *International Journal of Hydrogen Energy*. 2019;44:11717-11733
- [7] Islam M, Basnayake R, Korzeniewski C. A study of formaldehyde formation during methanol oxidation over PtRu bulk alloys and nanometer scale catalyst. *Journal of Electroanalytical Chemistry*. 2007;599:31-40
- [8] Ji F, Li C, Zhang J, Deng L. Heterogeneous photo-Fenton decolorization of methylene blue over LiFe(WO₄)₂ catalyst. *Journal of Hazardous Materials*. 2011;186:1979-1984
- [9] Duan F, Yang Y, Li Y, Cao H, Wang Y, Zhang Y. Heterogeneous Fenton-like degradation of 4-chlorophenol using iron/ordered mesoporous carbon catalyst. *Journal of Environmental Sciences*. 2014;26:1171-1179
- [10] Hu X, Liu B, Deng Y, Chen H, Luo S, Sun C, et al. Adsorption and heterogeneous Fenton degradation of 17 α -methyltestosterone on nano Fe₃O₄/MWCNTs in aqueous solution. *Applied Catalysis B: Environmental*. 2011;107:274-283
- [11] Molina R, Martínez F, Melero JA, Bremner DH, Chakinala AG. Mineralization of phenol by a heterogeneous ultrasound/Fe-SBA-15/H₂O₂ process: Multivariate study by factorial design of experiments. *Applied Catalysis B: Environmental*. 2006;66:198-207
- [12] Muthukumari B, Selvam K, Muthuvel I, Swaminathan M. Photoassisted hetero-Fenton mineralization of azo dyes by Fe(II)-Al₂O₃ catalyst. *Chemical Engineering Journal*. 2009;153:9-15
- [13] Vignesh K, Rajarajan M, Suganthi A. Visible light assisted photocatalytic performance of Ni and Th co-doped ZnO nanoparticles for the degradation of methylene blue dye. *Journal of Industrial and Engineering Chemistry*. 2014;20:3826-3833
- [14] Panda N, Sahoo H, Mohapatra S. Decolourization of methyl orange using Fentonlike mesoporous Fe₂O₃—SiO₂ composite. *Journal of Hazardous Materials*. 2011;185:359-365
- [15] Zhong X, Royer S, Zhang H, Huang Q, Xiang L, Valange S, et al.

- Mesoporous silica iron-doped as stable and efficient heterogeneous catalyst for the degradation of C.I. acid orange 7 using sono-photo-Fenton process. *Separation and Purification Technology*. 2011;**80**:163-171
- [16] Liu T, You H, Chen Q. Heterogeneous photo-Fenton degradation of polyacrylamide in aqueous solution over Fe(III)-SiO₂ catalyst. *Journal of Hazardous Materials*. 2009;**162**:860-865
- [17] Vu AT, Xuan TN, Lee CH. Preparation of mesoporous Fe₂O₃-SiO₂ composite from rice husk as an efficient heterogeneous Fenton-like catalyst for degradation of organic dyes. *Journal of Water Process Engineering*. 2019;**28**: 169-180
- [18] Chen JX, Zhu LZ. Catalytic degradation of Orange II by UV-Fenton with hydroxyl-Fe-pillared bentonite in water. *Chemosphere*. 2006;**65**: 1249-1225
- [19] Chen JX, Zhu LZ. Oxalate enhanced mechanism of hydroxyl-Fe-pillared bentonite during the degradation of Orange II by UV-Fenton process. *Journal of Hazardous Materials*. 2011; **185**:1477-1481
- [20] Feng JY, Hu XJ, Yue PL. Discoloration and mineralization of Orange II by using a bentonite clay-based Fe nanocomposite film as a heterogeneous photo-Fenton catalyst. *Water Research*. 2005;**39**:89-96
- [21] Perderiset M, Baillif P, Jaurand MC. Chemical analysis and photoelectron spectroscopy of the adsorption of macromolecules on the surface of attapulgite. *Journal of Colloid and Interface Science*. 1988;**121**:381-391
- [22] Zhang J, Chen H, Wang A. Study on superabsorbent composite. III. Swelling behaviors of polyacrylamide/attapulgite composite based on acidified attapulgite and organo-attapulgite. *European Polymer Journal*. 2005;**41**:2434-2442
- [23] Li A, Zhang JP, Wang AQ. Utilization of starch and clay for the preparation of superabsorbent composite. *Bioresource Technology*. 2007;**98**:327-332
- [24] Zhang T, Qian C, Dong L. Preparation of particle reusable heterogeneous catalyst Fe₃O₄/ATP for methylene blue decolorization. *International Journal of Environmental Science and Technology*. 2019;**10**: 343-349
- [25] Zhang T, Liu J, Chen M, Wang Y. Preparation of heterogeneous Fenton catalyst Fe/organo-attapulgite and its performance in sodium humate degradation. *Desalination and Water Treatment*. 2018;**107**:91-99
- [26] Solar P, Polonskyi O, Olbricht A, Hinz A, Shelemin A, Kylián O, et al. Single step generation of metal-plasma polymer multicore@shell nanoparticles from the gas phase. *Scientific Reports*. 2017;**7**: 8514-8519
- [27] Martinez L, Mayoral A, Espineira M, Roman E, Palomares FJ, Huttel Y. Core@ shell, Au@ TiO_x nanoparticles by gas phase synthesis. *Nanoscale*. 2017; **9**:6463-6470
- [28] Solaiyammal T, Murugakoothan P. Green synthesis of Au and Au@ TiO₂ core-shell structure formation by hydrothermal method for dye sensitized solar cell applications. *Journal of Materials Science: Materials in Electronics*. 2018;**29**:1-9
- [29] Guo XH, Ma JQ, Ge HG. CoFe₂O₄@ TiO₂@ Au core-shell structured microspheres: Synthesis and photocatalytic properties. *Russian Journal of Physical Chemistry A*. 2017; **91**:2643-2650

- [30] Shi BN, Wan JF, Liu CT, Yu XJ, Ma FW. Synthesis of $\text{CoFe}_2\text{O}_4/\text{MCM-41}/\text{TiO}_2$ composite microspheres and its performance in degradation of phenol. *Materials Science in Semiconductor Processing*. 2015;**37**:241-249
- [31] Sohail M, Xue H, Jiao Q, Li H, Khan K, Wang S, et al. Synthesis of well-dispersed $\text{TiO}_2/\text{CNTs}@ \text{CoFe}_2\text{O}_4$ nanocomposites and their photocatalytic properties. *Materials Research Bulletin*. 2018;**101**:83-89
- [32] Hang S, He Q, Ping S, Zeng S, Xu K, Li J, et al. One-pot synthesis of $\text{Au}@ \text{TiO}_2$ yolk-shell nanoparticles with enhanced photocatalytic activity under visible light. *Journal of Colloid and Interface Science*. 2017;**505**:884-891
- [33] Ma JQ, Guo SB, Guo XH, Ge HG. Liquid-phase deposition of TiO_2 nanoparticles on core-shell $\text{Fe}_3\text{O}_4 @ \text{SiO}_2$ spheres: Preparation, characterization, and photocatalytic activity. *Journal of Nanoparticle Research*. 2015;**17**:1-11
- [34] Wu J, Yang Y, Ding J. Green production of cyclohexanone oxime with a fixed-bed reactor using shaped titanosilicate catalysts. *Chinese Journal*. 2015;**60**:1538-1545
- [35] Caruso F. Nanoengineering of particle surfaces. *Advanced Materials*. 2010;**13**:11-19
- [36] Reiss P, Protiere M, Li L. Core/shell semiconductor nanocrystals. *Small*. 2009;**5**:154-168
- [37] Shi ZL, Du C, Yao SH. Preparation and photocatalytic activity of cerium doped anatase titanium dioxide coated magnetite composite. *Journal of the Taiwan Institute of Chemical Engineers*. 2011;**42**:652-657
- [38] Chou KS, Lin MY, Wu HH. Studies on the removal of 2-propanol by $\text{Ag}@ \text{Fe}_2\text{O}_3$ core-shell structured catalyst. *Journal of the Taiwan Institute of Chemical Engineers*. 2013;**44**:228-232
- [39] Jilani A, Abdel-Wahab MS, Hammad AH. *Advance Deposition Techniques for Thin Film and Coating*. London: IntechOpen; 2017
- [40] Shwetharani R, Chandan HR, Sakar M, Balakrishna GR, Reddy KR, Raghu AV. Photocatalytic semiconductor thin films for hydrogen production and environmental applications. *International Journal of Hydrogen Energy*. 2019. DOI: 10.1016/j.ijhydene.2019.03.149
- [41] Arconada N, Suarezb DAS, Portelab R, Coronadob JM, Sanchezb B, Castro Y. Synthesis and photocatalytic properties of dense and porous TiO_2 -anatase thin films prepared by sol-gel. *Applied Catalysis B: Environmental*. 2009;**86**:1-7
- [42] Sakthivel S, Shankar MV, Palanichamy M, Arabindoo B, Bahnemann DW, Murugesan V. Enhancement of photocatalytic activity by metal deposition: Characterization and photonic efficiency of Pt, Au, and Pd deposited on TiO_2 catalyst. *Water Research*. 2004;**38**:3001-3008
- [43] Jung JM, Wang M, Kim EJ, Park C, Hahn SH. Enhanced photocatalytic activity of Au -buffered TiO_2 thin films prepared by radio frequency magnetron sputtering. *Applied Catalysis B: Environmental*. 2008;**84**:389-392
- [44] Seong SG, Kim EJ, Kim YS, Lee KE, Hahn SH. Influence of deposition atmosphere on photocatalytic activity of $\text{TiO}_2/\text{SiO}_x$ double-layers prepared by RF magnetron sputtering. *Applied Surface Science*. 2009;**256**:1-5
- [45] Di Mauro A, Fragala ME, Privitera V, Impellizzeri G. ZnO for application in photocatalysis: From thin films to nanostructures. *Materials*

Science in Semiconductor Processing. 2017;**69**:44-51

[46] Chen YH, Tu KJ. Thickness dependent o photocatalytic activity of hematite thin films. *International Journal of Photoenergy*. 2012; **1110-662X**:1-6

[47] Schultz AM, Salvador PA, Rohrer GS. Enhanced photochemical activity of α -Fe₂O₃ films supported on SrTiO₃ substrates under visible light illumination. *Chemical Communications*. 2012;**48**:2012-2014

[48] Bhachu DS, Sathasivam S, Carmalt CJ, Parkin IP. PbO modified TiO₂ thin films: A route to visible light photocatalysts. *Langmuir*. 2014;**30**: 624-630

[49] Islam MR, Rahman M, Farhad SFU, Podder J. Structural, optical and photocatalysis properties of sol-gel deposited Aldoped ZnO thin films. *Surface and Interface Analysis*. 2019;**16**: 120-126

[50] Elias M, Uddin MN, Hossain MA, Saha JK, Siddiquey IA, Sarker DR, et al. An experimental and theoretical study of the effect of Ce doping in ZnO/CNT composite thin film with enhanced visible light photo-catalysis. *International Journal of Hydrogen Energy*. 2019;**44**:20068-20078

[51] Xia M, Chen C, Long M, Chen C, Cai W, Zhou B. Magnetically separable mesoporous silica nanocomposite and its application in Fenton catalysis. *Microporous and Mesoporous Materials*. 2011;**145**:217-223

[52] Matta R, Hanna K, Chiron S. Fenton-like oxidation of 2,4,6-trinitrotoluene using different iron minerals. *Science of the Total Environment*. 2007;**385**:242-251

[53] Kwan WP, Voelker BM. Rates of hydroxyl radical generation and organic

compound oxidation in mineral-catalyzed Fenton-like systems. *Environmental Science & Technology*. 2005;**39**:9303-9308

[54] Zhang Y, Wu P, Chen Z, Zhou L, Zhao Y, Lai Y, et al. Synergistic effect in heterogeneous Fenton degradation of tetrabromobisphenol a by MWCNT and β -CD co-modified Fe₃O₄. *Materials Research Bulletin*. 2019;**113**:14-24

[55] Zhang N, Xue C, Wang K, Fang Z. Efficient oxidative degradation of fluconazole by a heterogeneous Fenton process with Cu-V bimetallic catalysts. *Chemical Engineering Journal*. 2020; **380**:122516

[56] Francis O, Kuben GK, Sittert CGCE, Poomani GP. Recent progress in the development of semiconductor-based photocatalyst materials for applications in photocatalytic water splitting and degradation of pollutants. *Advanced Sustainable Systems*. 2017: 1700006

[57] Ahmed SN, Haider W. Heterogeneous photocatalysis and its potential applications in water and wastewater treatment: A review. *Nanotechnology*. 2018;**29**: 342001

[58] Reddy KR, Reddy CV, Nadagouda MN, Shetti NP, Jaesool S, Aminabhavi TM. Polymeric graphitic carbon nitride (g-C₃N₄)-based semiconducting nanostructured materials: Synthesis methods, properties and photocatalytic applications. *Journal of Environmental Management*. 2019; **238**:25-40

[59] Ravikumar CH, Mahto MSA, Nanjundaiah RT, Thippeswamy R, Teixeira SR, Balakrishna RG. Observation of oxo-bridged yttrium in TiO₂ nanostructures and their enhanced photocatalytic hydrogen generation under UV/visible light irradiations.

Materials Research Bulletin. 2018;**104**: 212-219

[60] D'Souza LP, Muralikrishna S, Chandan HR, Ramakrishnappa T, Balakrishna RG. Neodymium doped titania as photoanode and graphene oxide-CuS composite as a counter electrode material in quantum dot solar cell. *Journal of Materials Research*. 2015; **30**:3241-3251

[61] Schiffman HRCJD, Balakrishna RG. Quantum dots as fluorescent probes: Synthesis, surface chemistry, energy transfer mechanisms, and applications. *Sensors and Actuators B: Chemical*. 2018;**258**:1191-1214

[62] Ibhaddon A, Fitzpatrick P. Heterogeneous photocatalysis: Recent advances and applications. *Catalysts*. 2013;**3**:189

[63] Lu L, Shan R, Shi Y, Wang S, Yuan H. A novel TiO₂/biochar composite catalysts for photocatalytic degradation of methyl orange. *Chemosphere*. 2019;**222**:391-398

[64] Sun S, Zhao R, Xie Y, Liu Y. Photocatalytic degradation of aflatoxin B1 by activated carbon supported TiO₂ catalyst. *Food Control*. 2019;**100**: 183-188

[65] Zhang C, Zhou M, Ren G, Yu X, Ma L, Yang J, et al. Heterogeneous electro-Fenton using modified iron-carbon as catalyst for 2,4-dichlorophenol degradation: Influence factors, mechanism and degradation pathway. *Water Research*. 2015;**70**: 414-424

[66] Ghasemi M, Khataee A, Gholami P, Soltani RDC. Template-free microspheres decorated with Cu-Fe-NLDH for catalytic removal of gentamicin in heterogeneous electro-Fenton process. *Journal of Environmental Management*. 2019;**248**: 109236

[67] Zhang T, Chen M, Yu S. Decolorization of methylene blue by an attapulgite-based heterogeneous Fenton catalyst: Process optimisation. *Desalination and Water Treatment*. 2017;**63**:275-282

[68] Sun Y, Tian P, Ding D, Yang Z, Wang W, Xin H, et al. Revealing the active species of Cu-based catalysts for heterogeneous Fenton reaction. *Applied Catalysis B: Environmental*. 2019;**258**: 117985

[69] Elhalil A, Elmoubarki R, Farnane M, Machrouhi A, Sadiq M, Mahjoubi FZ, et al. Photocatalytic degradation of caffeine as a model pharmaceutical pollutant on Mg doped ZnO-Al₂O₃ heterostructure. *Environmental Nanotechnology, Monitoring and Management*. 2018;**10**:63-72

[70] Wang J, Yang F, Wang S, Zhong H, Wu Z, Cao Z. Reactivation of nano-Fe₃O₄/diethanolamine/rGO catalyst by using electric field in Fenton reaction. *Journal of the Taiwan Institute of Chemical Engineers*. 2019;**99**:113-122

Applications of Chemical Kinetics in Heterogeneous Catalysis

Zhenhua Zhang, Li-Ping Fan and Yue-Juan Wang

Abstract

Chemical kinetics is a key subdiscipline of physical chemistry that studies the reaction rate in every elemental step and corresponding catalytic mechanism. It mainly concludes molecular reaction dynamics, catalytic dynamics, elemental reaction dynamics, macrodynamics, and microdynamics. Such a research field has wide applications in heterogeneous catalysis. Based on the Arrhenius plot fitted by the catalytic conversions below 15% without the mass transfer effect and heat transfer effect, the apparent activation energy echoing with the intrinsically catalytic sites and the pre-exponential factor echoing with the relative number of active sites can be, respectively, derived from the slope and intercept of the Arrhenius plots, which can be used to compare the intrinsically catalytic activity of different catalysts and the relative amount of active sites. Reaction orders of both reactants and products are derived from the reaction rate equation and also fitted by the catalytic conversions below 15% without the mass transfer effect and heat transfer effect. According to the acquired reaction orders, the reaction mechanism can be proposed and even defined in some simple reactions. Therefore, investigations of chemical kinetics are of extreme importance and meaning in heterogeneous catalysis.

Keywords: Arrhenius equation, reaction rate equation, apparent activation energy, reaction order, heterogeneous catalysis

1. Introduction

Chemical kinetics, also known as reaction kinetics or chemical reaction kinetics, is a key branch of physical chemistry. Its main task is to investigate the rate during chemical process and to propose the catalytic mechanism of chemical process by a method of research object acting as a nonequilibrium dynamic system whose properties change with time [1, 2]. Through the study of chemical kinetics, it can reasonably guide us to know how to control the reaction conditions and improve the main reaction rate, in order to increase the production of chemical products, and also guide us to learn how to suppress or slow down the reaction rate of side reactions to reduce the consumption of raw materials, reduce the burden of separation operations, and eventually improve the product quality. Chemical kinetics can provide general knowledge on how to avoid explosion of dangerous goods, material corrosion, and aging and deterioration of products. It can also carry out optimal design and control for the industrialization of scientific research results and select the most suitable operating conditions for the existing production. Generally speaking, chemical kinetics is one

of the main theoretical bases of chemical reaction engineering, accompanied by the chemical thermodynamics for the improved study of chemical reactions.

Chemical kinetics is of great antiquity with continuous improvements. Date back to the first half of the twentieth century, a great deal of research was devoted to the parameter determination, theoretical analysis, and using these parameters to study the reaction mechanism. However, investigation of the reaction mechanism was extremely difficult at that time, which was dominantly limited by the abilities of probe and analyze reaction intermediates. As time goes on, the study of free radical chain reaction kinetics was generally carried out in the late twentieth century, which brought two development trends for chemical kinetics. One was for the study of elemental reaction dynamics, and the other was to urgently establish a method for detecting active intermediates. Such researches were accompanied by the development of electronics and laser technology. Notably, Herschbach, Lee, and Polanyi, three famous scientists in this field, were awarded the Nobel Prize in chemistry in 1986, which marked the importance of chemical kinetics and indicated the current progress and the achieved level.

Nowadays, chemical kinetics has become an indispensable tool in both chemical discipline development and scientific research. The application in heterogeneous catalysis is a typical example [3]. Heterogeneous catalysis, possessing most of the catalytic reactions in the industry, refers to the catalytic reaction that occurs at the interface of two phases. The heterogeneously catalytic reaction generally occurs on the catalyst surface on which the reactant molecular adsorbs, diffuses, activates, reacts, and desorbs to acquire the final products. Therefore, the surface compositions and structures of catalytic materials are extremely critical in determining the catalytic properties [4]. The adsorption center on catalyst surface is often the center of catalytic activity, which is denoted as active site. The reactant molecule bonds to the active site to form surface adsorption complex, which is denoted as active intermediate species. The existence of active site on catalyst surface can affect the formation and activation of active intermediate species, thus altering the reaction path and consequently the required activation energy [5, 6].

In this chapter, two important kinetic equations, the Arrhenius equation and the reaction rate equation, were comprehensively introduced, accompanied by the applications in heterogeneous catalysis. Through the introduction of the Arrhenius equation, the apparent activation energy (E_a) and pre-exponential factor (A) can be calculated based on the Arrhenius plots fitted by the catalytic conversions below 15% without the mass transfer effect and heat transfer effect, which can reflect the intrinsically catalytic sites and relative number of active sites, respectively. The reaction mechanism involving rate-determining elementary reaction step can be proposed by the reaction order derived from reaction rate equation plotted by the catalytic conversions below 15% without the mass transfer effect and heat transfer effect. Understanding the structure and number of active sites and catalytic mechanism, it can guide us insights into the understanding for a catalytic reaction and thereby provide a research fundamental for the design and synthesis of high-performance catalysts.

2. Applications of kinetic equations in heterogeneous catalysis

2.1 The Arrhenius equation and its applications in heterogeneous catalysis

The Arrhenius equation is an empirical formula with chemical reaction rate changing with temperature, which was established by Svante August Arrhenius, a famous scientist in Sweden. This equation can be expressed in different forms

containing the differential expression (Eq. (1)), antiderivative form expression (Eq. (2)), derivative form expression (Eq. (3)), and exponential form expression (Eq. (4)), as listed below. Among them, k represents the rate constant, R represents the gas molar constant, T represents the thermodynamic temperature, E_a represents the apparent activation energy, and A represents the pre-exponential factor. The Arrhenius equation can be used to calculate the apparent activation energy, the optimal reaction temperature and time, and the reaction rate constant in a chemical reaction.

$$\frac{d \ln k}{dT} = \frac{E_a}{RT^2} \quad (1)$$

$$\ln k = \frac{-E_a}{RT} + \ln A \quad (2)$$

$$\ln \frac{k_2}{k_1} = \frac{-E_a}{R} \left(\frac{1}{T_2} - \frac{1}{T_1} \right) \quad (3)$$

$$k = e^{\frac{-E_a}{RT}} \quad (4)$$

As shown in the above listed equations, it shows a wide applicability in catalytic reactions, including not only gas-phase reactions but also liquid-phase reactions, as well as most of complex catalytic reactions. However, the precondition of this equation in use is to assume that E_a is an independent constant without relating to temperature. Therefore, the results derived from this equation is well agreeing with the real experiment results within a certain temperature range.

This equation is of wide applications in heterogeneous catalysis. Typical in the catalytic oxidation of CO, a representative probe reaction in heterogeneous catalysis [7–12], the Arrhenius equation is often used as an evaluation standard to compare the intrinsic activity of different catalysts and relative amount of active sites. Bao et al. [7] reported a crystal-plane-controlled surface restructuring and catalytic performance of Cu_2O nanocrystals in CO oxidation with excess O_2 . As shown in **Figure 1**, the relationships of catalyst structure and catalytic property were deeply explored. Based on the microscopic and spectroscopic characterization results (detailed descriptions shown in Ref. [7]), the surface compositions and

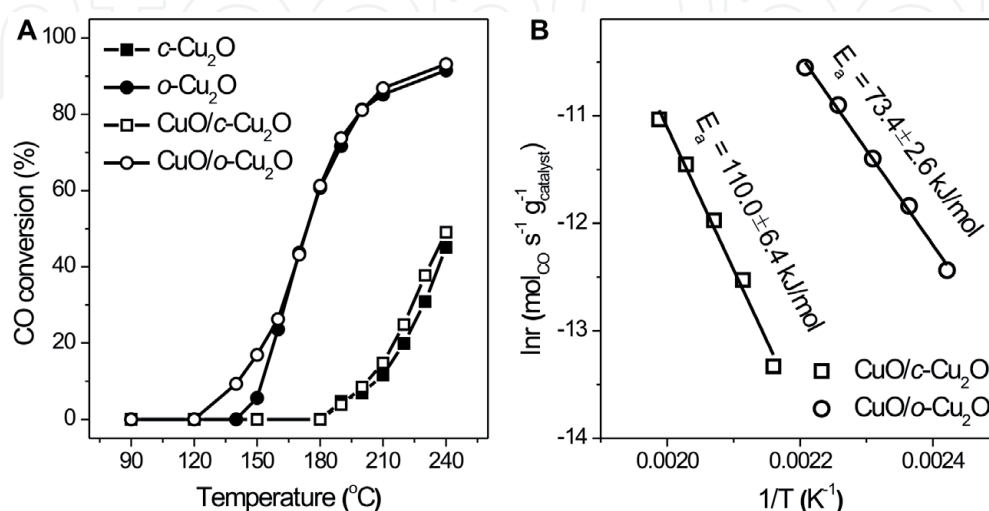


Figure 1. (A) Catalytic performance of $c\text{-Cu}_2\text{O}$, $o\text{-Cu}_2\text{O}$, $\text{CuO}/c\text{-Cu}_2\text{O}$, and $\text{CuO}/o\text{-Cu}_2\text{O}$ in CO oxidation reaction and (B) the Arrhenius plot of CO oxidation catalyzed by $\text{CuO}/o\text{-Cu}_2\text{O}$ and $\text{CuO}/c\text{-Cu}_2\text{O}$ [7]. Copyright © 2011, Wiley-VCH Verlag GmbH & Co.

structures of the restructured CuO/Cu₂O catalysts were distinctly identified. Their corresponding catalytic performance in CO oxidation with the plotted Arrhenius equation was also conducted. The derived E_a value plays a key role in comparing the intrinsic activity of surface sites on different catalysts based on the slope of the Arrhenius plots. CuO/Cu₂O octahedra (denoted as CuO/o-Cu₂O) show a lower E_a value of $73.4 \pm 2.6 \text{ kJ mol}^{-1}$ than CuO/Cu₂O cubes (denoted as CuO/c-Cu₂O) with a E_a value of $110.0 \pm 6.4 \text{ kJ mol}^{-1}$, indicating that CO oxidation catalyzed by the CuO of CuO/o-Cu₂O surface is more intrinsically active than the CO oxidation catalyzed by the CuO of CuO/c-Cu₂O surface. Density functional theory (DFT) calculations results demonstrate that they exist in different catalytic reaction mechanisms involved in different CuO/Cu₂O surface structures. The CuO/Cu₂O(100) surface is terminated with two-coordinated oxygen (O_{2c}) atoms, which result in a typical Mars-Van Krevelen (MvK) mechanism proceeded, while three-coordinated Cu (Cu_{3c}) and three-coordinated oxygen (O_{3c}) atoms are terminated on the CuO/Cu₂O(111) surface, which results in a Langmuir-Hinshelwood (LH) mechanism proceeded. These results clearly establish the catalyst structure-catalytic property relationships based on experimental observations and DFT simulations.

Similar results have been extensively reported in many other heterogeneous catalytic reactions, which were used by the calculated E_a values derived from the Arrhenius plots to compare the intrinsic activity [13–15]. Another example is in the identification of the most active Cu facet for low-temperature water gas shift reaction (**Figure 2**) [13]. Three types of Cu nanocrystals were prepared by a morphology-preserved reduction strategy from corresponding Cu₂O nanocrystals. Microscopic structural characterization results and in situ diffuse reflectance infrared Fourier transformed spectra (DRIFTS) of CO adsorption at 123 K confirm the Cu cubes (denoted as c-Cu), octahedra (denoted as o-Cu), and rhombic dodecahedra (denoted as d-Cu), respectively, enclosed with {100}, {111}, and {110} crystal planes (detailed descriptions shown in Ref. [13]). A morphology-dependent catalytic performance was observed on Cu nanocrystal catalyzed low-temperature water gas shift reaction, and the catalytic activity follows an order of c-Cu > d-Cu > o-Cu (**Figure 2A**). However, various Cu nanocrystals are different in particle sizes and surface structures and thus lead to the differently specific BET surface areas and catalytic sites in water gas shift reaction, respectively. As a result, it is difficult to compare the intrinsic activity of c-Cu and d-Cu nanocrystals in

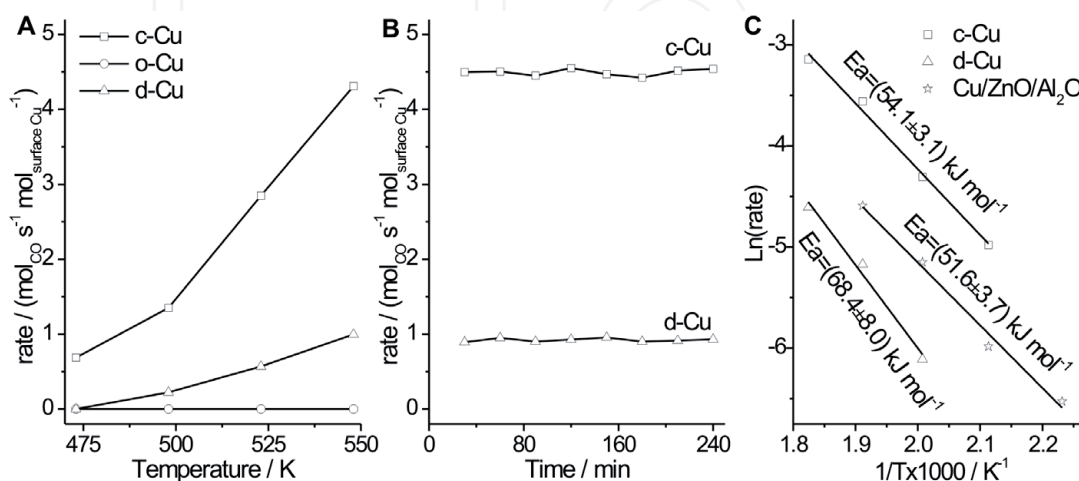


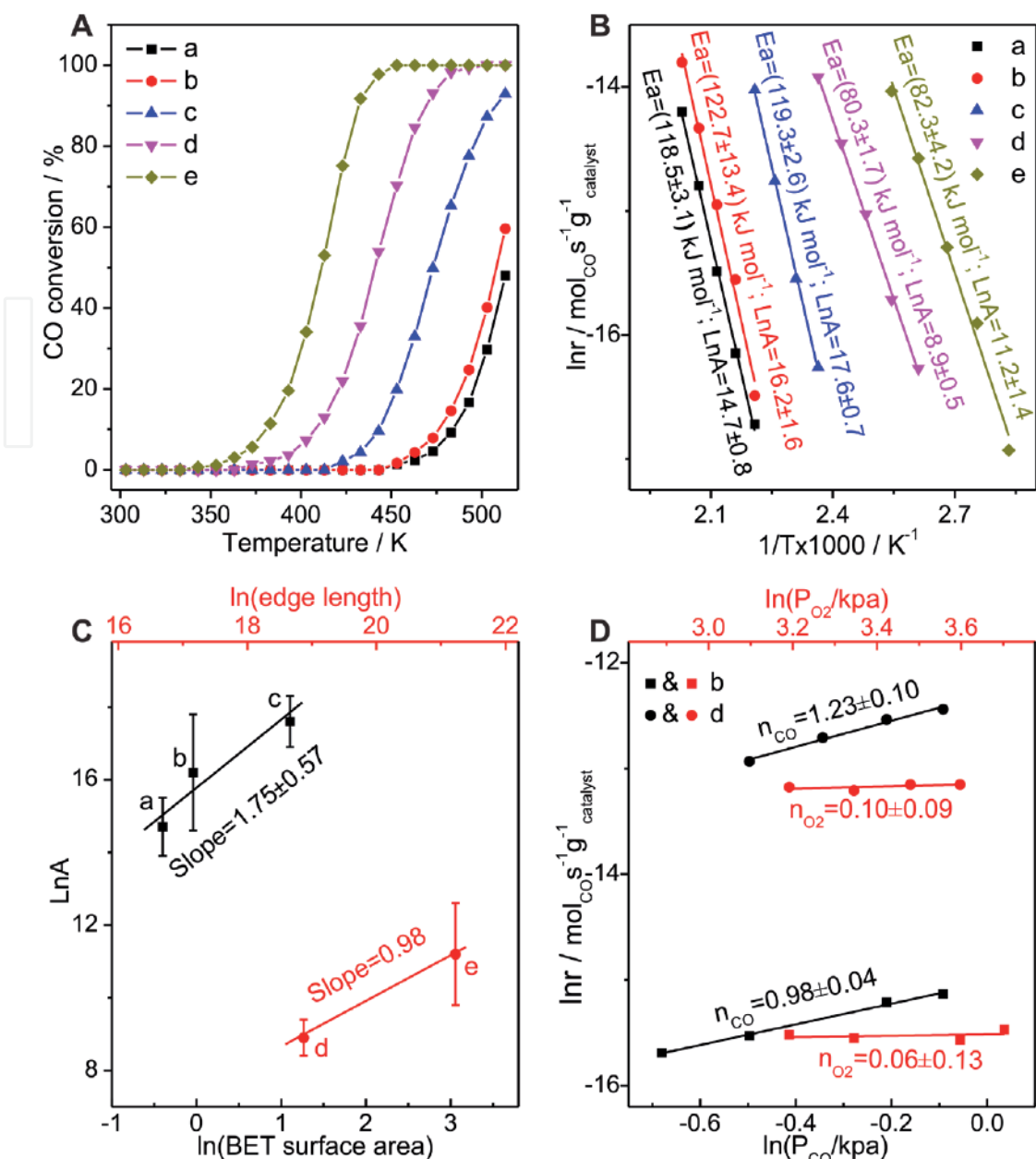
Figure 2.

(A) Reaction rate ($\text{mol}_{\text{CO}} \text{s}^{-1} \text{mol}_{\text{surface Cu}}^{-1}$) of Cu cubes, Cu octahedra, and Cu rhombic dodecahedra in the water gas shift reaction as a function of reaction temperature; (B) reaction rate ($\text{mol}_{\text{CO}} \text{s}^{-1} \text{mol}_{\text{surface Cu}}^{-1}$) of Cu cubes and rhombic dodecahedra at 548 K in the water gas shift reaction as a function of reaction time; (C) the Arrhenius plots of Cu cubes, rhombic dodecahedra, and commercial Cu/ZnO/Al₂O₃ catalyst in the water gas shift reaction [13]. Copyright © 2017, Nature Publishing Group.

water-gas shift reaction except o-Cu nanocrystals due to its catalytically inert under the reaction conditions. Subsequently, the Arrhenius equation was plotted based on the catalytic conversions below 15% without the mass transfer effect and heat transfer effect to compare the catalytic performance of intrinsically active sites. The calculated E_a value is $54.1 \pm 3.1 \text{ kJ mol}^{-1}$ for c-Cu nanocrystals, which is lower than d-Cu nanocrystals with a E_a value of $68.4 \pm 8.0 \text{ kJ mol}^{-1}$ and similar to commercial Cu/ZnO/Al₂O₃ catalyst with a E_a value of $51.6 \pm 3.7 \text{ kJ mol}^{-1}$ (**Figure 2C**). This indicates that the catalytic reaction proceeds more facile on c-Cu nanocrystals enclosed with {100} crystal planes, and thus, c-Cu nanocrystals are the most active Cu facet for low-temperature water gas shift reaction.

The above-mentioned results are a relatively straightforward and convenient method in the use of the Arrhenius equation. For more in-depth use, the Arrhenius equation can also have been utilized to identify the role and contribution of different active sites of a catalyst nanoparticle to the catalytic reaction based on the calculated E_a and pre-exponential factor A values derived from the Arrhenius equation [8]. c-Cu₂O nanocrystals in different sizes were synthesized by the established methods and subsequently evaluated in the oxidation of CO with excess O₂. The catalytic activities of the restructured CuO/c-Cu₂O catalysts increase with the size decrease (**Figure 3A**), apparently in consistent with their specific BET surface areas. However, their corresponding E_a values are distinctly different. c-Cu₂O nanocrystals in large sizes show a higher E_a value of about 120 kJ mol^{-1} than those in fine sizes with a E_a value of about 80 kJ mol^{-1} (**Figure 3B**), indicating that they exhibit different structures of active sites. Until here, it is still unclear which site contributes to the catalytic performance; thus, the relative relationships of different surface sites to the number of active sites, including facet sites and edge sites, are plotted in order to identify the structure of active sites on different c-Cu₂O nanocrystals. Under the same catalytic reaction conditions, the calculated A values derived from the intercept of the Arrhenius equation are positively related to the density of active sites. Thereby, the calculated $\ln(A)$ values of the CuO/c-Cu₂O catalysts were, respectively, plotted as a function of $\ln(\text{BET surface area})$ and $\ln(\text{edge length})$. As shown in **Figure 3C**, the $\ln(A)$ values of CuO/c-Cu₂O-1029, CuO/c-Cu₂O-682, and CuO/c-Cu₂O-446 are proportional to $\ln(\text{BET surface area})$ with a slope value of 1.75 ± 0.57 , and the $\ln(A)$ values of CuO/c-Cu₂O-109 and CuO/c-Cu₂O-34 are proportional to $\ln(\text{edge length})$ with a slope value of 0.98. These results are in consistent with the kinetic analysis results of DFT calculations, in which the calculated reaction rate expression based on the elementary reactions exhibits a slope value of 2 between $\ln(\text{reaction rate})$ and $\ln(\text{CuO/Cu}_2\text{O}(100) \text{ surface site})$ and a slope value of 1 between $\ln(\text{reaction rate})$ and $\ln(\text{CuO/Cu}_2\text{O}(110) \text{ surface site})$. Furthermore, the reaction orders of CO and O₂ derived from reaction rate equation (described below) in two representative CuO/c-Cu₂O catalysts are calculated (**Figure 3D**), whose values are also in consistent with the DFT calculation results. These kinetic analysis results in combination with DFT calculations successfully demonstrate the structure of active sites with the switch of dominant surface sites contributing to the catalytic activity in CO oxidation reaction from face sites for large c-Cu₂O nanocrystals to edge sites for fine c-Cu₂O nanocrystals.

The Arrhenius equation is also suitable for some complex reactions [16–18], such as the oxidative dehydrogenation of propane (ODHP) to selectively produce propene. You et al. [16] reported that the NbO_x/CeO₂-rod catalysts applied for such a reaction and the calculated E_a values derived from the Arrhenius plots with stable C₃H₈ conversions below 15% without the mass transfer effect and heat transfer effect are dependent on the catalyst structure (**Figure 4**). NbO_x/CeO₂-rod catalysts show a higher E_a value of about 65 kJ mol^{-1} than that of CeO₂ rods with a E_a value of about 45 kJ mol^{-1} , proving that the loading of NbO_x onto CeO₂ rods suppresses their

**Figure 3.**

(A) Stable light-off curves of the CuO/c-Cu₂O structures in different sizes during the oxidation of CO and (B) the corresponding Arrhenius plots; (C) calculated apparent pre-exponential factors ($\ln A$) as a function of the measured BET surface area and the calculated edge length; (D) reaction rates as a function of the partial pressures of CO and O₂: (a) CuO/c-Cu₂O-1029, (b) CuO/c-Cu₂O-682, (c) CuO/c-Cu₂O-446, (d) CuO/c-Cu₂O-109, and (e) CuO/c-Cu₂O-34 [8]. Copyright © 2019, Wiley-VCH Verlag GmbH & Co.

intrinsically catalytic activity. These results clearly demonstrate a wide application for the Arrhenius equation in heterogeneous catalysis. As the science advance, its physical significant is constantly being interpreted with a large amount of analysis of experimental data; therefore, it has a comprehensive guiding significance for chemical kinetics.

2.2 Reaction rate equation and its application in heterogeneous catalysis

Reaction rate equation is an equation of utilizing the concentration or partial pressure of reactants to calculate the reaction rate of chemical reaction. The general expression (Eq. (5)) and differential expression (Eq. (6)) are listed, in which r represents the reaction rate, k represents the rate constant, A and B represent the reactants, and x and y represent the reaction orders of A and B , respectively.

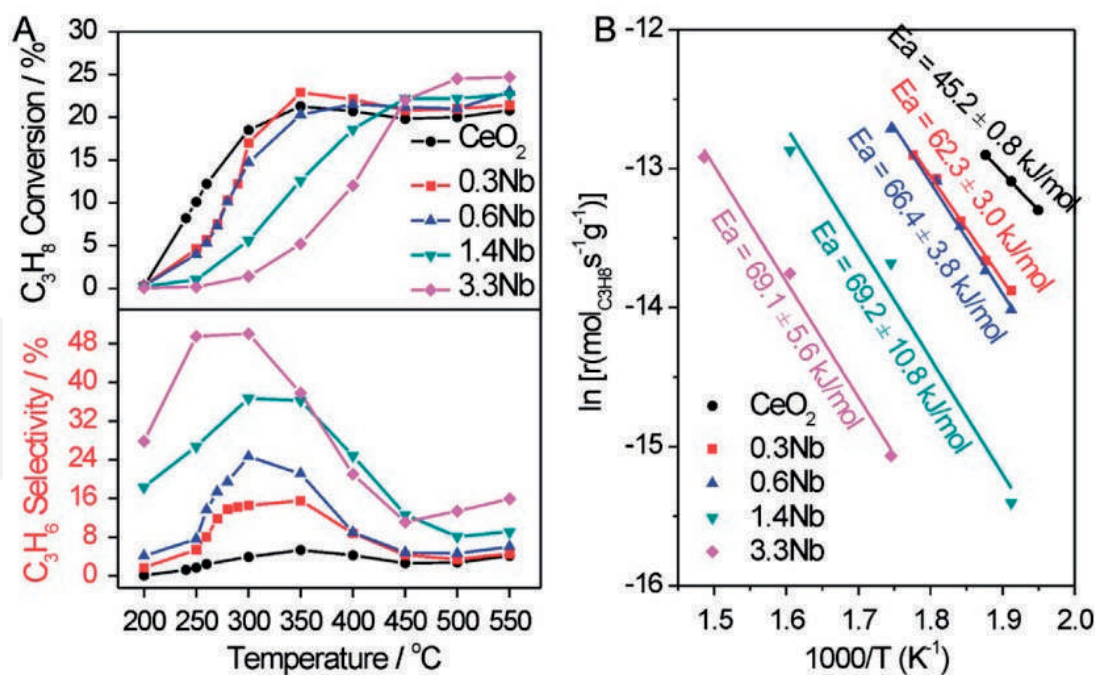


Figure 4. (A) C₃H₈ conversion and C₃H₆ selectivity of CeO₂ rods and NbO_x/CeO₂ catalysts in the oxidative dehydrogenation of propane reaction and (B) the corresponding Arrhenius plots with calculated apparent activation energies (E_a) [16]. Copyright © 2017, Elsevier.

The reaction orders are determined by the reaction process. Normally, the reaction order is equal to the stoichiometric number of chemical reaction in elementary reaction, while the values are generally not equal in nonelementary reaction. Therefore, it has a complex reaction rate expression in many catalytic reactions that lead to a difficult identification of reaction mechanism.

$$r = k [A]^x [B]^y \quad (5)$$

$$\ln \left(\frac{d[A]}{dt} \right) = \ln k + n \ln [A] \quad (6)$$

For a sample heterogeneous catalytic reaction involving a typical MvK mechanism, such as the above-mentioned CO oxidation reaction in **Figure 3D** [8], the calculated reaction orders of CO and O₂ are 1 and 0, respectively, indicating that the catalytic reaction is only dependent on CO but not on O₂. Such dependence suggests the adsorption of CO and O₂ onto catalyst surface proceeded step by step, as well as the rate-determining step prior to the O₂ adsorption process. Thereby, it can be reasonably proposed that the CO oxidation reaction catalyzed by the facet sites and edge sites of CuO/c-Cu₂O catalysts is both proceeding with the MvK mechanism.

But for complex reactions, the reaction mechanism is hardly proposed by the reaction orders [19–21]. However, the reaction orders are still useful to speculate the important catalytic process, especially in determining the rate-determining step of catalytic reaction [22–25]. A typical example is in the preparation of formic acid, an important chemical in the H₂ storage and other industrial applications, from CO₂ hydrogenation. The support plays a key role in determining the catalytic mechanism of CO₂ hydrogenation into formic acid, which has been confirmed in our previous report by using two common metal oxide (CeO₂ and ZnO) supported Pd catalysts dominantly based on the apparent kinetic analysis and in situ DRIFTS results [22]. The calculated E_a values are similar on Pd/CeO₂ catalysts with different Pd loadings but distinctly different on Pd/ZnO catalysts with different Pd

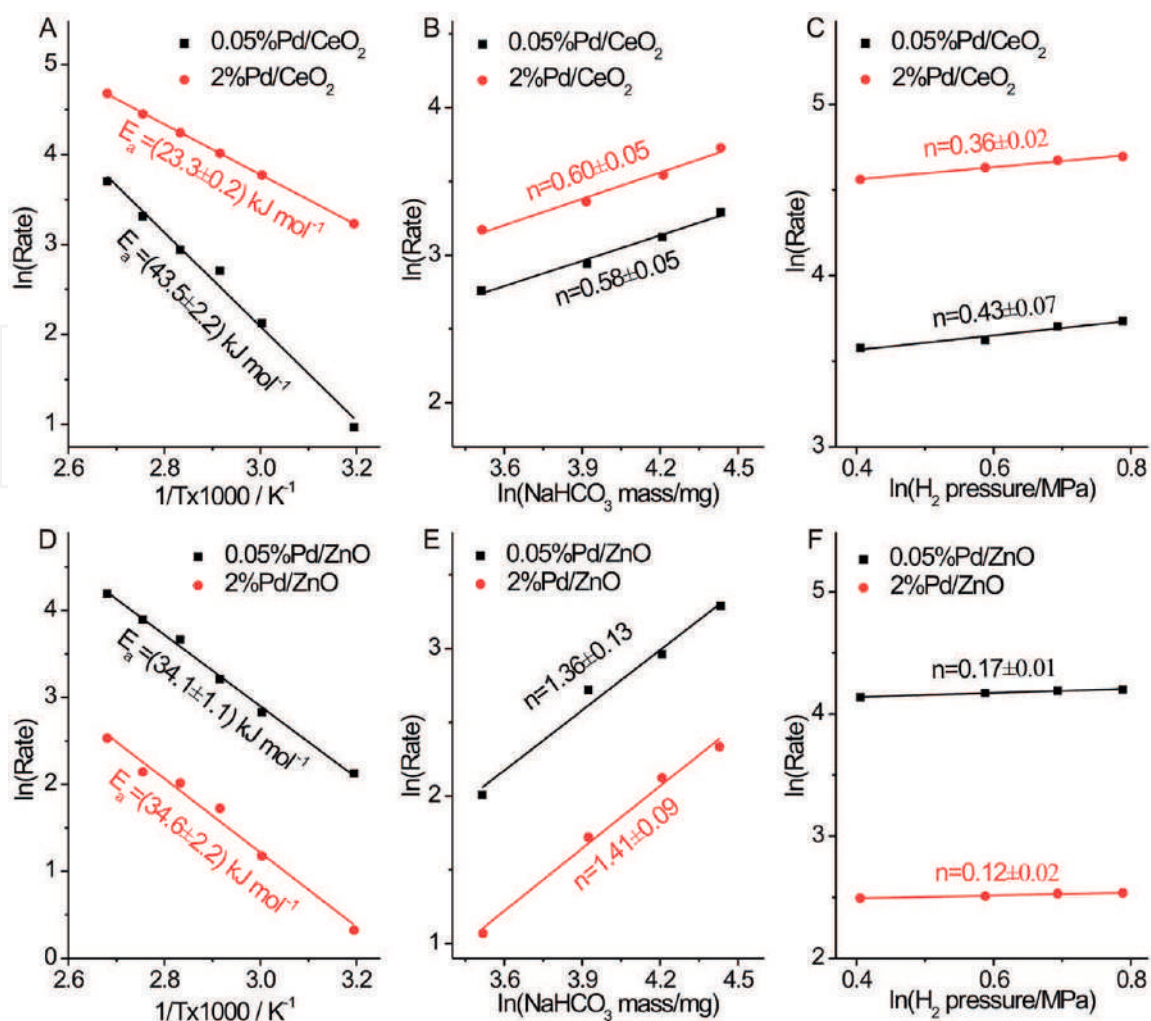


Figure 5.

The Arrhenius plots of (A) 0.05%Pd/CeO₂ and 2%Pd/CeO₂ catalysts and (D) 0.05%Pd/ZnO and 2%Pd/ZnO catalysts; CO₂ reaction orders of (B) 0.05%Pd/CeO₂ and 2%Pd/CeO₂ catalysts and (E) 0.05%Pd/ZnO and 2%Pd/ZnO catalysts at 373 K; and H₂ reaction orders of (C) 0.05%Pd/CeO₂ and 2%Pd/CeO₂ catalysts and (F) 0.05%Pd/ZnO and 2%Pd/ZnO catalysts at 373 K [22]. Copyright © 2019, Elsevier.

loadings (**Figure 5A** and **D**), suggesting that the catalytic performance on Pd/CeO₂ catalysts is affected by the Pd structures. The reaction orders of CO₂ and H₂ clearly demonstrate that the rate-determining step of CO₂ hydrogenation to formic acid on Pd/ZnO catalysts involves a CO₂-contained elementary reaction due to a relatively higher CO₂ reaction order (~ 1.4) (**Figure 5B** and **E**) and of CO₂ hydrogenation to formic acid on Pd/CeO₂ catalysts involves a H₂-contained elementary reaction due to a relatively higher H₂ reaction order (~ 0.4) (**Figure 5C** and **F**). H₂ is generally activated on Pd, and thus, the structure of Pd affects the catalytic performance of Pd/CeO₂ catalysts but not that of Pd/ZnO catalysts, in consistent with their calculated E_a results.

This conclusion is further proved by Pd/ZrO₂ catalyzed CO₂ hydrogenation into formate (**Figure 6**) [23]. Experimental observation results in CO₂-TPD profiles (detailed description shown in Ref. [23]) showed the basicity densities following an order of 2%Pd/ZrO₂-T (Tetragonal ZrO₂) > 2%Pd/ZrO₂-M&T (Mixed ZrO₂) \approx 2%Pd/ZrO₂-M (Monoclinic ZrO₂), in consistent with the intrinsic activity order. Comparing the reaction orders of H₂ and CO₂ on 2%Pd/ZrO₂-T and 2%Pd/ZrO₂-M catalysts, similar H₂ reaction orders were observed, while the CO₂ reaction orders were higher on 2%Pd/ZrO₂-M catalyst than that on 2%Pd/ZrO₂-T catalyst. These results clearly demonstrate that the catalytic performance of Pd/ZrO₂ catalyst in CO₂ hydrogenation into formate is strongly dependent on the

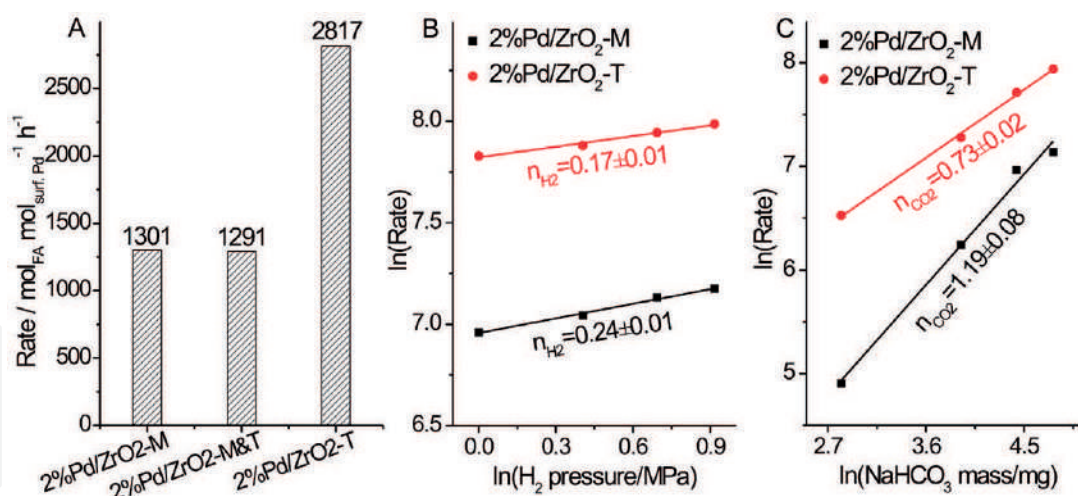


Figure 6.
 (A) Production rate (mol_{HCOO} · mol_{surf. Pd}⁻¹ h⁻¹) of formate on representative various 2%Pd/ZrO₂ catalysts based on the surface Pd atoms; reaction orders of (B) H₂ and (C) bicarbonate of 2%Pd/ZrO₂-M and 2%Pd/ZrO₂-T catalysts [23]. Copyright © 2019, Elsevier.

surface basicity densities, 2%Pd/ZrO₂-T support holds the higher surface basicity densities, and thus, Pd/ZrO₂-T catalyst is more active in catalyzing the formate production.

Reaction rate equation is the real reflection of chemical reaction rate. It has been widely used as an important method in investigating the catalytic mechanism. However, several factors, including temperature, chemical reaction, concentration, pressure, order, solvent, light, and catalyst, strongly affect the rate of a chemical reaction. Among them, temperature usually plays a key factor. Generally, the rate of a chemical reaction increases with an increase in reaction temperature because higher kinetic energy can result in more collisions between the reactant molecules. The increase of collision chance will cause the catalytic reaction more likely to happen. The temperature effect on reaction rate can be quantified by the Arrhenius equation. Notably, some reaction rates are negatively affected by the temperature, while some others are independent of temperature. The chemical reaction, concentration, pressure, and order directly determine the reaction rate. In chemical reaction, the complexity of the reaction and the state of the reactants are important. Such as, the reaction of a powder in a solution always proceeds faster than the reaction of a large chunk of a solid. Concentration, pressure, and order are the important parameters of reaction rate equation and thus directly affect the reaction rate. Solvent, light, and catalyst are the external factors that generally do not participate in a reaction but affect the reaction rate. In familiar with these influence factors, it can guide us to better understand and apply the reaction rate equation.

3. Summary and outlook

In summary, this chapter introduced the Arrhenius equation and reaction rate equation, two important equations in chemical kinetics, and their applications in heterogeneous catalysis in detail. By the analysis of some specific reactions in the documents, the Arrhenius equation could be used to calculate the E_a and A values in catalytic reaction, which were related to the intrinsic activity of the number of active sites, respectively. The reaction rate equation could be used to calculate the reaction order of a single reactant that was useful in speculating the contribution of a single reactant in catalytic reaction. Through these investigations of chemical kinetic equations in catalytic reaction and further combining with DFT

calculations, it well proposed the structure of active sites and the catalytic mechanism in catalytic reaction and thus established the concept of catalyst structure-catalytic property relationships. These would be promising to guide the structural design and controlled synthesis of novel efficient catalytic materials in the future.

Nowadays, the development of chemical kinetics is very rapid and the contained fields gradually enlarged with the research mode from basement state turning to excitation state, from small molecule turning to big molecule, and from gas phase turning to condensed phase. Benefiting from the improvement of advanced characterization skills, especially in the development of surface analysis and intermediate tracking skills, the catalytic science has become the frontier field of chemical kinetics. Furthermore, the progress of basic theory method also accelerates the application and development of chemical kinetics in catalytic science. The combination of theory and experiment can help to gain a deep insight into how various elementary reactions occur. The combination of more precise experimental results with more precise theoretical research is a powerful driving force for the continued development of this research field. Practice once again proves that the close combination of theory and experiment is the only way for the development of science.

Acknowledgements

Thanks to Li-Ping Fan and Yue-Juan Wang who provided the partial writing materials and also commented on the manuscript. This work was financially supported by Shuang-long Scholars Program, Special Foundation of Youth Scholars of Zhejiang Normal University, and Natural Science Foundation of Zhejiang Province (LQ20B030007).

Conflict of interest


The authors declare no conflict of interest.

Author details

Zhenhua Zhang*, Li-Ping Fan and Yue-Juan Wang
Key Laboratory of the Ministry of Education for Advanced Catalysis Materials,
Institute of Physical Chemistry, Zhejiang Normal University, Jinhua, China

*Address all correspondence to: hanyuzh@mail.ustc.edu.cn

IntechOpen

© 2020 The Author(s). Licensee IntechOpen. Distributed under the terms of the Creative Commons Attribution - NonCommercial 4.0 License (<https://creativecommons.org/licenses/by-nc/4.0/>), which permits use, distribution and reproduction for non-commercial purposes, provided the original is properly cited. 

References

- [1] Gillespie DT. Deterministic limit of stochastic chemical kinetics. *Journal of Physical Chemistry B*. 2009;**113**: 1640-1644. DOI: 10.1021/jp806431b
- [2] Gillespie DT. Stochastic simulation of chemical kinetics. *Annual Review of Physical Chemistry*. 2007;**58**:35-55. DOI: 10.1146/annurev.physchem.58.032806.104637
- [3] Frennet A, Hubert C. Transient kinetics in heterogeneous catalysis by metals. *Journal of Molecular Catalysis A: Chemical*. 2000;**163**:163-188. DOI: 10.1016/S1381-1169(00)00385-X
- [4] Huang W. Crystal plane-dependent surface reactivity and catalytic property of oxide catalysts studied with oxide nanocrystal model catalysts. *Topic in Catalysis*. 2013;**56**:1363-1376. DOI: 10.1007/s11244-013-0139-6
- [5] Huang W. Surface chemistry of solid catalysts. *Scientia Sinica Chimica*. 2018;**48**:1076-1093. DOI: 10.1360/N032018-00033
- [6] Chen S, Xiong F, Huang W. Surface chemistry and catalysis of oxide model catalysts from single crystals to nanocrystals. *Surface Science Reports*. 2019;**74**:100471. DOI: 10.1016/j.surfrep.2019.100471
- [7] Bao H, Zhang W, Hua Q, Jiang Z, Yang J, Huang W. Crystal-plane-controlled surface restructuring and catalytic performance of oxide nanocrystals. *Angewandte Chemie International Edition*. 2011;**50**:12294-12298. DOI: 10.1002/anie.201103698
- [8] Zhang Z, Wu H, Yu Z, Song R, Qian K, Chen X, et al. Site-resolved Cu₂O catalysis in the oxidation of CO. *Angewandte Chemie International Edition*. 2019;**58**:4276-4280. DOI: 10.1002/anie.201814258
- [9] Bai Y, Zhang W, Zhang Z, Zhou J, Wang X, Wang C, et al. Controllably interfacing with metal: A strategy for enhancing CO oxidation on oxide catalysts by surface polarization. *Journal of the American Chemical Society*. 2014;**136**:14650-14653. DOI: 10.1021/ja506269y
- [10] Bao H, Zhang Z, Hua Q, Huang W. Compositions, structures, and catalytic activities of CeO₂@Cu₂O nanocomposites prepared by the template-assisted method. *Langmuir*. 2014;**30**:6427-6436. DOI: 10.1021/la501406w
- [11] Zhang Z, Song R, Yu Z, Huang W. Crystal-plane effect of Cu₂O templates on compositions, structures and catalytic performance of Ag/Cu₂O nanocomposites. *CrystEngComm*. 2019;**21**:2002-2008. DOI: 10.1039/c8ce02164c
- [12] Li D, You R, Yang M, Liu Y, Qian K, Chen S, et al. Morphology-dependent evolutions of sizes, structures, and catalytic activity of Au nanoparticles on anatase TiO₂ nanocrystals. *Journal of Physical Chemistry C*. 2019;**123**:10367-10376. DOI: 10.1021/acs.jpcc.9b00262
- [13] Zhang Z, Wang S-S, Song R, Cao T, Luo L, Chen X, et al. The most active Cu facet for low-temperature water gas shift reaction. *Nature Communications*. 2017;**8**:488-497. DOI: 10.1038/s41467-017-00620-6
- [14] Bu Y, Weststrate CJ, Niemantsverdriet JW, Fredriksson HOA. Role of ZnO and CeO_x in Cu-based model catalysts in activation of H₂O and CO₂ dynamics studied by in situ ultraviolet-visible and X-ray photoelectron spectroscopy. *ACS Catalysis*. 2016;**6**:7994-8003. DOI: 10.1021/acscatal.6b02242
- [15] Graciani J, Mudiyansele K, Xu F, Baber AE, Evans J, Senanayake SD,

- et al. Highly active copper-ceria and copper-ceria-titania catalysts for methanol synthesis from CO₂. *Science*. 2014;**345**:546-550. DOI: 10.1126/science.1253057
- [16] You R, Zhang X, Luo L, Pan Y, Pan H, Yang J, et al. NbO_x/CeO₂-rods catalysts for oxidative dehydrogenation of propane: Nb-CeO₂ interaction and reaction mechanism. *Journal of Catalysis*. 2017;**348**:189-199. DOI: 10.1016/j.jcat.2016.12.012
- [17] Sun B, Gu C, Ma J, Liang B. Kinetic study on TEMPO-mediated selective oxidation of regenerated cellulose. *Cellulose*. 2005;**12**:59-66. DOI: 10.1023/B:CELL.0000049409.56806.da
- [18] Sinev I, Kardash T, Kramareva N, Sinev M, Tkachenko O, Kuchеров A, et al. Interaction of vanadium containing catalysts with microwaves and their activation in oxidative dehydrogenation of ethane. *Catalysis Today*. 2009;**141**:300-305. DOI: 10.1016/j.cattod.2008.04.021
- [19] Jia A-P, Hu G-S, Meng L, Xie Y-L, Lu J-Q, Luo M-F. CO oxidation over CuO/Ce_{1-x}Cu_xO_{2-δ} and Ce_{1-x}Cu_xO_{2-δ} catalysts: Synergetic effects and kinetic study. *Journal of Catalysis*. 2012;**289**:199-209. DOI: 10.1016/j.jcat.2012.02.010
- [20] Li N, Chen Q-Y, Luo L-F, Huang W-X, Luo M-F, Hu G-S, et al. Kinetic study and the effect of particle size on low temperature CO oxidation over Pt/TiO₂ catalysts. *Applied Catalysis B: Environmental*. 2013;**142-143**:523-532. DOI: 10.1016/j.apcatb.2013.05.068
- [21] Liu H-H, Wang Y, Jia A-P, Wang S-Y, Luo M-F, Lu J-Q. Oxygen vacancy promoted CO oxidation over Pt/CeO₂ catalysts: A reaction at Pt-CeO₂ interface. *Applied Surface Science*. 2014;314725-314734. DOI: 10.1016/j.apsusc.2014.06.196
- [22] Zhang Z, Zhang L, Yao S, Song X, Huang W, Hülsey MJ, et al. Support-dependent rate-determining step of CO₂ hydrogenation to formic acid on metal oxide supported Pd catalysts. *Journal of Catalysis*. 2019;**376**:57-67. DOI: 10.1016/j.jcat.2019.06.048
- [23] Zhang Z, Zhang L, Hülsey MJ, Yan N. Zirconia phase effect in Pd/ZrO₂ catalyzed CO₂ hydrogenation into formate. *Molecular Catalysis*. 2019;**475**:110461. DOI: 10.1016/j.mcat.2019.110461
- [24] Harrington DA. The rate-determining step in electrochemical impedance spectroscopy. *Journal of Electroanalytical Chemistry*. 2015;**737**:30-36. DOI: 10.1016/j.jelechem.2014.06.003
- [25] Oh H-S, Nong H-N, Reier T, Gliech M, Strasser P. Oxide-supported Ir nanodendrites with high activity and durability for the oxygen evolution reaction in acid PEM water electrolyzers. *Chemical Science*. 2015;**6**:3321-3328. DOI: 10.1039/c5sc00518c

Advancements in the Fenton Process for Wastewater Treatment

Min Xu, Changyong Wu and Yuexi Zhou

Abstract

Fenton is considered to be one of the most effective advanced treatment processes in the removal of many hazardous organic pollutants from refractory/toxic wastewater. It has many advantages, but drawbacks are significant such as a strong acid environment, the cost of reagents consumption, and the large production of ferric sludge, which limits Fenton's further application. The development of Fenton applications is mainly achieved by improving oxidation efficiency and reducing sludge production. This chapter presents a review on fundamentals and applications of conventional Fenton, leading advanced technologies in the Fenton process, and reuse methods of iron containing sludge to synthetic and real wastewaters are discussed. Finally, future trends and some guidelines for Fenton processes are given.

Keywords: Fenton, Fenton-like, Fenton sludge, reuse, application

1. Introduction

The presence of many organic pollutants in wastewater, surface water, and groundwater may result from contaminated soil, agricultural runoff, industrial wastewater, and hazardous compounds storage leakage [1]. These organic pollutants, such as volatile phenols, benzene, and benzene derivatives, are considered highly toxic and low biodegradable. In some instances, conventional treatment methods such as biological processes are not sufficient to remove them. In order to improve water quality, advanced treatment is needed to remove the refractory organics.

Fenton is an effective advanced treatment process. The hydroxyl radical ($\cdot\text{OH}$) can be generated from the reaction between aqueous ferrous ions and hydrogen peroxide (H_2O_2), and it can destroy refractory and toxic organic pollutants in wastewater [2]. Fenton discovered the Fenton reaction in 1894, and he reported that H_2O_2 could be activated by ferrous (Fe^{2+}) salts to oxidize tartaric acid. However, its application as an oxidizing process for destroying toxic organics was achieved until the late 1960s [3]. Fenton was mainly used to treat wastewater by radical oxidation and flocculation. H_2O_2 is catalyzed by ferrous ions to decompose into $\text{HO}\cdot$ and to trigger the production of other radicals, which can fully oxidize organic matters. The hydroxyl radical ($\cdot\text{OH}$) has a strong oxidation capacity (standard potential = 2.80 V versus standard hydrogen electrode) [4]. Hydroxyl radicals can effectively oxidize refractory organic pollutants in wastewater and even completely mineralized them into CO_2 , water, and inorganic salts [5]. Meanwhile,

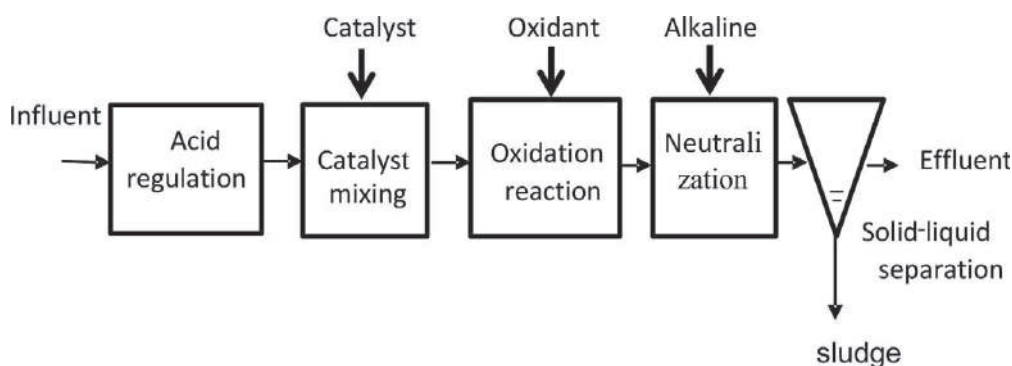


Figure 1.
Schematic diagram of the Fenton process.

the iron complex produced in the treatment of wastewater by Fenton will play the role of flocculant.

The conventional Fenton continuous flow process configuration, as illustrated in **Figure 1**, including acid regulation, catalyst mixing, oxidation reaction, neutralization, and solid–liquid separation. Fenton has many advantages, such as its high performance and simplicity (operated at room temperature and atmospheric pressure) for the oxidation of organics [6] and its non-toxicity [7] (H_2O_2 can break down into environmentally safe species like H_2O and O_2). However, Fenton also has some inherent disadvantages, which limit its application and promotion. For example, strict pH range, high H_2O_2 consumption, and the accumulation of ferric sludge that affects the oxidation efficiency [8, 9]. In order to overcome these disadvantages, the enhancement of the Fenton process has attracted much attention from researchers. Both heterogeneous and homogeneous catalysts were used to replace Fe^{2+} , including ferric oxide [10], iron minerals [11], and nano zero-valent iron [12].

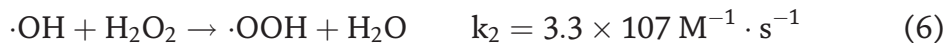
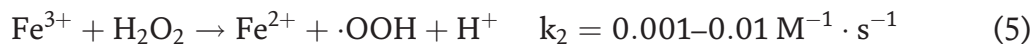
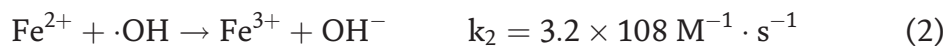
On the one hand, the loss of iron and the consequent sludge generation can be reduced by using reductant or transition metal, giving rise to a heterogeneous Fenton process. On the other hand, some external energy was introduced into the Fenton and Fenton-like processes to form photo-Fenton/Fenton-like processes [13, 14], electro-Fenton-like processes [15, 16], and so on [17, 18]. Hence, this work mainly summarizes the recent advancements in the Fenton process related to improving Fenton oxidation efficiency and minimizing sludge production. It also describes the main drawbacks and potential applications based on recent developments. Some recommendations are also stated in the Conclusions section.

2. Fenton process

Currently, two mechanisms have been proposed to explain the degradation of organic matters by Fenton reaction. One is the Harber-Weiss mechanism [19], which considered that active oxide species $\cdot\text{OH}$ are generated to degrade organics in Fenton reaction. The other is the mechanism of high iron oxide intermediates, which was proposed by Bray and Gorin [20]. They suggested that the strong oxidizing iron substances (FeO^{2+} , FeO^{3+}) were produced in Fenton reaction, rather than $\cdot\text{OH}$. With the development of spectroscopy and chemical probe method, it is generally accepted that the formation of $\cdot\text{OH}$ initiates the Fenton oxidation.

The traditionally accepted Fenton mechanism is represented by Eqs. (1)–(7) [21].





According to the above equation, ferrous iron (Fe^{2+}) was rapidly oxidized to ferric ions (Fe^{3+}), while Fe^{2+} is regenerated from the so-called Fenton-like reaction between Fe^{3+} and H_2O_2 at a very slow rate. Equation (1) is usually considered as the core of the Fenton reaction.

The Fenton process is usually operated under the solution pH value of 3. The oxidation activity of $\cdot\text{OH}$ is related to the solution pH. The oxidation potential of $\cdot\text{OH}$ increases and the oxidation capacity is enhanced with decreasing pH [22, 23]. In addition, the activity of Fenton reagent is reduced with increasing pH due to the lack of active Fe^{2+} , in which the formation of inactive iron oxohydroxides and ferric hydroxide precipitate. Meanwhile, auto-decomposition of H_2O_2 appears at high pH [24].

At very low pH values, iron complex species $[\text{Fe}(\text{H}_2\text{O})_6]^{2+}$ and stable oxonium ion $[\text{H}_3\text{O}_2]^+$ exist, which reduces the reactivity between Fe^{2+} and H_2O_2 [25, 26]. Therefore, the efficiency of the Fenton process to degrade organic compounds is reduced both at high and low pH. In addition, there are many competitive reactions in the Fenton reaction system. In Fenton oxidation, the reaction rate is dependent on the iron dosage, while the extent of mineralization is directly related to the concentration of oxidant.

It is important to understand the mutual relationships between Fenton reagent in terms of $\cdot\text{OH}$ production and consumption. These relationships were investigated and classified them into three categories according to the quantity of the $[\text{Fe}^{2+}]_0/[\text{H}_2\text{O}_2]_0$ ratio (initial concentration of Fe^{2+} versus initial concentration of H_2O_2) [27]. Their results showed that $[\text{Fe}^{2+}]_0/[\text{H}_2\text{O}_2]_0$ ratio and organics can affect the competition in Fenton reaction paths.

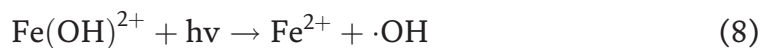
The main disadvantages for the application of the Fenton process are the relatively high cost of H_2O_2 and the high amount of ferric sludge produced in the neutralization step of the treated solution before disposal. These drawbacks and the more increasingly stringent water regulations are a challenge to develop solutions addressed to improve the Fenton technology. On one hand, the energy was introduced into Fenton to enhance the $\cdot\text{OH}$ generation, such as photo-Fenton, electro-Fenton, and so on. On the other hand, iron-based catalysts and reuse of Fenton sludge were developed as a Fenton-like reaction.

3. Enhanced Fenton process

3.1 Photo-Fenton process

The classic Fenton reaction efficiency was affected by the conversion rate from Fe^{3+} to Fe^{2+} . Recent methods have promoted the in situ circulation from Fe^{3+} to Fe^{2+} . A combination of hydrogen peroxide and UV radiation with Fe^{2+} or Fe^{3+} oxalate ion [photo-Fenton (PF) process] produces more $\cdot\text{OH}$ compared to the conventional Fenton method [28]. The hydroxy- Fe^{3+} complexes after Fenton reaction mainly exists in the form of $\text{Fe}(\text{OH})^{2+}$ at pH 2.8–3.5. The photochemical regeneration of Fe^{2+} by photo-reduction (Eq. (8)) of ferric Fe^{3+} occurs in the photo-Fenton

reaction. The newly generated Fe^{2+} reacts with H_2O_2 and generates $\cdot\text{OH}$ and Fe^{3+} , and the cycle continues:



Direct photolysis of H_2O_2 (Eq. (9)) produces $\cdot\text{OH}$, which can be used for the degradation of organic compounds, and in turn increases the rate of degradation of organic pollutants [29].



However, photo-Fenton gives a better degradation of low concentration organic pollutants. Because the high concentration organic pollutants could reduce the absorb radiation of iron complex, which needs a longer radiation time and more H_2O_2 dosage.

Excess H_2O_2 can easily capture $\cdot\text{OH}$. In order to improve the efficiency of photo-Fenton, several organic ligands such as EDTA, EDDS, oxalate, and other organic carboxylic acid were added and complexed with Fe^{3+} under photocatalysis [29, 30]. The positive effects achieved by these ions can be attributed to the following aspects: (i) iron-ligands having higher ability compete for UV light in a wide wavelength range compared to other Fe^{3+} -complexes, and promoting the reduction of ferric ion to ferrous ion and accordingly, regeneration of higher amounts of $\cdot\text{OH}$, (ii) Promoting H_2O_2 activation and $\cdot\text{OH}$ radical generation, (iii) improving iron dissolution at pH 7.0, and (iv) operating over the broad range of the solar radiation spectrum [14].

Compared with the classic Fenton, photo-Fenton has many advantages. A photo-induced $\text{Fe}^{3+}/\text{Fe}^{2+}$ redox cycle could decrease the dosage of catalyst in Fenton, which effectively reduce the formation of iron sludge [31–33]. Meanwhile, solar or UV light can increase the utilization of H_2O_2 , and possess photolysis on several small molecule organics. However, photo-Fenton has many disadvantages, such as low utilization of visible light, the required UV energy for a long time, high energy consumption, and cost.

3.2 Electro-Fenton process

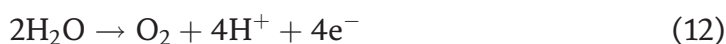
Electrochemical processes can be combined with Fenton processes (EF processes) during WW treatment to improve the Fenton processes. Fe^{2+} and H_2O_2 were produced by the electrochemical method as Fenton reagent. The electro-Fenton process follows the reaction shown below [34, 35], where H_2O_2 can be generated in situ via a two-electron reduction of dissolved oxygen on the surface of the cathode in an acidic solution when the electrochemical process is applied (reaction Eq. (10)).



Also, the produced ferric ion from Eq. (1) can be reduced to Fe^{2+} by electrochemical regeneration of Fe^{3+} ions on the cathode surface:



Water was oxidized to oxygen ta the anode (Eq. (12)):



$\cdot\text{OH}$ was also generated at the surface of a high-oxygen overvoltage anode from water oxidation:



Compared with tradition Fenton reaction, electro-Fenton has certain advantages, including (i) the production of H_2O_2 in situ via an electrochemical processes is beneficial for an increase in the organics degradation efficiency, a decrease in the cost, and a reduction in the risks associated with transportation; (ii) ferrous ion is regenerated through the reduction of ferric ions on the cathode, which reduces the production of iron sludge; and (iii) realizing the diversification of organics degradation pathway, such as Fenton oxidation, anodic oxidation, flocculation, and electric adsorption [36].

Electro-Fenton gives a better degradation of alachlor than the tradition Fenton. However, electro-Fenton processes have some problems with respect to H_2O_2 production. The production of H_2O_2 is slow because oxygen has low solubility in water and the current efficiency under reduced pH ($\text{pH} < 3$) is low. In addition, the efficiency of the electro-Fenton process depends on electrode nature, pH, catalyst concentration, electrolytes, dissolved oxygen level, current density, and temperature [37].

3.3 Sono-Fenton process

The combined treatment using ultrasound with Fenton reagent is known as sono-Fenton, which provides a synergistic effect on organic degradation [38, 39]. Ultrasound can enhance the Fenton's oxidation rate due to the generation of more $\cdot\text{OH}$ caused by the cavitation within ultrasonic irradiation.

The physical effect of cavitation is the generation of intense convection in the medium through the phenomena of microturbulence and shock waves, whereas the chemical effect of cavitation is the generation of radical species, such as oxygen ($\cdot\text{O}$), hydroperoxyl ($\cdot\text{OOH}$), and $\cdot\text{OH}$ through the dissociation of solvent vapor during transient collapse of cavitation bubbles [40]. On the other hand, Fe^{3+} continuously reacts with H_2O_2 , according to Eq. (5). A part of Fe^{3+} after a Fenton reaction exists in the form of $\text{Fe}-\text{OOH}^2$. $\text{Fe}-\text{OOH}^2$ can be quickly decomposed into Fe^{2+} and $\cdot\text{OOH}$; thereby, the phenomenon promotes the $\text{Fe}^{3+}/\text{Fe}^{2+}$ redox cycle [41]. In addition, ultrasound provides stirring and mass transfer effects to promote the diffusion of reactants in solution and improve the efficiency of Fenton reaction. However, sono-Fenton has some disadvantages, such as high cost and energy-intensive, so it is limited in practical application.

3.4 Fenton combined with other wastewater treatment technologies

The physical, chemical, and biological technologies have been widely used to treat wastewater. However, most of the real wastewater contains many organic pollutants with high toxicity and low biodegradability [42]. So that biological technologies are not enough. Moreover, the physical and chemical techniques are often effective for color, macromolecular organics, and suspended matter removal.

In order to improve the wastewater quality, advanced treatment needs the removal of refractory organics from the wastewater. In recent years, Fenton has been used to treat refractory wastewater by combining it with other wastewater-treatment technologies. The application of the Fenton oxidation process, as a pre-treatment, oxidizes refractory organics and improves the biodegradability, solubility, and coagulation, which are beneficial to the subsequent treatment.

Fenton was proved to be a feasible technique as the pre-oxidation for polluted pharmaceutical wastewater. Fenton as a pre-treatment process increased the BOD₅/COD value from 0.26 to 0.5, and also removed chloramphenicol, diclofenac, p-aminophenol, benzoic acid, and other toxic organics in the final effluent results from the Fenton-biological treatment processes [43].

Compared with biological treatment alone, Fenton-biological treatment processes improved COD removal [44]. Fenton combined with membrane filtration was also used to treat pharmaceutical wastewater. Although single nanofiltration (NF) and Fenton could effectively remove pharmaceutical active compounds, high organic load favored membrane fouling, and resulting in flux decline. The calcium salts were found to be the main fouling on the NF membrane surface. Fenton as the pre-treatment could ensure higher flux for the NF process. Also, the Fenton-NF system was found to be a promising method for wastewater from the pharmaceutical industry containing etodolac [45].

On the other hand, lime/unhair effluent, which contain highly loaded organic hazardous wastes, have been effectively treated by the Fenton-membrane filtration system at the pilot-scale [46]. Fenton was used also as a post-treatment of other treatment technologies for degrading residual organics, including physico-chemical and biological treatment. Compared with the aerobic sequencing batch reactor (SBR), SBR-Fenton could improve the TOC removal rate of textile wastewater up to 12% [47]. The solar photo-Fenton process was found to be an efficient process in removing phytotoxicity from Olive mill wastewater samples [48]. A COD and phenol removal as high as 94 and 99.8% could be achieved in coagulation/flocculation combined with the solar photo-Fenton system [48]. This combined technology, taking into account its reasonable overall cost, can be applied in somewhere with plenty of sunshine. Based on the technological and economic analysis performed, all combined treatment technologies will provide better performance than single treatment.

The Fenton process, combined with biological technologies, has shown quite low operational cost. The integrated Fenton-membrane processes were found efficient in removing organics from the industry wastewater. The phenolic compounds concentrated in the concentrate flow by membrane filtration could be recovered and further valorized in various industries. Although the combined Fenton and membrane technologies show the relatively higher overall cost of the combined membrane technologies, it is necessary to estimate the accuracy of the potential profit from the sale and valorization of these by-products recovered by this process.

4. The application of modified iron source as heterogeneous catalysts in Fenton reactions

The Fenton reaction in which iron salts are used as a catalyst is defined as a homogeneous Fenton process. Nevertheless, there are some disadvantages, including (i) the formation of ferric hydroxide sludge at pH values above 4.0 and its removal, (ii) difficulty in catalyst recycle and reuse, (iii) high energy consumption, and (iv) limitation of operating pH range. Therefore, the application of modified iron source as heterogeneous catalysts in Fenton reaction to overcome the shortcomings of homogeneous catalysis has been widely studied. Different heterogeneous catalysts have been used in Fenton reactions, including zero valent iron [49], iron pillared clays [50], and iron minerals [51]. **Figure 2** shows various types of heterogeneous Fenton-like catalysts.

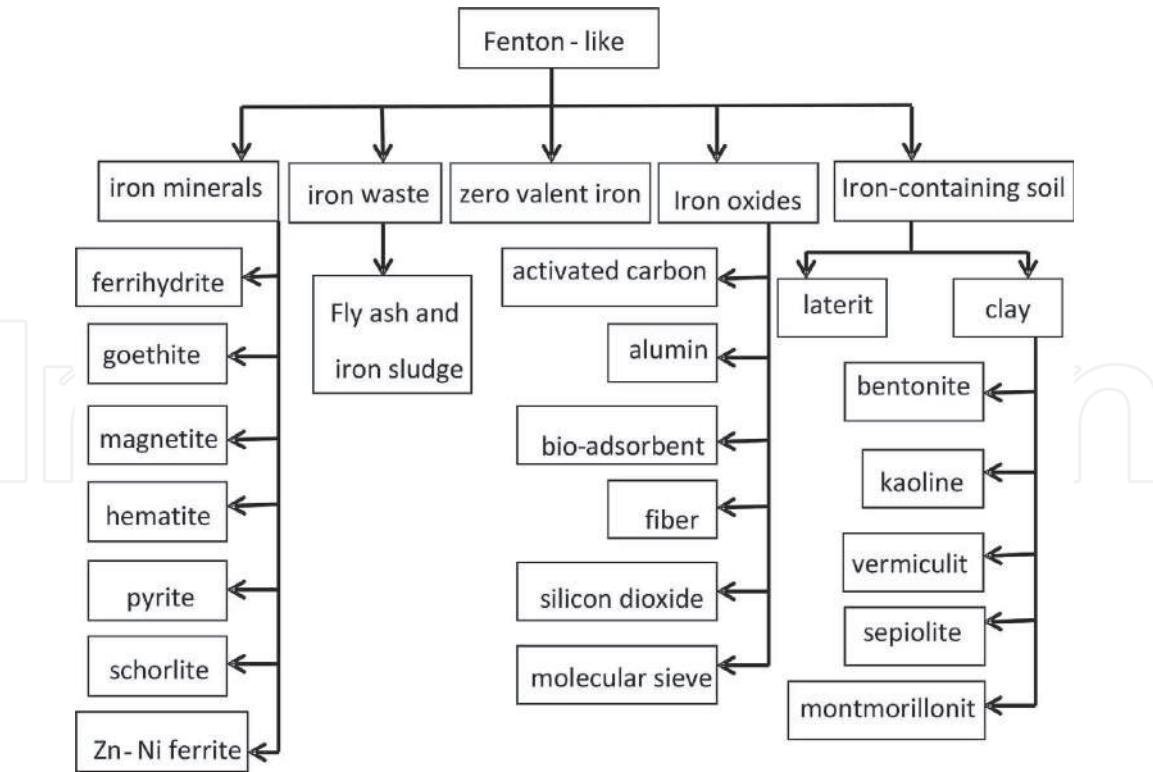


Figure 2.
Iron-containing catalysts.

4.1 Fenton-like reactions using zero-valent iron

Recently, zero-valent iron (Fe^0) has been increasingly used in the heterogeneous Fenton system, due to its large specific surface area and high reactivity. It is reported that the removal of contaminants in the Fe^0 induced heterogeneous Fenton system involves two steps [52–54]: (i) H_2O_2 decomposes on or near the Fe^0 surface to form Fe^{2+} (Eq. (14)); (ii) then, Fenton reaction occurs, Fe^{2+} reacts with H_2O_2 to produce $\cdot\text{OH}$ (Eq. (1)), and contaminants are degraded. Meanwhile, the produced Fe^{3+} is further reduced to Fe^{2+} (Eq. (15)).



The degradation of trichloroethylene (TCE) in nano-scale zero-valent iron (nZVI) Fenton systems with $\text{Cu}(\text{II})$ was investigated [55]. TCE was significantly degraded (95%) in 10 min in the nZVI Fenton system with 20 mM $\text{Cu}(\text{II})$ at initial pH 3, while slight degradation (25%) was observed in nZVI Fenton system without $\text{Cu}(\text{II})$ at the same experimental condition. Because of the high activity on the Fe^0 surface, Fe^0 could easily coalesce into aggregates, which reduced the reactivity. The particle size of Fe^0 is too small to recycle and separate at the end of the treatment.

4.2 Fenton-like reactions using iron oxides

Different physicochemical characteristics of these oxides make them favorable for oxidative reactions, where the surface area, pore size/volume, and the

crystalline structure have significant effects on their activities. The amorphous Fe_2O_3 with the largest surface area has the lowest catalytic efficiency, while the higher efficiency was achieved with crystalline $\alpha\text{-Fe}_2\text{O}_3$, which has a significantly lower surface area [56]. In the Fenton process, magnetite has gained considerable attention than other iron oxides due to its unique characteristic: the magnetically easy separation of magnetite catalysts from the reaction system as a result of its magnetic property.

In many cases, magnetite offered better performance due to the presence of Fe^{2+} cations in its structure [57]. A comparison of the catalytic activity of amorphous iron (III) oxide, maghemite, magnetite, and goethite mixed with quartz was carried out by Hanna et al. [58] for methyl red degradation in presence of H_2O_2 . The authors indicated that the oxidation state of iron in the oxides was the critical parameter, considering that Fe^{2+} is superior to Fe^{3+} in Fenton processes. In this study, magnetite exhibited the highest rate constant normalized to surface area per unit mass of oxide (SSA) at neutral pH value.

4.3 Fenton-like reactions using other iron-containing catalysts

The characteristic of iron materials mainly determines the oxidation efficiency in the heterogeneous Fenton reaction. The design of iron-containing catalysts can improve the activity and stability of the heterogeneous Fenton reaction. In recent years, heterogeneous Fenton catalysts have also been developed in the following aspects: (1) iron-loaded material, that is, iron is loaded on the porous materials, such as carbon nanotubes, clay and molecular sieves by a simple method. These materials are considered as potential heterogeneous Fenton catalysts because of low cost, high specific surface area, rich active sites, and easy separation, (2) new iron-containing materials. In the homogeneous Fenton-like processes, the catalysts used in the Fenton-like processes include Fe^{3+} , Cu^{2+} , Mn^{2+} , Co^{2+} , and Ag^+ . Sometimes organic or inorganic ligands are also used for complexing and stabilizing the metal ion over a wide pH range. The ligands studied include, but are not limited to, citrate, oxalate, edetic acid (EDTA), humic acids, and ethylenediamine succinic acid (EDDS). The catalysts based on different metal elements and ligands were developed to improve the degradation of organics, promote the $\text{Fe}^{3+}/\text{Fe}^{2+}$ redox cycle and decrease the sludge production [59, 60].

5. Reuse of the iron-containing sludge after Fenton reaction

A large amount of ferric sludge generated from the Fenton treatment. The practical applications of the Fenton process are limited, mainly because of neutralization after oxidation. The discharge of ferric sludge easily causes secondary pollution because of residual organics adsorbed and accumulated in ferric sludge from treated wastewater. The disadvantage is, therefore, the main obstacle limiting the development and application of the Fenton process [61].

Two approaches have been studied to minimize the production of sludge as a by-product of the Fenton process, including heterogeneous catalysts and the reuse of the iron-containing sludge [61]. However, the catalytic activity is usually weakened after repetitive use due to active iron leaching [62] or the decay of active catalytic sites [63]. Recently, the reuse of iron-containing Fenton sludge has been drawing increasing interest from researchers world-wide.

5.1 Fenton-like reactions using iron-containing sludge

The iron-containing Fenton sludge was used as an iron source for the synthesis of ferrite catalysts that have drawn much more attention due to their potential application in the fields of catalysis in the Fenton process.

Zhang et al. [64] proposed a novel method for the reuse of Fenton sludge in the synthesis of nickel ferrite particles (NiFe_2O_4). In phenol degradation with H_2O_2 , NiFe_2O_4 alone, and $\text{NiFe}_2\text{O}_4\text{—H}_2\text{O}_2$, the phenol removal was as high as $95 \pm 3.4\%$. However, the phenol removal efficiencies were as low as $5.9 \pm 0.1\%$ and $13.5 \pm 0.4\%$ in H_2O_2 and NiFe_2O_4 alone, respectively. The leaching of iron ion from heterogeneous ferrite catalysts under the acid conditions is a common phenomenon. The leached iron amounted to $6.3 \pm 0.2\%$ of total iron, and the recovery ratio of NiFe_2O_4 catalyst in this study was found to be $97.1 \pm 1.7\%$ [64]. Notably, a rapid electron exchange between Ni^{2+} and Fe^{3+} ions in the NiFe_2O_4 structure could accelerate the conversion of Fe^{3+} to Fe^{2+} , which was beneficial for the Fenton reaction. In addition, the Fe^{3+} on the surface of NiFe_2O_4 particles and the leaching of iron ion from NiFe_2O_4 could also react with the H_2O_2 to induce Fenton reaction.

Therefore, phenol could be effectively removed [64]. Roonasi and Nezhad [65] compared the catalytic activity of nano ferrite M-Fenton sludge ($\text{M} = \text{Cu}, \text{Zn}, \text{Fe}$, and Mn), and CuFe_2O_4 achieved the best performance. Based on the previous studies, a new catalyst $\text{Cu}_2\text{O—CuFe}_2\text{O}_4$ was synthesized by co-sedimentation. Compared with CuFe_2O_4 , $\text{Cu}_2\text{O—CuFe}_2\text{O}_4$ improved the phenol removal. The phenol removal as high as $97.3 \pm 0.4\%$, and the leached iron amounted to 4.77% of total iron in $\text{Cu}_2\text{O—CuFe}_2\text{O}_4\text{—H}_2\text{O}_2$ reaction. The superior catalytic performance was mainly due to the synergistic effect of both Cu^+ and Cu^{2+} as well as $\text{Fe}^{2+}/\text{Fe}^{3+}$ redox pairs [66]. An electron bridge was formed between Cu^+ and Fe^{3+} , which accelerates the formation of Fe^{2+} species in order to boost the reaction rate [66].

5.2 Regenerated the iron-containing sludge by the electrochemical process

Fenton process was employed to treat synthetic dye wastewater with a supply of Fe^{2+} electrolytically generated from iron-containing sludge [67]. The concentration of Fe^{2+} increases linearly (r^2 of 0.94) with increasing electrolysis time, but the amount of total iron provided is enough and not the limiting factor for the electrogeneration of Fe^{2+} . In electro-Fenton reaction, Fe^{3+} and O_2 were reduced to Fe^{2+} and H_2O_2 at the same time on the cathode. So, there exists competition between Fe^{2+} and H_2O_2 production. In order to eliminate the competition and decrease the chemical cost of H_2O_2 , hypochlorous acid (HOCl) was instead of H_2O_2 [68]. Two iron sludge reuse modes were examined to treat 1,4-dioxane in this study: sequencing batch mode and separation batch mode. The current efficiency (CE) in the electrolytic cell is related to the initial iron concentration, the initial iron species, and operation pH. Fe^{3+} ions were perceived to be more suitable for use as the initial iron species in the electrochemical Fenton-type process, where the CE was found independent of the Fe^{3+} concentration. Compared with the sequencing batch mode, the iron recovery ratio was higher in the separation batch mode. Therefore, the separation batch mode is relatively suitable for iron sludge reuse for both the CE and the iron recovery rate [68].

5.3 Regenerated the iron-containing sludge by the thermal method

In order to remove the residual organics adsorbed in the waste sludge and minimize the sludge production. Baking the sludge was a common method [69, 70]. A higher the baking temperature led to less accumulation of organics in sludge.

The iron-containing sludge catalyst showed more activity (superior TPh, COD, and TOC removals) but higher leaching iron and less adsorption at high baking temperature. Also, the BOD₅/COD ratio was dropped by less than 50% [70]. However, the thermal methods will increase the overall cost and operational difficulty. Fe³⁺/Fe²⁺ redox cycle cannot be effectively realized in thermal system, thus, decreasing the catalytic ability of the iron-containing sludge catalyst.

5.4 Regenerated the iron-containing sludge by reduction

Some organic ligands (such as EDTA, EDDS) are used for complexing and regenerating iron-containing sludge to promote the Fe³⁺/Fe²⁺ redox cycle. These organic ligands effectively inhibited the precipitation of Fe³⁺. However, organic ligands such as EDTA were difficult to be biodegraded, which remained in the water and caused the second pollution. These organic ligands cannot efficiently promote the Fe³⁺/Fe²⁺ redox cycle, so reductants were required to help the Fe³⁺ reduction.

Organic reductants such as ascorbic acid, glutamic acid, and catechol were usually used in the Fenton-based process to accelerate the Fe³⁺/Fe²⁺ cycle, enhance the performance of Fenton reaction and expand the range of operation pH. On the other hand, organic reductants can react with ·OH. Because the selectivity of the reaction between reductants and ·OH is different, the degradation efficiency of pollutants is different.

The investigation evaluated the efficacy of the ferric oxy-hydroxide sludge continuous reuse in the Fenton-based treatment of landfill leachate in a sequencing batch reactor with and without the addition of supplementary ferrous iron [71]. The mechanism of the ferric oxy-hydroxide sludge-activated hydrogen peroxide oxidation in the presence of strong complexing and reducing agents was proposed.

Three iron-dissolution mechanisms could be distinguished: protonation, complexation, and reduction. First, in the case of the H₂O₂/sludge system, the probability of iron dissolution by protonation is objectively high at favorable acidic conditions applied. Second, the dissolution of iron by complexation involves the attachment of a complexing ligand onto the ferric oxy-hydroxide surface; humic and fulvic acids, main subclasses in landfill leachate, contain a high density of functional groups, which can conjugate iron ions to form ion-ligand complexes. Third, these complexing ligands were partially dissolved at pH 3, and bound to the protonated OH-group, thus ending in ultimate decomposition of the Fe³⁺-ligand complex into the bulk solution. Last, both humic and fulvic acids, as effective reductants, reduced Fe³⁺ via electron transfer mechanism [72].

Besides, the addition of a Fe²⁺ activator to the ferric oxy-hydroxide sludge-activated Fenton-based systems increases the total phenols removal rate and reuse cycles. The supplementation of the Fe²⁺ activator could ensure the full utilization of the oxidant.

Organics as quinone- and hydroquinone-structure compounds (such as tannic acid, lignin, phenol, and among others) may assist the Fenton oxidation by reducing Fe³⁺ to Fe²⁺. The lost iron can be used by these organics to form complexes and reduced in the H₂O₂/sludge cycle. Comparing the reducing efficiency of iron-containing sludge by the quinone-structure organics, it is found that H₂O₂/sludge/TN system gave the best performance after adding the quinone-structure organics. Tannins are considered to be strong metal-chelating and reducing agents [73]. They exhibit anti-oxidation (act as ·OH scavengers) and pro-oxidation (promote ·OH generation in the presence of transition metals) properties in biological systems (living organisms).

A comprehensive study of the catalytic performance of Fe³⁺ in the presence of tannic acid during the Fenton-based treatment of 2,4,6-trichlorophenol (TCP) was

performed [74]. The addition of TN significantly promoted the degradation of TCP. H_2O_2 dose and ferric sludge load for water treatment in the presence of TN should be optimized to balance Fe^{3+} reduction to boost the Fenton reaction and $\cdot\text{OH}$ scavenging to remove TN from water. The Fe^{3+} reductive mechanism by tannic acid incorporated tannic acid- Fe^{3+} complex formation and decay through an electron transfer reaction to form Fe^{2+} .

TN availability in wastewater allows for the reuse of non-regenerated ferric sludge for Fenton-based oxidation without any supplementary Fe^{2+} . The positive effect of TN in the $\text{Fe}^{3+}/\text{H}_2\text{O}_2$ system can be explained by its monomer of gallic acids. Gallic acid complexed with Fe^{3+} to form two complexes that protonated $[\text{Fe}(\text{LH})]^{2+}$ and deprotonated $[\text{Fe}(\text{L})]^+$ from pH 1.0 to 3.0. These complexes were decomposed into Fe^{2+} and the quinone group by electron transfer, while Fe^{2+} reacted with H_2O_2 to accelerate the TCP removal [74].

The reuse methods of iron-containing sludge have been successfully proved with synthetic aqueous solutions of highly toxic compounds, such as phenols and chlorophenols. However, the decontamination of real wastewater by these enhanced technologies has been so far scarcely performed. The main reason is that real wastewater contains many organic pollutants with high toxicity and low biodegradability. These pollutants cannot completely mineralize. Organic pollutants will be continuously accumulated in reused iron-containing sludge that produced from treating real wastewater by the Fenton process. The phenomenon causes the low efficiency of the Fenton reaction.

6. Conclusions

During the last few years, many research efforts have been made toward the improvement of the Fenton process. Hybrid methods such as photo-Fenton, electro-Fenton, and sono-Fenton are not economically viable techniques to degrade large volumes of effluent disposed of by the industries. Most experimental studies have been conducted at the laboratory scale; thus, a more detailed investigation is required for the Fenton process to be considered feasible for industrial treatment plants. Further research on the advancement of the Fenton process is needed to demonstrate the economic and commercial feasibility of this process.

Although heterogeneous catalysts demonstrate considerable advances for the elimination of contaminants, there are still drawbacks related to the low oxidation rates, which appeared when pH values above four along with iron leaching, leading to an increase in the H_2O_2 consumption. Future studies should address the stability of the process for broader operational conditions to avoid metal leaching of into the reaction solution and their negative effects on the environment. These combined methods and heterogeneous systems expected to reduce the production of Fenton sludge. However, the high cost of combined methods, the leaching of active iron, and the decay of active catalytic sites should limit the reduction of Fenton sludge.

At present, regenerating the Fenton sludge is crucial for future studies. The use of Fenton sludge as a catalyst for the Fenton process has been tested mainly after thermal regeneration and subsequent re-dissolution of iron-containing solids by acid, chemical regeneration with reducing agent, and electrochemical reduction. The decontamination of real effluents by these enhanced technologies has been so far scarcely performed. The main reason is that real wastewater contains many complex organic pollutants with high toxicity and low biodegradability. These pollutants cannot completely mineralize. Significant attention should be devoted in the future on the development of rate expressions (based on reaction mechanisms),

identification of reaction intermediates, identification of scale-up parameters, and cost-effectiveness analysis.

Acknowledgements

The work is financially supported by the China special S&T project on treatment and control of water pollution (2017ZX07402002).

Author details


Min Xu^{1,2}, Changyong Wu^{1*} and Yuexi Zhou^{1*}

1 State Key Laboratory of Environmental Criteria and Risk Assessment,
Chinese Research Academy of Environment Sciences, Beijing, China

2 College of Water Science, Beijing Normal University, Beijing, China

*Address all correspondence to: changyongwu@126.com and zhouyuexi@263.net

IntechOpen

© 2020 The Author(s). Licensee IntechOpen. Distributed under the terms of the Creative Commons Attribution - NonCommercial 4.0 License (<https://creativecommons.org/licenses/by-nc/4.0/>), which permits use, distribution and reproduction for non-commercial purposes, provided the original is properly cited. 

References

- [1] Babuponnusami A, Muthukumar K. A review on Fenton and improvents to the Fenton process for wastewater treatment. *Journal of Environmental Chemical Engineering*. 2014;**2**:557-572
- [2] Lucas MS, Dias AA, Sampaio A, Amaral C, Peres JA. Degradation of a textile reactive Azo dye by a combined chemical-biological process: Fenton's reagent-yeast. *Water Research*. 2007;**41**: 1103-1109
- [3] Huang CP, Dong C, Tang Z. Advanced chemical oxidation: Its present role and potential future in hazardous waste treatment. *Waste Management*. 1993;**13**(5-7):361-377
- [4] Oturan AA, Aaron JJ. Advanced oxidation processes in water/ wastewater treatment: Principles and applications-a review. *Critical Reviews in Environmental Science and Technology*. 2014;**44**:2577-2641
- [5] Gallard H, De Laat J. Kinetic modeling of Fe(III)/H₂O₂ oxidation reactions in dilute aqueous solution using atrazine as a model organic compounds. *Water Research*. 2000;**34**: 3107-3116
- [6] Bigda RJ. Consider Fenton's chemistry for wastewater treatment. *Chemical Engineering Progress*. 1995;**91**: 62-66
- [7] Duarte F, Maldonado-Hódar FJ, Madeira LM. Influence of the characteristics of carbon materials on their behavior as heterogeneous Fenton catalysts for the elimination of the azo dye Orange II from aqueous solutions. *Applied Catalysis B: Environmental*. 2011;**103**:109-115
- [8] Yuan SH, Gou N, Alshawabkeh AN, Gu AZ. Efficient degradation of contaminants of emerging concerns by a new electro-Fenton process with Ti/MMO cathode. *Chemosphere*. 2013; **93**:2796-2804
- [9] Wang NN, Zheng T, Zhang GS, Wang P. A review on Fenton-like processes for organic wastewater treatment. *Journal of Environmental Chemical Engineering*. 2016;**4**:762-787
- [10] Matta R, Hanna K, Chiron S. Fenton-like oxidation of 2,4,6-trinitrotoluene using different iron minerals. *The Science of the Total Environment*. 2007;**385**:242-251
- [11] Shinya A, Bergwall L. Pyrite oxidation: Review and prevention practices. *Journal of Vertebrate Paleontology*. 2007;**27**:145A-145A
- [12] Babuponnusami A, Muthukumar K. Removal of phenol by heterogeneous photo electro Fenton-like process using nano-zero valent iron. *Separation and Purification Technology*. 2012;**98**: 130-135
- [13] Dehghani M, Shahsavani E, Farzadkia M, Samaei MR. Optimizing photo- Fenton like process for the removal of diesel fuel from the aqueous phase. *Journal of Environmental Health Science and Engineering*. 2014;**12**:1-17
- [14] Pourn SR, Aziz ARA, Daud WMAW. Review on the main advances in photo-Fenton oxidation system for recalcitrant wastewaters. *Journal of Industrial and Engineering Chemistry*. 2015;**21**:53-69
- [15] Alfaya E, Iglesias O, Pazos M, Sanroman MA. Environmental application of an industrial waste as catalyst for the electro-Fenton-like treatment of organic pollutants. *RSC Advances*. 2015;**5**:14416-14424
- [16] Brillas E, Sires I, Oturan MA. Electro-Fenton process and related electrochemical technologies based on

- Fenton's reaction chemistry. Chemical Reviews. 2009;**109**:6570-6631
- [17] Wang CK, Shih YH. Degradation and detoxification of diazinon by sono-Fenton and sono-Fenton-like processes. Separation and Purification Technology. 2015;**140**:6-12
- [18] Carta R, Desogus F. The enhancing effect of low power microwaves on phenol oxidation by the Fenton process. Journal of Environmental Chemical Engineering. 2013;**1**:1292-1300
- [19] Haber F, Weiss J. The catalytic decomposition of hydrogen peroxide by iron salts. Proceedings of the Royal Society of London, Series A. 1934; **147**(861):332-351
- [20] Bray WC, Gorin MH. Ferryl ion, a compound of tetravalent iron. Journal of the American Chemical Society. 1932; **54**(5):2124-2125
- [21] Neyens E, Baeyens J. A review of classic Fenton's peroxidation as an advanced oxidation technique. Journal of Hazardous Materials. 2003;**B98**(1-3): 33-50
- [22] Pignatelli JJ, Oliveros E, Mackay A. Advanced oxidation processes for organic contaminant destruction based on the Fenton reaction and related chemistry. Critical Reviews in Environmental Science and Technology. 2006;**36**:1-84
- [23] Duysterberg CK, Mylon SE, Waite TD. pH effects on iron-catalyzed oxidation using Fenton's reagent. Environmental Science and Technology. 2008;**42**:8522-8527
- [24] Szpyrkowicz L, Juzzolino C, Kaul SN. A comparative study on oxidation of disperse dye by electrochemical process, ozone, hypochlorite and Fenton reagent. Water Research. 2001;**35**: 2129-2136
- [25] Kavitha V, Palanivelu K. Destruction of cresols by Fenton oxidation process. Water Research. 2005;**39**:3062-3072
- [26] Xu XR, Li XY, Li XZ, Li HB. Degradation of melatonin by UV, UV/H₂O₂, Fe²⁺/H₂O₂ and UV/Fe²⁺/H₂O₂ processes. Separation and Purification Technology. 2009;**68**:261-266
- [27] Yoon J, Lee Y, Kim S. Investigation of the reaction pathway of ·OH radicals produced by Fenton oxidation in the conditions of wastewater treatment. Water Science and Technology. 2000; **44**:15-21
- [28] Zepp RG, Faust BC, Hoigné J. Hydroxyl radical formation in aqueous reaction (pH 3-8) of iron(II) with hydrogen peroxide the photo-Fenton reaction. Environmental Science and Technology. 1992;**26**(2): 313-319
- [29] Zuo Y, Hoigne J. Formation of hydrogen peroxide and depletion of oxalic acid in atmospheric water by photolysis of iron(III) –oxalato complexes. Environmental Science and Technology. 1992;**26**:1014-1022
- [30] Katsumata H, Kaneco S, Suzuki T, Otha K, Yobiko Y. Photo-Fenton degradation of alachlor in the presence of citrate solution. Journal of Photochemistry and Photobiology A. 2006;**180**:38-45
- [31] Bandala ER, Brito L, Pelaez M. Degradation of domoic acid toxin by UV-promoted Fenton-like processes in seawater. Desalination. 2009;**45**: 135-145
- [32] Giri AS, Golder AK. Chloramphenicol degradation in Fenton and photo-Fenton: Formation of Fe²⁺-chloramphenicol chelate and reaction pathways. Industrial and Engineering Chemistry Research. 2014;**53**: 16196-16203

- [33] Xiao D, Guo Y, Lou X, Fang C, Wang Z, Liu J. Distinct effects of oxalate versus malonate on the iron redox chemistry: Implications for the photo-Fenton reaction. *Chemosphere*. 2014; **103**:354-358
- [34] Mohajeri S, Abdul Aziz H, Hasnain Isa M, Ali Zahed M, Adlan MN. Statistical optimization of process parameters for landfill leachate treatment using electro-Fenton technique. *Journal of Hazardous Materials*. 2009; **176**:749-758
- [35] Guinea E, Arias C, Cabot PL, Garrido JA, Rodríguez RM, Centella F, et al. Mineralization of salicylic acid in acidic aqueous medium by electrochemical advanced oxidation processes using platinum and boron-doped diamond as anode and cathodically generated hydrogen peroxide. *Water Research*. 2008; **42**: 499-511
- [36] Panizza M, Cerisola G. Electro-Fenton degradation of synthetic dyes. *Water Research*. 2009; **43**:339-344
- [37] Pipi ARF, De Andrade AR, Brillas E, Sirés I. Total removal of alachlor from water by electrochemical processes. *Separation and Purification Technology*. 2014; **132**:674-683
- [38] Ranjit PJD, Palanivelu K, Lee CS. Degradation of 2,4-dichlorophenol in aqueous solution by sono-Fenton method. *Korean Journal of Chemical Engineering*. 2008; **25**:112-117
- [39] Ioan I, Wilson S, Lundanes E, Neculai A. Comparison of Fenton and sono-Fenton bisphenol A degradation. *Journal of Hazardous Materials*. 2007; **142**:559-563
- [40] Chakma S, Moholkar VS. Physical mechanism of sono-Fenton process. *AIChE Journal*. 2013; **59**:4303-4313
- [41] Neppolian B, Jung H, Choi H, Lee JH, Kang JW. Sonolytic degradation of methyl tert-butyl ether: The role of coupled Fenton process and persulphate ion. *Water Research*. 2002; **S36**: 4699-4708
- [42] Wu CY, Zhou YX, Sun QL, Fu LY, Xi HB, Yu Y, et al. Applying hydrolysis acidification-anoxic-oxic process in the treatment of petrochemical wastewater: Form bench scale reactor to full scale wastewater plant. *Journal of Hazardous Materials*. 2016; **309**:185-191
- [43] Badawy MI, Wahaab RA, El-Kalliny AS. Fenton-biological treatment processes for the removal of some pharmaceuticals from industrial wastewater. *Journal of Hazardous Materials*. 2009; **167**:567-574
- [44] Martinez NSS, Fernandez JF, Segura XF, Ferrer AS. Pre-oxidation of an extremely polluted industrial wastewater by the Fenton's reagent. *Journal of Hazardous Materials*. 2003; **B101**:315-322
- [45] Vergili I, Gencdal S. Applicability of combined Fenton oxidation and nanofiltration to pharmaceutical wastewater. *Desalination and Water Treatment*. 2015; **56**:3501-3509
- [46] Abdel-Shafy HI, El-Khateeb MA, Mansour MSM. Treatment of leather industrial wastewater via combined advanced oxidation and membrane filtration. *Water Science and Technology*. 2016; **23**:26-43
- [47] Blanco J, Torrades F, De la Varga M, García-Montano J. Fenton and biological-Fenton coupled processes for textile wastewater treatment and reuse. *Desalination*. 2011; **286**:394-399
- [48] Ioannou-Ttofa L, Michael-Kordatou I, Fattas SC, Eusebio A, Ribeiro B, Rusan M, et al. Treatment efficiency and economic feasibility of biological oxidation membrane filtration and

separation processes, and advanced oxidation for the purification and valorization of olive mill wastewater. *Water Research*. 2017;**114**: 1-13

[49] Mylon SE, Sun QA, Waite TD. Process optimization in use of zero valent iron nanoparticles for oxidative transformations. *Chemosphere*. 2010; **81**:127-131

[50] Chen Q, Wu P, Dang Z, Zhu N, Li P, Wu J, et al. Iron pillared vermiculite as a heterogeneous photo-Fenton catalyst for photocatalytic degradation of azo dye reactive brilliant orange X-GN. *Separation and Purification Technology*. 2010;**71**: 315-323

[51] Lan Q, Li F, Sun CX, Liu CS, Li XZ. Heterogeneous photodegradation of pentachlorophenol and iron cycling with goethite, hematite and oxalate under UVA illumination. *Journal of Hazardous Materials*. 2010; **174**:64-70

[52] Fu FL, Wang Q, Tang B. Effective degradation of Cl acid red 73 by advanced Fenton process. *Journal of Hazardous Materials*. 2010;**174**:17-22

[53] Pagano M, Volpe A, Lopez A, Mascolo G, Ciannarella R. Degradation of chlorobenzene by Fenton-like processes using zero-valent iron in the presence of Fe^{3+} and Cu^{2+} . *Environmental Technology*. 2011;**32**: 155-165

[54] Pecci L, Montefoschi G, Cavallini D. Some new details of the copper-hydrogen peroxide interaction. *Biochemical and Biophysical Research Communications*. 1997;**235**:264-267

[55] Choi K, Lee W. Enhanced degradation of trichloroethylene in nano-scale zero-valent iron Fenton system with Cu(II) . *Journal of Hazardous Materials*. 2012;**211**:146-153

[56] Hermanek M, Zboril R, Medrik I, Pechousek J, Gregor C. Catalytic efficiency of iron (III) oxides in decomposition of hydrogen peroxide: Competition between the surface area and crystallinity of nanoparticles. *Journal of the American Chemical Society*. 2007;**129**:10929-10936

[57] Matta R, Hanna K, Kone T, Chiron S. Oxidation of 2,4,6-trinitrotoluene in the presence of different iron-bearing minerals at neutral pH. *Chemical Engineering Journal*. 2008;**144**:453-458

[58] Hanna K, Kone T, Medjahdi G. Synthesis of the mixed oxides of iron and quartz and their catalytic activities for the Fenton-like oxidation. *Catalysis Communications*. 2008;**9**: 955-959

[59] Song Z, Wang N, Zhu LH, Huang AZ, Zhao XR, Tang HQ. Efficient oxidative degradation of triclosan by using enhanced Fenton-like process. *Chemical Engineering Journal*. 2012; **198-199**:379-387

[60] Huang WY, Brigante M, Wu F, Mousty C, Hanna K, Mailhot G. Assessment of the Fe(III) -EDDS complex in Fenton-like processes: From the radical formation to the degradation of bisphenol A. *Environmental Science and Technology*. 2013;**47**:1952-1959

[61] Bolobajev J, Kattel E, Viisimaa M, Goi A, Trapido M, Tenno T, et al. Reuse of ferric sludge as an iron source for the Fenton-based process in wastewater treatment. *Chemical Engineering Journal*. 2014;**255**:8-13

[62] Ji F, Li C, Zhang J, Deng L. Efficient decolorization of dye pollutants with $\text{LiFe(WO}_4)_2$ as a reusable heterogeneous Fenton-like catalyst. *Desalination*. 2011;**269**(1-3):284-290

[63] Takbas M, Yatmaz HC, Bektas N. Heterogeneous photo-Fenton oxidation

of reactive azo dye solutions using iron exchanged zeolite as a catalyst. *Microporous and Mesoporous Materials*. 2008;**115**(3):594-602

[64] Zhang H, Liu JG, Ou CJ, Faheem SJY, Yu HX, Jiao ZH, et al. Reuse of Fenton sludge as an iron source for NiFe_2O_4 synthesis and its application in the Fenton-based process. *Journal of Environmental Sciences*. 2016;**5**:1-8

[65] Roonasi P, Nezhad AY. A comparative study of a series of ferrite nanoparticles as heterogeneous catalysts for phenol removal at neutral pH. *Materials Chemistry and Physics*. 2016; **172**:143-149

[66] Faheem M, Jiang XB, Wang LJ, Shen JY. Synthesis of Cu_2O - CuFe_2O_4 microparticles from Fenton sludge and its application in the Fenton process: The key role of Cu_2O in the catalytic degradation of phenol. *RSC Advances*. 2018;**8**:5740-5748

[67] Li CW, Chen YM, Chiou YC, Liu CK. Dye wastewater treated by Fenton process with ferrous ions electrolytically generated from iron-containing sludge. *Journal of Hazardous Materials*. 2007;**144**: 570-576

[68] Kishimoto N, Kitamura T, Kato M, Otsu H. Reusability of iron sludge as an iron source for the electrochemical Fenton-type process using $\text{Fe}^{2+}/\text{HOCl}$ system. *Water Research*. 2013;**47**: 1919-1927

[69] Cao GM, Sheng M, Niu WF, Fei YL, Li D. Regeneration and reuse of iron catalyst for Fenton-like reactions. *Journal of Hazardous Materials*. 2009; **172**:1446-1449

[70] Rossi AF, Martins RC, Quinta-Ferreira RM. Reuse of homogeneous Fenton's sludge from detergent industry as Fenton's catalyst. *Journal of*

Advanced Oxidation Technologies. 2013;**16**(2):298-305

[71] Kattel E, Trapido M, Dulova N. Treatment of landfill leachate by continuously reused ferric oxyhydroxide sludge-activated hydrogen peroxide. *Chemical Engineering Journal*. 2016;**304**:646-654

[72] Voelker BM, Sulzberger B. Effects of fulvic acid on Fe(II) oxidation by hydrogen peroxide. *Environmental Science and Technology*. 1996;**30**: 1106-1114

[73] Bolobajev J, Trapido M, Goi A. Role of organic wastewater constituents in iron redox cycling for ferric sludge reuse in the Fenton-based treatment. *International Journal of Chemical, Molecular, Nuclear, Materials and Metallurgical Engineering*. 2016;**10**(4): 352-357

[74] Bolobajev J, Trapido M, Goi A. Interaction of tannic acid with ferric iron to assist 2,4,6-trichlorophenol catalyst decomposition and reuse of ferric sludge as a source of iron catalyst in Fenton-based treatment. *Applied Catalysis B: Environmental*. 2016;**187**: 75-82